Title	Cavity ring-down spectroscopy instrumentation for airborne detection of nitrogen oxides
Authors	Dubé, W. P.
Publication date	2018
Original Citation	Dubé, W. P. 2018. Cavity ring-down spectroscopy instrumentation for airborne detection of nitrogen oxides. PhD Thesis, University College Cork.
Type of publication	Doctoral thesis
Rights	© 2018, William P. Dubé. - http://creativecommons.org/licenses/by-nc-nd/3.0/
Download date	2025-08-17 05:34:55
Item downloaded from	https://hdl.handle.net/10468/6560

Ollscoil na hÉireann, Corcaigh
National University of Ireland, Cork

University College Cork, Ireland
Coláiste na hOllscoile Corcaigh

Cavity ring-down spectroscopy instrumentation

for airborne detection of nitrogen oxides

Thesis presented by

William P. Dubé, BSME

For the degree of
Doctor of Philosophy

University College Cork
Department of Physics

May 2018

Head of Department: Professor John McInerney
Supervisor: Professor Albert A. Ruth
Examiners: Professor Weidong Chen, Professor John Wenger

Declaration

This is to certify that the work I am submitting is my own and has not been submitted for another degree, either at University College Cork or elsewhere. All external references and sources are clearly acknowledged and identified within the contents. I have read and understood the regulations of University College Cork concerning plagiarism.

_____

William P. Dubé

Dedication

It takes a village to raise a PhD! This thesis would never have become reality without the huge support of my UCC advisor Dr. Andy Ruth, my NOAA boss Dr. Steven Brown, and my beloved wife Dr. Eva Håkansson. I also owe much of the success in airborne measurements to my great colleagues at NOAA and University of Colorado/CIRES, and at multiple other institutions that we have collaborated with over the years. Thank you all for advancing the field of atmospheric research and for helping me make this lifelong dream come true!

Preface

I was recruited by the United States National Oceanic and Atmospheric Administration (NOAA) in Boulder, Colorado, USA in 2003. My first project concerned the development of CaRDS instrumentation for airborne deployment. During the 1990s, the general opinion had been that CaRDS instruments could not be deployed on airborne platforms due to their size and lack of ruggedness. When I was told that this was the common belief, I did not agree that it had to be that way. My supervisor, Dr. Steven Brown, shared the opinion that airborne deployment of CaRDS should be possible.

One year after I started at NOAA, we had taken CaRDS from the lab to an airplane with great success. Based on my new design and several improvements in the experimental setup, the first airborne deployment of a CaRDS instrument on the NOAA P-3 Hurricane Hunter airplane in 2004 for in-situ measurements of NO_3 and N_2O_5 became possible. It required a huge engineering effort, but is a prime example of applied physics and engineering.

During the next 13 years, I continued to develop CaRDS for airborne deployment. CaRDS instruments fully or partially conceived and designed by me have been deployed in a large number of field measurements, which have resulted in an increased understanding of the chemistry of the troposphere. Several of my designs, were later copied by other research groups. The UCC group led by Dr. Andy Ruth is taking my approach for light-weight, low-power CaRDS instruments to a new level with a new instrument currently being built. This instrument represents the state-of-the-art in the field.

While the airborne deployment was the first huge leap in the use of CaRDS for atmospheric measurements of nitrogen oxides, the development has also resulted in successive improvements in reliability, ruggedness, accuracy, and sensitivity. Airborne measurements with CaRDS instruments are now routine.

Abstract

Pulsed laser cavity ring-down spectroscopy (CaRDS) is a highly sensitive method for direct absorption spectroscopy that has been applied to in-situ detection of NO_3, N_2O_5, NO_2, NO, and O_3, as well as NO_x and NO_y in the atmosphere from a variety of airborne platforms. CaRDS instruments have traditionally been large and delicate laboratory instruments. The successful leap from laboratory instruments with high maintenance requirements to compact and rugged field instruments for airborne deployment was made possible through the extensive engineering work and new innovations presented in this thesis.

The necessary improvements were mainly in the six following areas: 1) Instrument rack design and vibration isolation, 2) Automated aerosol filter changer, 3) Low loss inlet design and flow control, 4) Optical cage design, 5) Clamped/nudged mirror mount, and 6) Purge system improvements. The result was a series of compact, reliable, and rugged field instruments with high sensitivity and accuracy.

The first airborne deployment was performed in 2004. The designs have been copied by several other research groups, and airborne measurements with CaRDS instruments are now considered routine.

Table of contents

1. Introduction

This thesis describes the development and optimization of airborne pulsed cavity ring-down spectroscopy (CaRDS) instrumentation for the highly sensitive detection of nitrogen oxides and ozone in the free troposphere.

1.1 Motivation to the thesis and contributions

Nitrogen oxides in the troposphere are primary pollutants derived from combustion of fossil fuels. They are key constituents regulating the abundance of ozone and hence are important for climate and air quality. Many of the chemical reaction mechanisms involving nitrogen oxides are driven by sunlight, however, nitrogen oxides also play an important role in the nighttime tropospheric chemistry. The nighttime chemistry involves species that are unstable in sunlight, such as the nitrate radical, NO_3, and its equilibrium partner, N_2O_5.

To characterize the processes that govern the atmospheric chemistry both during daytime and nighttime, measurement instruments with high sensitivity are necessary as the abundance of the species of interest can be inherently low. The CaRDS principle offers the needed sensitivity, but the corresponding instruments have traditionally been difficult to deploy outside a laboratory environment. CaRDS instruments have generally been built on optical tables using conventional optics components, and these designs were highly sensitive to vibrations, ambient temperature, and pressure. Thermal and mechanical stresses, combined with components designed for laboratory use rather than field use, would cause cavity mirrors to drift out of alignment. Early (lab-based) instrumentation in CaRDS required high maintenance and daily alignments and were unsuitable for airborne deployment.

Through extensive engineering work, the first airborne deployment of a CaRDS instrument was performed in 2004. Continuous development resulted in a series of compact, reliable, and rugged field instruments with high sensitivity and accuracy. The designs have been copied by several other research groups, and airborne measurements with CaRDS instruments are now considered routine.

The author was instrumental in the development of these trail-breaking field measurements from airplanes and other mobile platforms. This thesis focusses on the physical and engineering aspects of two CaRDS instruments developed at NOAA (Boulder): "ARNOLD" (*Atmospheric Ring-down Nitrogen Oxide Laser Detector*) and "NOxCaRD" (*Nitrogen Oxides by Cavity Ring Down*). The thesis is based on five selected publications [1-5] published over the past 13 years, where some or all the data was collected using these two instruments. The five publications are presented in full in chapters 3 through 7. The two instruments are presented in sections 2.1 and 2.2.

The author's main contributions in the development of CaRDS instruments for airborne detection of nitrogen oxides are in the following six areas (references refer to the publication(s) where

the respective design features were used for the measurements). Engineering details and experimental aspects will be discussed in detail in Chapter 8.

1. **Instrument rack design:** Welded 4130 chrome-moly steel racks replacing the traditional riveted aluminum rack design resulted in higher strength, lower weight, lower cost, and better vibration isolation. Publications [1, 2, 4].

2. **Automated filter changer:** An inlet aerosol filter is necessary for measurements of NO_3 and N_2O_5, but the filter has to be changed hourly because collected contaminants react with the substances of interest, resulting in unacceptable inlet losses. A fully automated filter changer allowed increased filter change frequency while decreasing down-time during filter changes, and allowed the instrument to be operated in the pressurized cabin while sampling the outside, unpressurized, air. The gaps in the measurements due to filter changes were greatly reduced resulting far less missed data. Publications [1, 2, 4].

3. **Low loss inlet design and flow control:** Inlet design improvements include a coaxial flow type zero air addition scheme that does not introduce disruptive inlet pressure variations and a low loss Teflon machining technique. Portions of the inlet were manufactured using a special Computer Numerical Control (CNC) low NO_3/N_2O_5 loss machining technique. The improved inlet designs were first used in [2], and have been used in all airborne deployments afterwards [3-5]. The work also included integration of flow controllers.

4. **Cage design:** A cage design addressed the problem with the mirrors drifting out of alignment, and further reduced the vibration sensitivity. The cage design in a CaRDS instrument was first used in [3], and has very successfully been used in the multichannel instruments "NOxCaRD" and "ACES" (*Airborne Cavity Enhanced Spectrometer*, not presented in detail in this thesis but included in the selected publications), and will be implemented in the next generation of "ARNOLD" instruments. Publications [3, 5].

5. **Clamped/nudged mirror mount:** A clamped/nudged mirror mount design further reduced the need for re-alignment of the mirrors. In contrast with traditional CaRDS instruments requiring daily alignments, the instrument NOxCaRD, using nudged and clamped cage mirror mounts, has been operated for several years without alignment. Publication [5].

6. **Purge system improvements:** Improvements in the purge system, which keeps the contaminated air from reaching the mirrors, increased the effective cavity length and increased both accuracy and sensitivity of the measurements. Publications [1, 5].

All of the design aspects, except for the filter changer (item 2), feature presently in a collaborative project with University College Cork (UCC). The project aims at the construction of a lightweight, autonomous CaRDS instrument for the CARIBIC program (www.caribic-

atmospheric.com). The instrument is referred to as "CARDINO" *(CARIBIC Autonomous Ring-Down Instrument for Nitrogen Oxides*) and will be the world's lightest four channel, autonomous, CaRDS instrument which will be deployed in a cargo container onboard an Airbus 340-600 on regular commercial passenger flight around the globe. CARDINO will be used to detect N_2O_5, NO_3, NO_2 and O_3 in the upper and lower troposphere for long-term global climatological monitoring.

1.2 Pulsed cavity ring-down spectroscopy (CaRDS)

In a conventional direct optical absorption experiment the incident and transmitted intensities (I_0 and I respectively) of a light beam, propagating through a sample of path length L, are measured. The absorption of the sample is related to the attenuation of the light intensity which is expressed by the well-known Lambert-Beer law:

$$I = I_0 \exp(-\alpha L) \tag{1-1}$$

where $\alpha(\lambda)$ is the wavelength dependent absorption coefficient, which is usually given in [cm^{-1}]. The absorption coefficient $\alpha(\lambda) \equiv N\,\sigma(\lambda)$ is normally expressed as the product of the number density N [cm^{-3}] and the specific wavelength-dependent absorption cross-section σ [cm^2] of the absorbing species. For inherently weak absorptions (i.e. ln (I/I_0) < 10^{-6}), which occur in gas-phase absorption measurements, the main problem with conventional methods is that, the change of intensity of the light passing through the sample is very small compared with the initial light intensity. Thus, the sensitivity is generally limited by fluctuations in I_0. In other words, it is difficult to achieve an adequate signal-to-noise ratio to distinguish the difference between I_0 and I. The approach to measure absorption coefficients with the cavity ring-down method virtually eliminates this problem, since the experimental principle is based on the measurement of a *rate* rather than a *magnitude* of an intensity change. The cavity ring-down approach is also combined with the creation of a very long absorption path length, which is a well-known way of improving the sensitivity in measurements of small absorption coefficients ($\alpha = L^{-1} \ln(I/I_0)$).

In cavity ring-down absorption spectroscopy (CaRDS) the light pulse from a (potentially tunable) laser is coupled into an optically stable high-finesse cavity formed by two highly reflective dielectric mirrors which are separated by a distance L_0. In the following the round-trip time of the laser pulse in the resonator is assumed to be longer than the laser pulse duration so that interference and mode effects can be neglected. If the reflectivity R of the mirrors is high enough (typically $R \sim 0.99999$ in the visible) the light pulse can be stored in the cavity for tens of microseconds, which corresponds to several thousand passes of the pulse depending on the mirror separation L_0. The light intensity in the cavity decreases due to the overall losses of the cavity. This decay is monitored by measuring the transmitted intensity of the light pulses by means of an appropriate detector on the exit side of the resonator (usually photomultiplier tubes (PMT) or photodiodes are employed for that purpose, see Figure 1-1).
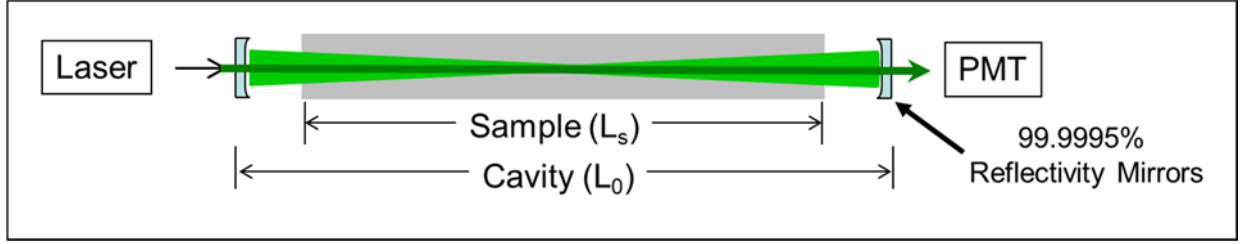
Figure 1-1: Typical Components of a CaRDS setup. PMT: Photomultiplier Tube.

The empty cavity: In an empty (evacuated) cavity the intensity measured after the first pass will be $I_0 = T^2 I_{in}$, where $T = 1-R$ is the transmission of each mirror and I_{in} is the intensity of the input laser pulse. During each round-trip (=two passes) the pulse intensity is attenuated by a factor of R^2 leading to an intensity of $I_k = I_0 R^{2k} = I_0 \exp(2k \ln(R))$ after k round-trips. Replacing the discrete number of round-trips k by the continuous parameter time, $t = k(2L_0/c)$, leads to an expression for the time-dependence of the laser pulse intensity, which is measured at the cavity exit (*c* is the speed of light)

$$I(t) = I_0 \exp\left(\frac{c \ln(R)}{L_0} t\right) \tag{1-2}$$

The decay time of this exponential decay is called ring-down time

$$\tau_0(\lambda) = \frac{L_0}{c|\ln(R(\lambda))|} \qquad (\ln R \approx R\text{-}1 < 0), \tag{1-3}$$

which is solely dependent on the mirror reflectivity at a given mirror separation L_0. By scanning the laser wavelength and measuring τ_0 the wavelength-dependence of the mirror reflectivity can be determined. For the derivation of equation 1-2 it was assumed that diffraction losses of the cavity are negligible. This is a valid assumption since in practice cavity conditions can be found, almost always, where this is the case.

The filled cavity: In a cavity which contains a gas sample the absorption of the respective species will increase the total losses per pass by $\sim\exp(-\alpha L_0)$ according to Lambert-Beer's law; please note that the losses in principle contain absorption and scattering losses. It is important that losses due to scattering of the light in the cavity are kept to a minimum (e.g. through aerosol filters) and much smaller than the losses due to the limited mirror reflectivity. From the intensity after k round-trips in the cavity, $I_k = I_0 (R \exp(\alpha L_0))^{2k}$, the time-dependence of the intensity exiting the cavity can be written as

$$I(t) = I_0 \exp\left(-\frac{\alpha L_0 + |\ln(R)|}{L_0} ct\right). \tag{1-4}$$

In this case the reciprocal ring-down time τ^{-1} is proportional to the total losses per round-trip:

$$\tau^{-1}(\lambda) = \left(\alpha(\lambda) + \frac{|\ln(R(\lambda))|}{L_0}\right) c \tag{1-5}$$

The absorption coefficient of the gas α is derived by fitting equations 1-4 and 1-5 to the measured intensity decay for the empty and the filled cavity and subsequently subtracting the respective reciprocal ring-down times:

$$\alpha = \frac{1}{c}\left(\frac{1}{\tau} - \frac{1}{\tau_0}\right) \tag{1-6}$$

An absorption *spectrum* can in principle be measured if a tunable laser is used and τ^{-1} is plotted versus the wavelength λ, taking into account the "background" of the empty--resonator, $c \ln(R) / L_0$, which is solely dependent on the mirror reflectivity. This is the reason why CaRD spectroscopy is practically intensity-independent and only limited by the shot-to-shot noise of the laser.

Figure 1-1 shows a typical experimental scheme illustrating the (pulsed) cavity ring-down principle. It should be noted that in practice L_0 is to be replaced by the sample length, L_S, inside the cavity, because the cavity mirrors are generally purged with a clean gas for protection of the mirrors. Purging the mirrors is essential as mirror surfaces are, by their very nature, very sensitive to contamination and degradation by volatile organic compounds (VOC) and aerosols, which are difficult to remove entirely from gas samples. The purging of the mirrors shortens the sample length to $L_S < L_0$, depending on purge conditions. Although the two "purge" volumes keep the mirrors clean, the boundary between the sample volume and the purge volumes is not perfectly defined. There is diffusion across the boundary in both directions. The purge flow, although typically small in comparison to the gas sample flows, also dilutes the sample flow slightly. Both of these effects tend to make the measurement slightly sensitive to pressure changes and changes in the sample flow.

Sensitivity and detection limits

From equation 1-5 it becomes obvious that the better the mirror reflectivity, i.e. the longer the ring-down time, the smaller absorption coefficients can be measured. Formally the

sensitivity of the CaRD method is defined through the relative decrease of the light intensity per pass, δI, which is related to the quantities in a CaRD experiment in the following way [45]:

$$\delta I \equiv \frac{I_0 - I}{I_0} \approx \alpha L_0 = (1 - R)\frac{\Delta\tau}{\tau} \tag{1-7}$$

where $\Delta\tau$ is the change of the ring-down time with and without the absorption (or loss in general) in the cavity. The smallest measurable absorption coefficients therefore depend on the smallest detectable change in the ring-down time according to equation 1-7. In other words, the accuracy with which the ring-down time can be measured determines the size of the smallest measurable absorption coefficient. This is in agreement with the fact, that ring-down times can be determined more accurately the longer the ring-down decays are. The time constants of the cavities discussed in this thesis are of the order of tens to hundreds of microseconds. These time constants correspond to path lengths of tens of kilometers to nearly one hundred kilometers, as shown in Figure 1-2. This long path length is what makes CaRDS a very sensitive absorption spectroscopy method.
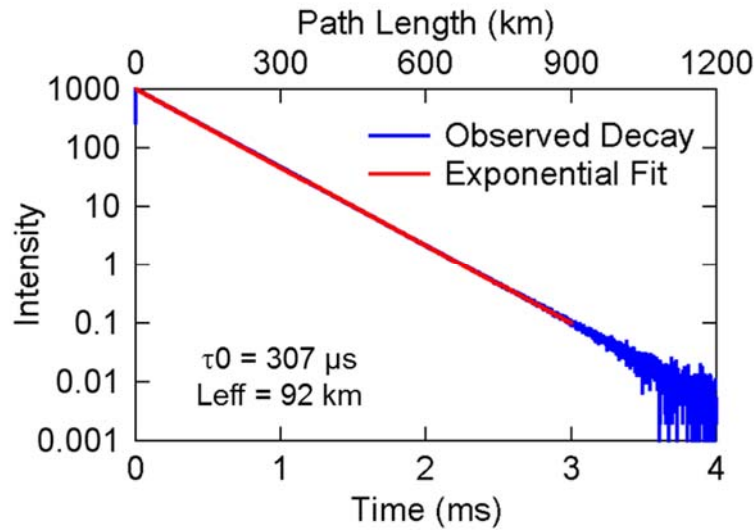
Figure 1-2: Example of the decay of light intensity in a stable cavity as a function of time including the corresponding fit of the data. $L_{eff} = L_S/(1-R)$

1.3 Selected publications

This thesis is based on the five selected publications presented below [1-5], of which the applicant is 1st author of one, 2nd author of three, and 3rd author of one. Currently these publications have a total of 332 citations, or on average 66.4 citations per publication.

A. **Aircraft instrument for simultaneous, in-situ measurements of NO_3 and N_2O_5 via pulsed cavity ring-down spectroscopy**

W.P. Dubé, S.S. Brown, H.D. Osthoff, M.R. Nunley, S.J. Ciciora, M.W. Paris, R.J. McLaughlin, A.R. Ravishankara.

Rev. Sci. Instr. 77 (2006) 034101.

Contribution: ~65 %

Responsibilities: Conceived and designed the CaRDS instrument "ARNOLD". This was the first successful deployment of a CaRDS instrument on an airborne platform. This is a descriptive paper of the instrument and measurement technique.

Citations: 109 (Google Scholar, January 2018)

Figure 1-3: Front page of Publication A [1].

B. **Determination of inlet transmission and conversion efficiencies for in-situ measurements of the nocturnal nitrogen oxides, NO_3, N_2O_5 and NO_2, via pulsed cavity ring-down spectroscopy**

H. Fuchs, **W.P. Dubé,** S. J. Ciciora, S. S. Brown.

Anal. Chem. 80 (2008) 6010-6017.

Contribution: ~35 %

Responsibilities: Contributed to the experimental design for the study. Designed the instrument, including selecting the lowest loss inlet material and developing specialized low loss machining technique for PFA (*Perfluoroalkoxy alkanes*, a material similar to Teflon).

Citations: 56 (Google Scholar, January 2018)
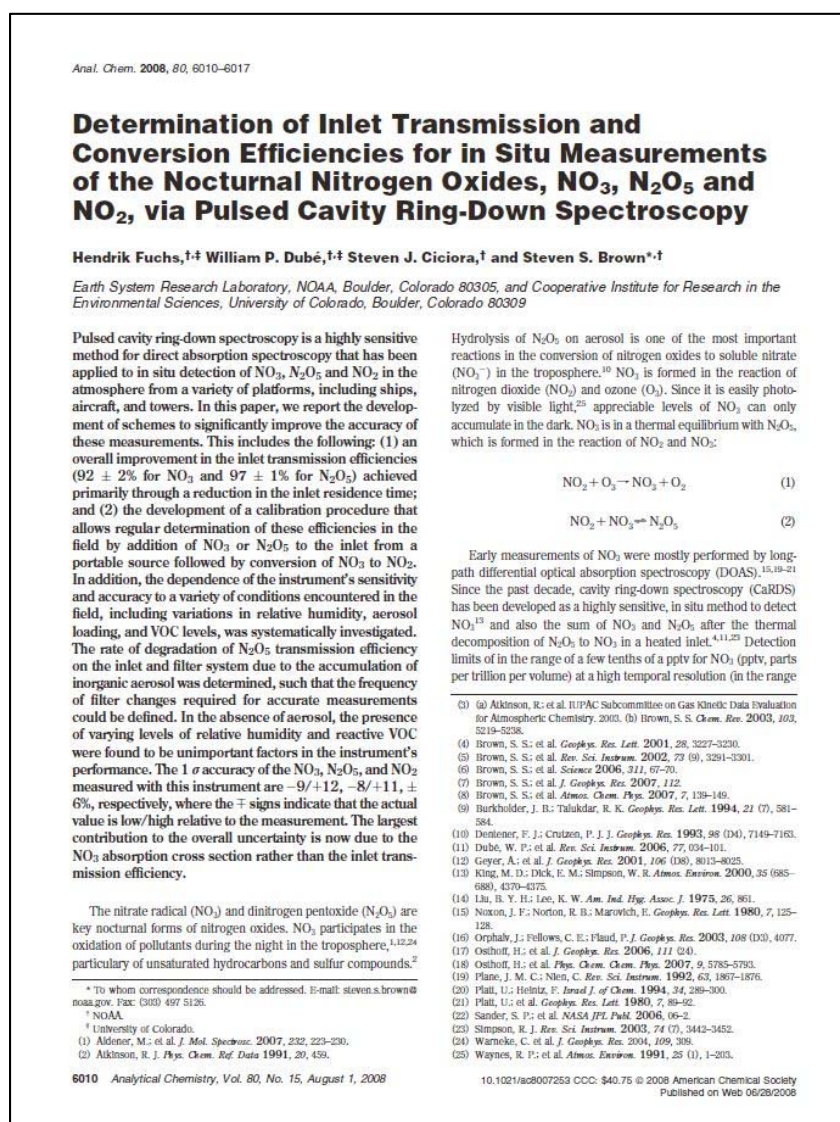
Figure 1-4: Front page of Publication B [2].

C. **A sensitive and versatile detector for atmospheric NO₂ and NOₓ based on blue diode laser cavity ring-down spectroscopy**

H. Fuchs, **W.P. Dubé,** B.M. Lerner, N.L. Wagner, E.J. Williams, S.S. Brown.

Environ. Sci. Technol. 43 (2009) 7831-7836.

Contribution: ~40 %

Responsibilities: Designed the major portion of the instrument, which was the first CaRDS instrument to use a 405 nm blue diode laser.

Citations: 70 (Google Scholar, January 2018)

Figure 1-5: Front page of Publication C [3].

D. **Diode laser-based cavity ring-down instrument for NO_3, N_2O_5, NO, NO_2 and O_3 from aircraft**

N.L. Wagner, **W.P. Dubé,** R.A. Washenfelder, C.J. Young, I.B. Pollack, T.B. Ryerson, S.S. Brown.

Atmos. Meas. Tech. 4 (2011) 1227-1240.

Contribution: ~45 %

Responsibilities: Designed the major revision of the instrument "ARNOLD", where it was equipped with dual diode lasers: 405 nm, and 662 nm.

Citations: 73 (Google Scholar, January 2018).

Atmospheric Measurement Techniques

Diode laser-based cavity ring-down instrument for NO_3, N_2O_5, NO, NO_2 and O_3 from aircraft

N. L. Wagner[1,2], W. P. Dubé[1,2], R. A. Washenfelder[1,2], C. J. Young[1,2], I. B. Pollack[1,2], T. B. Ryerson[1], and S. S. Brown[1]

[1]NOAA Earth System Research Laboratory, R/CSD7, 325 Broadway, Boulder, CO 80305, USA
[2]Cooperative Institute for Research in Environmental Sciences, University of Colorado, Boulder, CO 80309, USA

Abstract. This article presents a diode laser-based, cavity ring-down spectrometer for simultaneous in situ measurements of four nitrogen oxide species, NO_3, N_2O_5, NO, NO_2, as well as O_3, designed for deployment on aircraft. The instrument measures NO_3 and NO_2 by optical extinction at 662 nm and 405 nm, respectively; N_2O_5 is measured by thermal conversion to NO_3, while NO and O_3 are measured by chemical conversion to NO_2. The instrument has several advantages over previous instruments developed by our group for measurement of NO_2, NO_3 and N_2O_5 alone, based on a pulsed Nd:YAG and dye laser. First, the use of continuous wave diode lasers reduces the requirements for power and weight and eliminates hazardous materials. Second, detection of NO_2 at 405 nm is more sensitive than our previously reported 532 nm instrument, and does not have a measurable interference from O_3. Third, the instrument includes chemical conversion of NO and O_3 to NO_2 to provide measurements of total NO_x (= NO + NO_2) and O_x (= NO_2 + O_3) on two separate channels; mixing ratios of NO and O_3 are determined by subtraction of NO_2. Finally, all five species are calibrated against a single standard based on 254 nm O_3 absorption to provide high accuracy. Disadvantages include an increased sensitivity to water vapor on the 662 nm NO_3 and N_2O_5 channels and a modest reduction in sensitivity for these species compared to the pulsed laser instrument. The in-flight detection limit for both NO_3 and N_2O_5 is 3 pptv (2σ, 1 s) and for NO, NO_2 and O_3 is 140, 90, and 120 pptv (2σ, 1 s) respectively. Demonstrated performance of the instrument in a laboratory/ground based environment is better by approximately a factor of 2–3. The NO and NO_2 measurements are less precise than research-grade chemiluminescence instruments. However, the combination of these five species in a single instrument, calibrated to a single analytical standard, provides a complete and accurate picture of nighttime nitrogen oxide chemistry. The instrument performance is demonstrated using data acquired during a recent field campaign in California.

1 Introduction

The nitrate radical, NO_3 and its reservoir species, dinitrogen pentoxide (N_2O_5) are important trace gases in the nocturnal atmosphere (Wayne et al., 1991). NO_3 is formed by reaction of ozone with NO_2 (Reaction R1), and reacts with NO_2 to reversibly form N_2O_5 (Reaction R2).

$$O_3 + NO_2 \rightarrow NO_3 + O_2 \tag{R1}$$

$$NO_3 + NO_2 \leftrightarrows N_2O_5 \tag{R2}$$

These species are typically present at very modest levels during daytime (less than 1 pptv) because NO_3 undergoes rapid photolysis and reaction with NO, which is present during the day and in close proximity to large NO_x emission sources during the night.

$$
\begin{aligned}
NO_3 + h\upsilon &\rightarrow NO_2 + O \\
&\rightarrow NO + O_2
\end{aligned} \tag{R3}
$$

$$NO_3 + NO \rightarrow 2 NO_2 \tag{R4}$$

The nitrate radical is a strong oxidant and is consumed by reactions with biogenic VOCs and sulfur compounds, and some classes of highly reactive anthropogenic VOCs (Atkinson, 1991). N_2O_5 undergoes heterogeneous uptake to aerosol. Its hydrolysis leads either to non-photochemical conversion of NO_x to soluble nitrate via production of HNO_3 (Jones and Seinfeld, 1983), or to activation of photolabile halogens through formation of nitryl chloride, $ClNO_2$ (Finlayson-Pitts et al., 1989; Thornton et al., 2010). Thus,

Correspondence to: S. S. Brown
(steven.s.brown@noaa.gov)

Figure 1-6: Front page of Publication D [4].

E. **A measurement of total reactive nitrogen, NO$_y$, together with NO$_2$, NO, and O$_3$ via cavity ring-down spectroscopy**

R.J. Wild, P.M. Edwards, **W.P. Dubé,** K. Baumann, E.S. Edgerton, P.K. Quinn, J.M. Roberts, A.W. Rollins, P.R. Veres, C. Warneke, E.J. Williams, B. Yuan, S.S. Brown, Environ. Sci. Technol. 48 (2014) 9609-9615.

Contribution: ~30 %

Responsibilities: This paper describes the applicant's instrument design, "NOxCARD", in detail. The major design revisions included the cage design concept and the nudged mirror mounts, plus the addition of a NO$_y$ channel. This was the first time the nudged mirror mount design was used.

Citations: 24 (Google Scholar, January 2018).

Figure 1-7: Front page of Publication E [5].

In addition to these publications, the CaRDS development work presented in this thesis has been instrumental in the measurements for the following two publications in *Nature* [6, 7], where the applicant is one of the co-authors. These two publications will not be covered in detail in this thesis:

A large atomic chlorine source inferred from mid-continental reactive nitrogen chemistry

J.A. Thornton, J.P. Kercher, T.P. Riedel, N.L. Wagner, J. Cozic, J.S. Holloway, **W.P. Dubé,** G.M. Wolfe, P.K. Quinn, A.M. Middlebrook, B. Alexander, S.S. Brown.

Nature 464 (2010) 271-274.

Contribution: ~20 %

Responsibilities: Provided half of the instruments for the campaign, half of the measurements, and the N_2O_5 calibration source in support of the discovery.

Citations: 313 (Google Scholar, January 2018)

High winter ozone pollution from carbonyl photolysis in an oil and gas basin

P.M. Edwards, S.S. Brown, J.M. Roberts, R. Ahmadov, R.M. Banta, J.A. deGouw, **W.P. Dubé,** R.A. Field, J.H. Flynn, J.B. Gilman, [...], C.R. Thompson, M.K. Trainer, C. Tsai, P.R. Veres, R.A. Washenfelder, C. Warneke, R.J. Wild, C.J. Young, B. Yuan, R. Zamora.

Nature 514 (2014) 351–354.

Contribution: ~10 %

Responsibilities: Provided all three instruments (ARNOLD, NOxCaRD, ACES) and assisted in the measurements in this field campaign (ACES will only be covered very briefly in this thesis).

Citations: 74 (Google Scholar, January 2018)
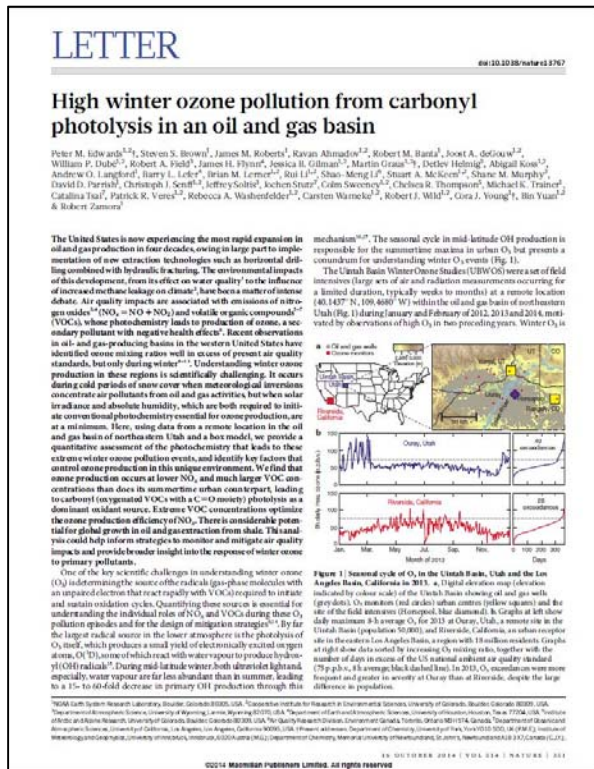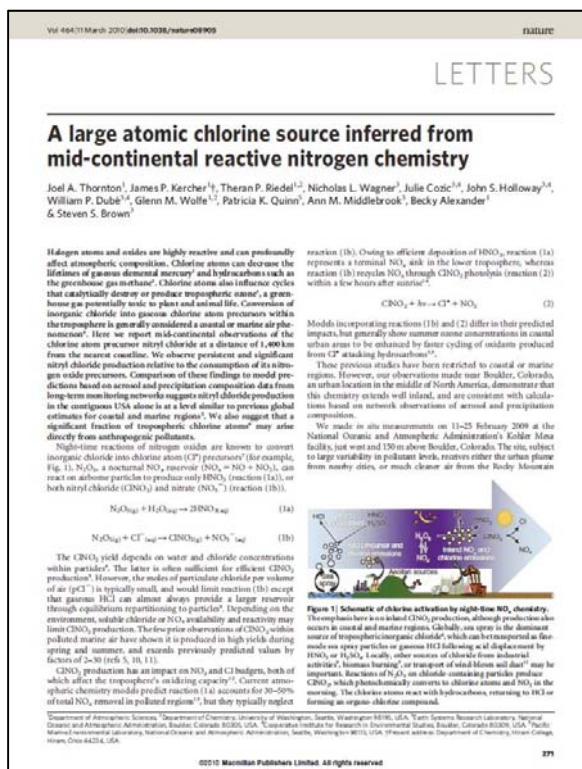
Figure 1-8: The two publications in Nature [6, 7] that are resulting from the development work published in this thesis.

2. Overview of airborne CaRDS instruments

The findings in the five publications selected for this thesis were crucially dependent on the two CaRDS instruments abbreviated as "ARNOLD" (*Atmospheric Ring-down Nitrogen Oxide Laser Detector*) and "NOxCaRD" (*Nitrogen Oxides by Cavity Ring Down*). These acronyms will be used throughout this thesis to refer to the two instruments. The majority of my work went into the design and development of both these devices. This section gives a brief overview of their development and evolution of features between ~2003 and 2017.

2.1 Instrument ARNOLD

The ARNOLD instrument was the first CaRDS instrument to be successfully deployed on an airborne platform. The first deployment was on the NOAA P-3 Hurricane Hunter airplane in 2004 (Figure 2-1 and Figure 2-2) which is described in the selected publication A (Chapter 3). It has been deployed in multiple field missions after that, both airborne and ground-based. Data from ARNOLD also provided the basis for the selected publications B (Chapter 4) and D (Chapter 6).

Figure 2-1: The NOAA P-3 Hurricane Hunter.

The design of ARNOLD was based on existing laboratory setups, and the optical components of the instrument were similar to an older ground-based, two channel NO_3 and N_2O_5 cavity ring down instrument, described in [8]. Because of this heritage, some features of the old instrument still remained after over a decade, such as an optical breadboard forming the base for the instrument.

ARNOLD was continuously improved, and the current version of ARNOLD with 6 channels (Figure 2-3) utilizes almost all of the improvements that are described in this thesis. Presently ARNOLD has a welded steel instrument rack, automated filter changer, low loss inlet, isothermic pressure reducer,

and an improved purge design. An upgraded version which also uses a cage design and nudged/clamped mirror mounts is currently under construction (illustrated in Figure 2-5). The next version of the ARNOLD instrument will also be significantly smaller and occupy only a single bay rack instead of a double bay rack (Figure 2-4). Features of the very first version and the latest version of ARNOLD (under construction) are compared in **Error! Reference source not found.**. An intermediate version of the new ARNOLD with the new optical cage system but the old instrument rack and data acquisition system is shown in section 8.4, where the cage system design in discussed in detail.

Table 2-1 : Comparison of features of the first and latest design of the ARNOLD instrument.

Feature	First version	Latest version (currently under construction)
First deployment	2004	2018
# of channels	2 channels	6 channels (2 × 662 nm, 4 × 405 nm)
Laser(s)	532 nm pumped dye laser used to create red light at 662 nm	One blue 405 nm diode laser and one red 662 nm diode laser
Species measured	NO_3, N_2O_5	NO_3, N_2O_5, NO, NO_2, O_3, NO_y
Volume	Double bay, 1100 mm × 525 mm × 880 mm	Single bay, 530 mm × 840 mm × 1200
Mass	135 kg	< 100 kg
Power consumption	700 W	800 W
Welded steel rack	Yes	Yes
Automated filter changer	Yes	Yes
Low loss inlet design	Yes	Yes
Cage design	No, optical system mounted on aluminum breadboard	Yes
Clamped/nudged mirror mount	No	Yes
Purge system improvements	No	Yes
Detection limit @ 1 second time response	Laboratory: 0.1 pptv for NO_3 0.1 pptv for N_2O_5 On aircraft: 0.2-0.5 pptv for NO_3 0.5-2 pptv for N_2O_5 [1]	Yet to be determined
Accuracy	25 % for NO_3. 20-40 % for N_2O_5, limited mainly by the uncertainty in the inlet transmission. [1]	Yet to be determined
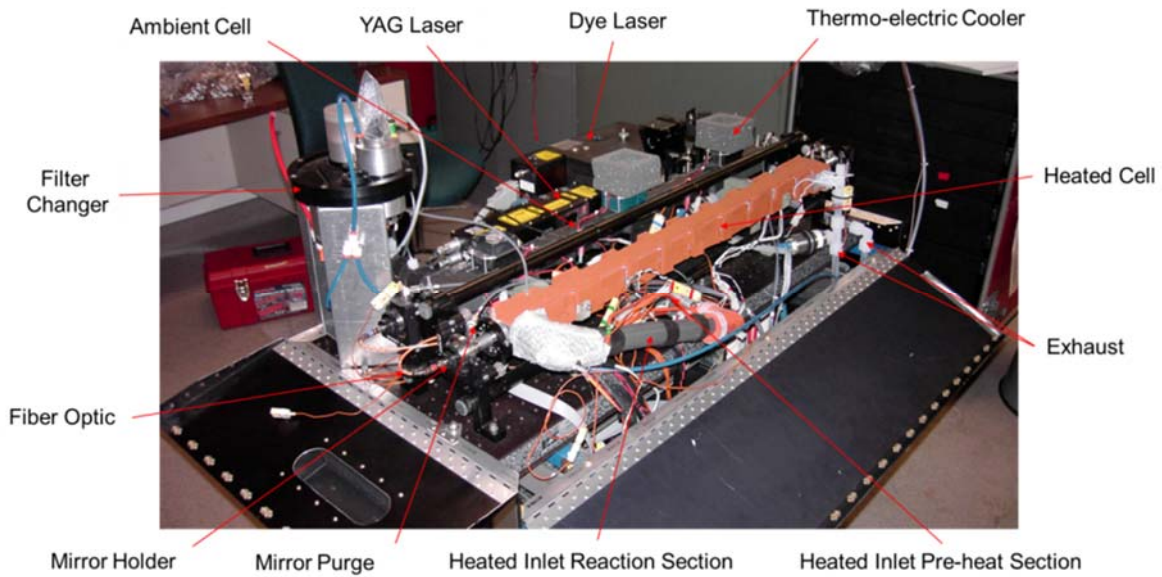
Figure 2-2: The first prototype of the ARNOLD instrument. Detailed description and illustration of the optical system is outlined in Publication A (Chapter 3).

Figure 2-3: The current 6-channel ARNOLD instrument installed in NOAA P-3 research aircraft. Results from the corresponding campaign are outlined in Publication D (Chapter 6).

Cage mounted optics

Single bay, welded
steel rack
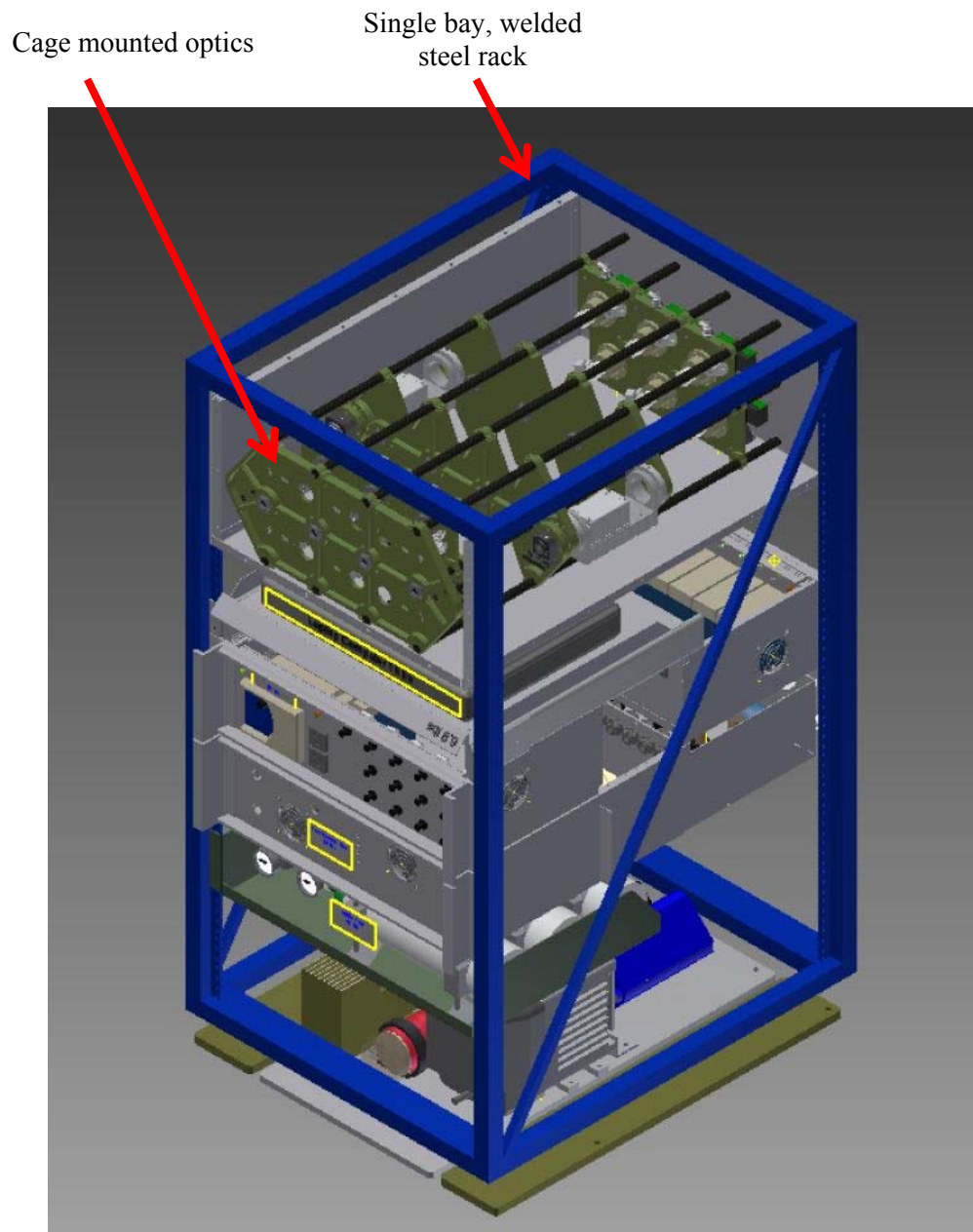
Figure 2-4: Rendering of the next version of ARNOLD, which is currently under construction.
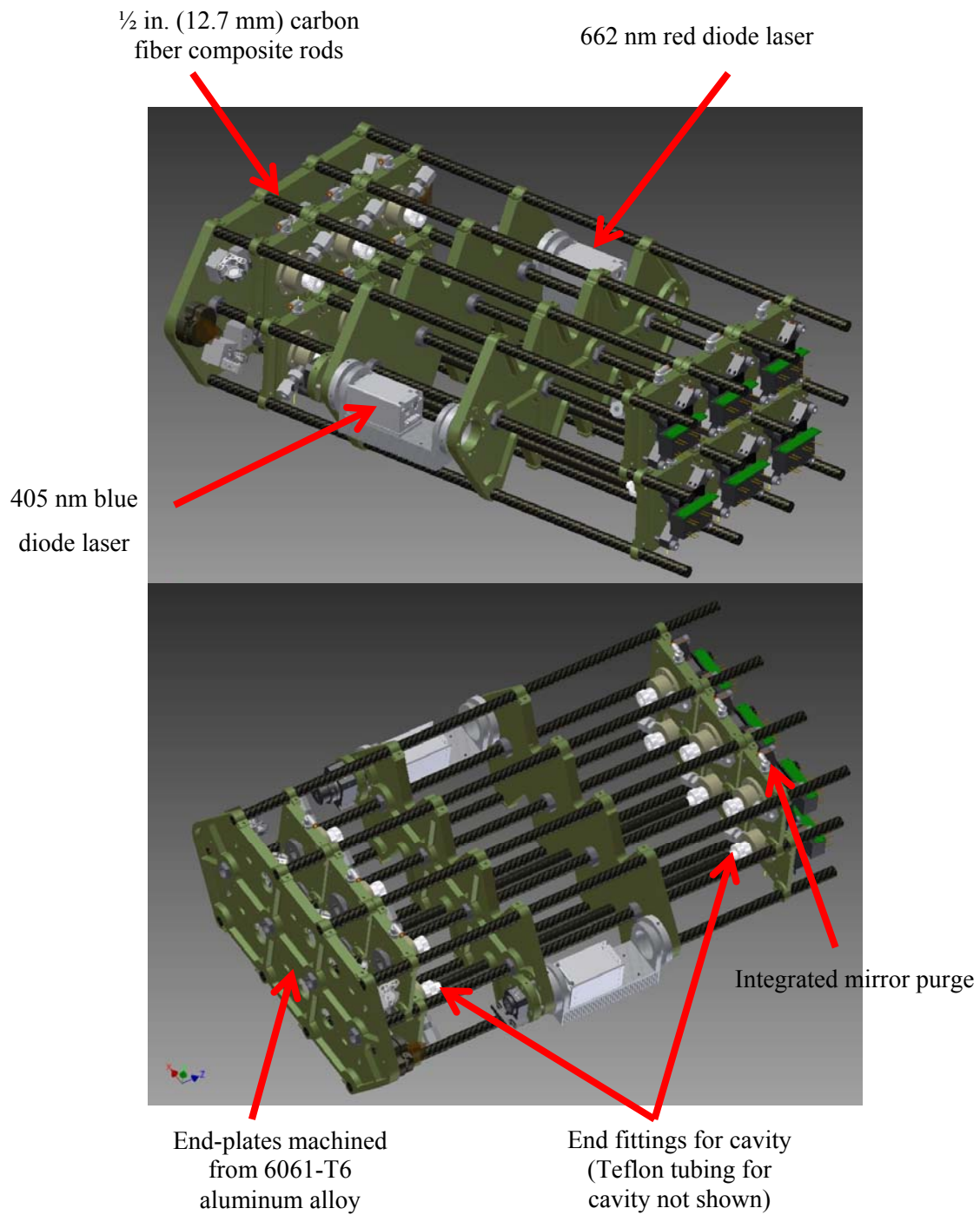
2.2 Instrument NOxCaRD

NOxCaRD is a compact CaRDS instrument suitable for both airborne and ground based platforms and was first deployed in 2009. It originally had two channels for the detection of NO_2 and NO. The current version has four channels for the additional detection of O_3 and NO_y.

NOxCaRD was originally conceived by Dr. Steven Brown at NOAA as a direct NO_2 detector. As opposed to the early versions of ARNOLD, a diode laser at 405 nm is utilized in NOxCaRD. The availability of compact lasers at this wavelength made it possible to build a CaRDS instrument that measured NO_2 concentrations directly in a spectral range with virtually negligible interference of other species such as O_3 or NO_3. This measurement approach is now also integrated in the current version of ARNOLD.

The main specifications of the instrument are listed in Table 2-1. NOxCaRD is more compact than ARNOLD, it requires low power and maintenance, and utilizes almost all of the engineering improvements which are subject of this thesis. NOxCaRD has a welded steel frame, a low loss inlet, an optical cage system (very similar to that of the latest version of ARNOLD, shown in Figure 2-5), and also clamped/nudged mirror mounts.

Figure 2-6a shows the optical cage system, Figure 2-6b shows its first deployment on the NOAA P-3 Hurricane Hunter airplane. NOxCaRD's small footprint is apparent in Figure 2-6c where the instrument is being loaded on to the relatively small NOAA Twin Otter airplane.

To our knowledge, NOxCaRD was the first CaRDS instrument in the world with the optical system mounted in a custom designed cage system. The carbon fiber rods provide stability against mechanical and thermal stress, and enormously increased the ruggedness of the instrument. The design is described in detail in publication E (Chapter 7). That publication, as well as publication C (Chapter 5), uses data from NOxCaRD.

Table 2-1: Specifications for the current version of the NOxCaRD instrument.

First deployment	2009 (2 channels), 2013 (4 channels).
# of channels	4 channels
Laser(s)	One blue 405 nm diode laser
Species measured	NO, NO_2, O_3, NO_y
Volume	Single bay, 1100 mm × 500 mm × 300 mm
Mass	95 kg
Power consumption	300 W (plus ~300 W for NO_y oven)
Welded steel rack	Yes
Automated filter changer	No
Low loss inlet design	No
Cage design	Yes
Clamped/nudged mirror mount	Yes
Purge system improvements	Planned upgrade
Precision	<30 pptv for NO_y @ 1 s time response <4 pptv for NO_y @ 1 min time response [5]
Detection limit	<22 pptv for NO_2 @ 1s time resolution [3]
Accuracy	3 % for NO_2 3 % for O_3 5 % for NO 12 % for NO_y [5] 5 % for NOx [3]

Figure 2-6: a) NOxCaRD instrument with 4 channels. b) NOxCaRD installed in the NOAA P-3 Hurricane Hunter airplane. c) NOxCaRD being loaded onto the NOAA Twin Otter airplane in 2017. Photo by C. Womark.

3. Publication A:

Aircraft instrument for simultaneous, in-situ measurement of NO_3 and N_2O_5 via pulsed cavity ring-down spectroscopy

Authors:

William P. Dubé,[1,2] Steven S. Brown,[1] Hans D. Osthoff,[1,2] Maya R. Nunleya,[3] Steven J. Ciciora,[1] Mark W. Paris,[1] Richard J. McLaughlin,[1] A. R. Ravishankara[1,4]

[1]*Earth System Research Laboratory, NOAA, Boulder, Colorado 80305, USA.*

[2]*Cooperative Institute for Research in the Environmental Sciences, University of Colorado, Boulder, Colorado 80309, USA.*

[3]*NOAA Educational Partnership Program MSI, Boulder, Colorado, USA*

[4]*Department of Chemistry and Biochemistry, University of Colorado, Boulder, Colorado, USA*

Abstract:

This article describes a cavity ring-down spectrometer (CaRDS) specifically designed and constructed for installation on the NOAA WP-3D Orion (P-3) aircraft for sensitive, rapid in-situ detection of NO_3 and N_2O_5. While similar to our previously described CaRDS instrument, this instrument has significant improvements in the signal-to-noise ratio, the time resolution, and in overall size and weight. The instrument utilizes a custom-built, automated filter changer that was designed and constructed to meet the requirement for removal of particulate matter in the airflow while allowing fully autonomous instrument operation. The CaRDS instrument has a laboratory detection sensitivity of 4×10^{-11} cm^{-1} in a 1 s integration time which corresponds to a detection limit of 0.1 pptv of NO_3. The typical detection sensitivities encountered in the field, however, were 0.5 pptv for NO_3 and 1 pptv for N_2O_5. The instrument accuracy is 25 % for NO_3 and 20 – 40 % for N_2O_5, limited mainly by the uncertainty in the inlet transmission. The instrument has been deployed on the P-3 aircraft as part of a

major field campaign in the summer of 2004 and during several ground and tower deployments near Boulder, CO, USA.

3.1 Introduction

The nitrate radical (NO_3) and dinitrogen pentoxide (N_2O_5) are important reactive intermediates in the atmospheric chemistry of nitrogen oxides [9]. They form from the oxidation of NO_2 by O_3 and the further association of NO_2 with NO_3.

$$NO_2 + O_3 \rightarrow NO_3 + O_2 \qquad\qquad (3\text{-}1)$$

$$NO_2 + NO_3 \leftrightarrow N_2O_5 \qquad\qquad (3\text{-}2)$$

Their formation is effectively reversed during the day by the reaction of NO_3 with NO (present in sunlight from NO_2 photolysis) and by efficient NO_3 photolysis (lifetime of ~5 s in direct sunlight) [10]. At night, reaction equation 3-1 can consume a significant fraction (50 %–90 %) of NO_2, particularly if the hydrolysis of N_2O_5 is rapid [11, 12]. Furthermore, NO_3 is a strong oxidant for a variety of hydrocarbons and sulfur compounds [13-15]. Thus, the fate of NO_3 and N_2O_5 is important to the cycling and removal of NO_x and to the oxidation of volatile organic compounds (VOC) in the nighttime atmosphere, and measurements of their concentrations are of substantial interest to atmospheric chemistry.

The majority of the database for atmospheric measurements of NO_3 comes from open path differential optical absorption spectroscopy (DOAS), which was first applied to the detection of NO_3 over 25 years ago [16-18]. These observations have been carried out both passively, using natural light sources (e.g., moonlight and starlight) for column density measurements [19, 20], and actively, using artificial light sources aligned over a multi-kilometer path [21, 22]. Reported detection sensitivities for active DOAS detection of NO_3 range from 0.2 pptv [23] (pptv denotes parts per trillion by volume) to several pptv [24, 25] with integration times on the order of minutes.

Because these techniques rely on the strong visible absorption bands of the nitrate radical, they do not detect N_2O_5 directly, although average N_2O_5 concentrations over the DOAS path can be calculated from simultaneous measurements of NO_3, NO_2, and temperature, as long as the variability in NO_2 and NO_3 is small over the path [26]. Until recently, the only in-situ technique for NO_3 detection was cryogenic collection followed by the electron spin resonance (ESR) spectroscopy [27, 28]. In the last few years, several sensitive, fast time response, real-time in-situ techniques have been developed for NO_3 detection. One of the principal advantages of these instruments is the capability to detect N_2O_5 directly via its thermal decomposition to NO_3 in a heated inlet. One recent approach has been cavity ring-down spectroscopy (CaRDS), a high sensitivity direct absorption technique. This method relies on the strong visible absorption bands of NO_3, similar to DOAS. Our group [8, 29], Simpson and coworkers

[30-32], and Ball et al. [33] have all reported CaRDS based instruments, with detection sensitivities for NO_3 or for the sum of NO_3 + N_2O_5 of 0.3–2 pptv with integration times from seconds to minutes. Recently Ball and coworkers [34, 35] have also demonstrated laboratory detection of NO_3 by a related technique using a broadband light source. Laser induced fluorescence (LIF) has been recently applied to NO_3 and N_2O_5 detection, as demonstrated by both Wood et al. [36, 37] and Matsumoto et al. [38] albeit with somewhat larger detection limits and integration times (4–80 pptv in 10–1 min) in the instruments reported to date. Finally, Slusher et al. [39] have applied chemical ionization mass spectrometry (CIMS) to detect the sum of NO_3 and N_2O_5 by their reactions with I^-, both of which yield NO_3^-.

This article describes a CaRDS instrument designed and tested for aircraft deployment. Included in the description are improvements in the sensitivity and the inlet design for NO_3 and N_2O_5 sampling implemented since the previous description of our ground and ship based instrument [8]. Also included are the data from a test flight on the NOAA P-3 aircraft in Tampa, FL in March of 2004, the first example of NO_3 or N_2O_5 measurements from an aircraft. To date, the instrument has been deployed at ground and tower sites near the NOAA laboratories in Boulder, Colorado, and on the NOAA P-3 aircraft during the New England Air Quality Study in Portsmouth, New Hampshire (http://www.al.noaa.gov/2004/) for six weeks in July and August, 2004.

3.2 Instrument Description

Cavity ring-down spectroscopy (CaRDS) is a high sensitivity, direct absorption technique based on the measurement of the time constant for single exponential decay of light intensity from an optical cavity [40, 41]. Measurement of this time constant in the presence (τ) and absence (τ_0) of an absorbing species gives an absolute measurement of the absorbance (α, cm^{-1}, also referred to as the absorption coefficient or the extinction), and, therefore, the absorber's number density [(A), molecules cm^{-3}] as long as the absorption cross-section (σ, cm^2 $molecule^{-1}$) and the transmission efficiency (T_E) for the target compound through the inlet system are known:

$$\alpha = \frac{1}{c}\left(\frac{1}{\tau} - \frac{1}{\tau_0}\right) \qquad (3\text{-}3a)$$

$$(A) = \alpha\frac{R_L}{\sigma T_E} \qquad (3\text{-}3b)$$

Here c is the speed of light, and R_L is the ratio of the cavity length to the length over which the sample is present in the cavity, as described below. There are now several varieties of cavity ring-down spectroscopy and related techniques such as integrated cavity output spectroscopy (ICOS), using both pulsed and cw laser light sources and broadband sources [42-44]. Pulsed CaRDS takes advantage of the passive coupling that occurs between nanosecond time scale pulsed lasers and high finesse optical

cavities as a result of the overlap of a relatively wide-bandwidth laser source (e.g., Nd:YAG (YAG denotes yttrium aluminum garnet) laser pumped dye lasers, $\Delta v \sim 3$ GHz) with multiple cavity resonances (free spectral range ~ 0.2 GHz) and the broadening of cavity resonances in the presence of laser pulses comparable to the cavity round trip time [45]. The passive coupling allows optimization of the instrument's sensitivity through the use of mirrors of arbitrarily high reflectivity. The disadvantages of pulsed CaRDS include the larger size and power requirements of pulsed laser systems in comparison to cw diode lasers, and the laser bandwidth effects [45, 46] that makes the detection of compounds on discrete mid or near infrared rovibrational features more difficult. Therefore, for atmospheric applications, pulsed CaRDS is most applicable to broad band absorption and/or scattering measurements, such as the quantification of aerosol extinction [47] or the detection of visible absorbers with wide bandwidths such as NO_3 or NO_2 [48].

3.2.1 Optics, electronics, and vibration isolation

Figure 3-1 shows the layout of the optical and inlet system for the aircraft NO_3 and N_2O_5 CaRDS instrument. Optically, the instrument is similar to the previously described ground-based, two channel NO_3 and N_2O_5 instrument [8]. The light source is a small footprint, pulsed, Nd:YAG laser (Big Sky Laser, ultra-CFR) pumped dye laser (Dakota Technologies, Northern Lights) that produces ~ 1 mJ, 6 ns pulses at a repetition rate of 33 Hz. The dye laser wavelength is tuned to a point on the broad maximum of the NO_3 absorption spectrum near 662 nm [49] that is not resonant with any of the weak, discrete water vapor absorptions in this region. Since the 662 nm NO_3 absorption band varies only slowly with wavelength (bandwidth = 80 cm^{-1}), it is possible to choose an arbitrary point near the peak of the NO_3 absorption band that minimizes the optical absorption due to water vapor. Periodic scans of the water vapor absorption spectrum in ambient air between 661–663 nm provided a convenient means of calibrating the dye laser wavelength, which was stable to ± 0.02 nm. The breadth of the NO_3 absorption band relative to the linewidth of the dye laser (0.5 cm^{-1}) ensures that there are no laser linewidth artifacts in the exponential ring-down traces [45]. The beam from the dye laser propagates through an optical isolator and a series of irises and lenses (50–100 cm focal length) to minimize the spot size at the end of the optical cavities. A 50/50 beamsplitter separates the laser output into two beams of approximately equal intensity, each of which is aligned on the axis of two separate optical cavities.

Each cavity is a stable resonator of near-confocal geometry, consisting of two 1 in. (25.4 mm) diameter, 1 m radius of curvature dielectric coated, high reflectivity mirrors, separated by 93 cm. Each mirror is mounted in a purge volume separated from the air sample by an orifice ($\sim 1/4$ in. (6.4 mm) diameter) and purged with dry zero air to maintain mirror cleanliness. The purge volumes have proven effective in preventing degradation in mirror reflectivity, which has been observed to remain constant or improve slightly, even during extended field deployments of six weeks or longer. The purge volumes are mounted in commercial, 2 in. (50.8 mm) optical mounts. Light transmitted through the rear cavity

mirror is collected using optical fiber and imaged on to a small, red-sensitive photomultiplier tube through a bandpass filter centered at 660 nm to reject the stray light at other wavelengths. Ring-down traces are digitized on a 16 bit oscilloscope card mounted in an external peripheral component interconnect (PCI) bus and analyzed on a laptop computer. Ring-down time constants are measured at 1 s time resolution from a linear fit to the natural logarithm of a co-added trace of 33 individual decay profiles. Figure 3-2 shows an example ring-down trace and exponential fit at 662 nm. The time constant in 830 mbar of laboratory air (in Boulder) is 183 μs, limited mainly by mirror reflectivity rather than Rayleigh scattering [50]. The mirror reflectivity, corrected for Rayleigh losses, is 99.9987 % (13 ppm total loss, where ppm denotes parts per million). The effective path length, shown on the top axis, is 55 km for one e-folding time and several hundred kilometers over the five lifetime range over which each decay is typically fitted.
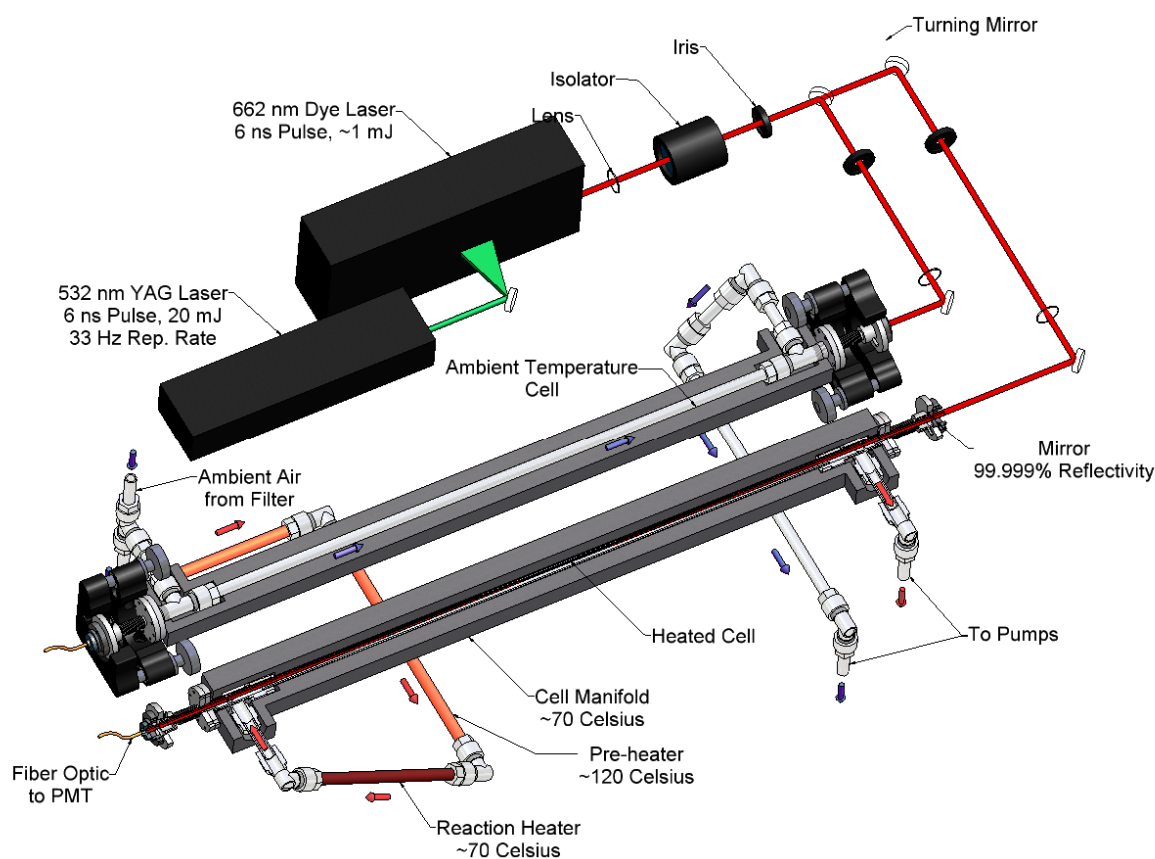
Figure 3-1: Layout of the optical and inlet systems.

The optical system is mounted on an aluminum breadboard attached to a custom-made steel frame that houses the computer, electronics, photomultiplier tubes, flow and temperature controllers, laser power supply, dye laser circulators, gas cylinders (NO, zero air, and He), and pumps. Figure 3-3(a) shows the arrangement and its mount inside the cabin of the P-3. The overall size and weight of the

instrument are 110 cm × 52.5 cm × 88 cm and 135 kg, respectively. Although this instrument is still relatively large, it is considerably smaller than our prototype instrument and it meets the requirements for installation on the P-3. Further size and weight reductions are anticipated in the future. Vibrations are always a concern on a mobile platform, particularly in a propeller-driven aircraft. Previous experience with field deployments of the pulsed CaRDS system on a ship [51] has shown, however, that it is rather robust with respect to vibration. Thus, the approach to vibration isolation was a bit different than typical, i.e. we chose not to vibration isolate the optical table from the frame and the support systems. Instead, the optical table was purposely coupled to the frame and the non-vibrating support equipment (such as the computer, gas bottles, flow controllers, etc.) This much larger mass was vibration isolated from the aircraft and the vibrating support equipment. This additional mass enhanced the vibration isolation between the optical table and the aircraft. Vibrations that propagated by the wire-rope vibration isolators was attenuated, to a degree, by the purposefully supple support frame. Moreover, the instruments and support equipment helped damping the leakage vibration before it reached the optical table. This approach proved quite successful as there were no vibration-related problems during the deployment of the instrument. The instrument's sensitivity, as measured by the precision of the ringdown time constant, was identical to that when the aircraft was on the ground without engines running and in flight.
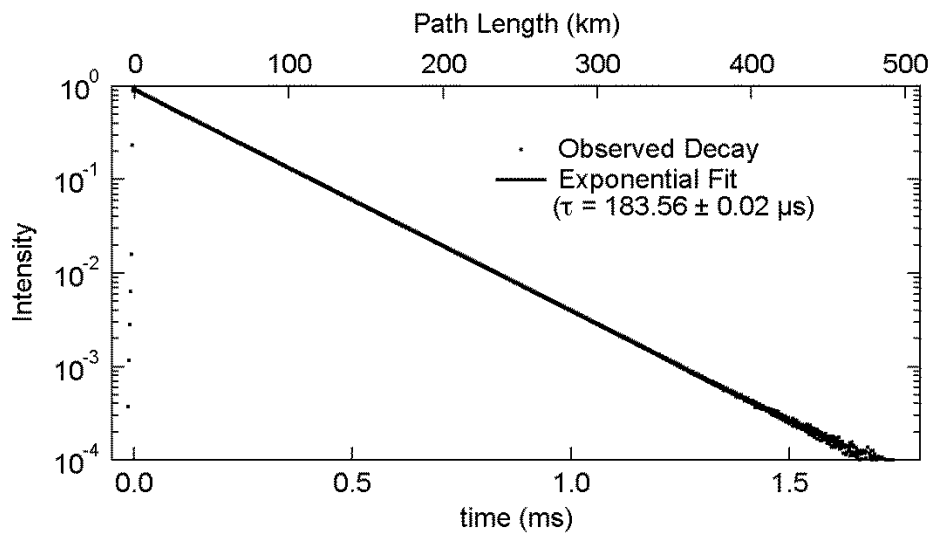
Figure 3-2: Ring-down trace with single exponential fit.
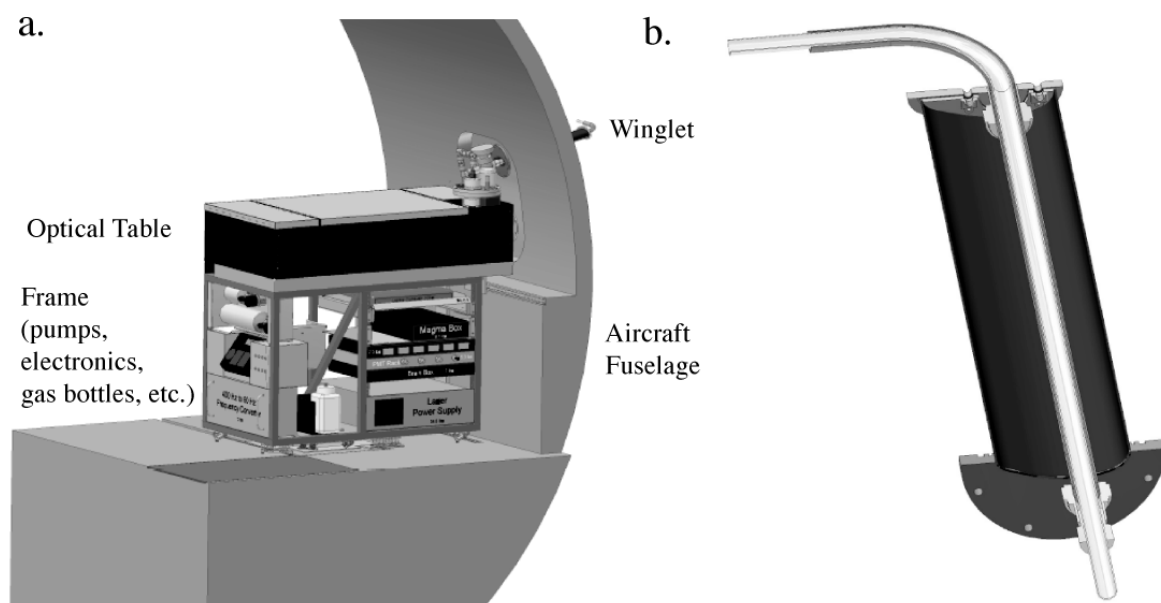
Figure 3-3: (a) Schematic of the instrument frame and optical table mounted in the P-3 fuselage. (b) Inlet fast flow system and winglet.

3.2.2 Inlet system

The inlet system consists of three parts: an initial, fast flow system that brings the air sample from outside the boundary layer of the aircraft into the cabin; a filter that removes ambient aerosol from the sampled air flow; and a slower flow system that brings the air sample on to the axes of the two ring-down cells. Aside from the filter housings, all components of the cells and all inlet plumbing are constructed of commercial 1/2 in. (12.7 mm) outer diameter (OD) PFA fittings and tubing.

The sampling position of the NO_3 and N_2O_5 instrument (on its first deployment) on the NOAA P-3 is somewhat rearward in the aircraft, where the estimated boundary layer thickness is ~30 cm. To ensure sampling of air outside this boundary layer, the fast flow portion of the inlet was housed in a winglet [Figure 3-3(b)] that protruded 46 cm from the outer fuselage skin. The sampling tube sheath is a thin-wall copper pipe with an internal diameter (ID) slightly larger than 1/2 in. (12.7 mm). This copper sheath protects and guides an inner liner made of 1/2 in. (12.7 mm) PFA tubing. The inner liner of the sampling inlet can be easily removed and replaced from inside the aircraft cabin. The flow rate through the fast flow system is 40–50 liter per minute (LPM), which is the sum of the full capacity of an oil-free diaphragm pump, measured at 25 LPM, and the controlled flows in the slow flow system, which totaled approximately 20 LPM. The flow rate in this section of the inlet is not critical so long as it is fast enough to suppress wall loss of NO_3 and N_2O_5 (see below). The slow flow system samples air from the fast flow manifold at a branch point just inside the aircraft fuselage. The air sample is filtered in the slow flow part of the inlet, immediately downstream of the branch point with the fast flow system. Filters are housed in and changed by an automated device, described in the next section. As shown in

Figure 3-1, the slow flow system branches into two air samples immediately below the filter, each of which is controlled with electronic mass flow controllers at the exhaust and a second diaphragm pump common to both flows. The pressure in the ring-down cells is not controlled and varies with the ambient pressure on the exterior of the aircraft. To maintain constant residence time within the slow flow systems, the data acquisition software sets the two flow rates to a constant volumetric flow as the cell pressure changes with aircraft altitude. The flow rate on the ambient temperature side (NO_3 detection) is 16 LPM volumetric, while on the heated side ($N_2O_5+NO_3$ detection), it is 8 LPM. These flow rates allow adequate residence time for NO titration of NO_3 to zero the absorption signal and thermal conversion of N_2O_5 to NO_3 while minimizing wall loss.

Insulation along the common section of the slow flow system serves to minimize the temperature rise between the (typically) colder air, sampled outside of the aircraft and the cabin temperature. This is important to minimize shifts in the NO_3– N_2O_5 equilibrium, which can lead to an artifact in the NO_3 signal when the ratio of N_2O_5 to NO_3 is large [52]. The temperature shift is measured and the required correction to the NO_3 signal modelled accordingly. During the NEAQS 2004 deployment, this correction was generally less than 2 % but occasionally as large as 15 % in large, cold NO_2 plumes. As shown in Figure 3-1, an aluminum manifold with Peltier elements maintains a constant temperature in the ambient channel along the ring-down axis, including the elbow fittings at the inlet and exhaust. The inside of the manifold is machined to the shape of the tubing and the fittings at the ends, and is split into a top and bottom half that are bolted together. This design allows periodic removal and exchange of the Teflon tubing to help suppress wall losses due to aging of the tubing between flights. It also maintains the alignment of the PFA tubing on the center of the optical detection axis. The temperature of the manifold is actively set by the data acquisition software to match that of the air flow immediately upstream of the manifold. This active temperature control is necessary to suppress turbulent flow noise arising from temperature gradients within the sampled air flow. The air sample entering the heated channel passes through two different heating stages of 45 cm each. The first is a preconverter stage that rapidly heats the incoming airflow and induces rapid thermal decomposition of N_2O_5. The preconverter stage is controlled to remain at a temperature of 120°C using a copper sheath wrapped in heat tape and silicone rubber insulation. A second, similarly constructed heating stage with a set temperature of 70 or 75°C allows the air sample to cool prior to entering the axis of the ring-down cell. Here, a single aluminum manifold, similar to that on the ambient channel but controlled at 70 or 75°C, maintains a constant temperature in the flow along the entire optical detection region.

In spite of attempts to maintain constant temperature throughout the flow along the optical detection axis, considerable noise in the heated channel was found. The noise is the result, presumably, of the temperature gradient between the ambient temperature purge volumes and the heated air sample. This gradient may induce some variable thermal lensing at the interface that slightly alters the alignment in the optical cavity. Introduction of a mixture of 20 % He in zero air to the purge volumes to

approximately match the refractive index of the heated air sample to the cooler purge volume partially offsets this noise (~2× reduction). Similar effects have been observed at surface pressure in the ambient channel when the air sample was much colder than the purge volumes. In summertime aircraft sampling, thermally induced noise was not important on the ambient side since the coldest air was sampled at the highest altitude, and the effect was smaller at lower pressures.

3.2.3   Automated filter changer

The largest component to the visible extinction signal in ambient air is typically due to scattering and absorption by aerosol. Not only is the aerosol extinction signal large, but it is also gives rise to a statistically noisy CaRDS signal due to small numbers of large, optically active particles in the detection volume [47]. Consequently, high sensitivity gas-phase pulsed CaRDS measurements require filtering of the aerosol. This requirement poses a significant challenge for the sampling of reactive trace gases and leads to by far the largest single source of uncertainty in sampling NO_3 and N_2O_5 with this instrument. To minimize loss of NO_3 and N_2O_5, 47 mm diameter, 2 μm pore size, 25 μm thick poly tetrafluoroethylene (PTFE) filters (Pall-Gelman) are used. Because of aging effects in the filters (see below), the filters are changed typically at 1 h intervals, although in some cases the changes occur more frequently. Thus, for the instrument to be fully autonomous, an automated filter changer had to be devised and constructed. It is shown in Figure 3-4.

The filter changer was designed with minimal gas contact surface in the flow path to minimize wall losses. Two funnel-like PFA pistons are sealed to either side of the PTFE filter. The pistons are withdrawn by applying a vacuum to the back side of the pistons to allow the filter to be exchanged. They are then moved back into place and held firmly against the filter by applying compressed air to the back sides of the pistons. A rotating disk transports filters from a stack contained in the fresh filter reservoir. The fresh filter is then moved into place between the two pistons by the rotating disk. Simultaneously, the used filter is moved away from between the pistons and transported to the used filter reservoir.

The interior of the device is sealed from the exterior to allow the filter changer to operate in the pressurized cabin of the aircraft. The interior of the filter changer case is vented to the aircraft exterior (ambient) pressure. Thus, when the pistons retract to change a filter, there is no significant air movement that might buffet the filter or contaminate the inlet. Also, cabin pressure integrity is maintained during a filter change. Since the pistons are actuated pneumatically, changes in the ambient pressure on the piston faces alter the net force acting on the pistons. Springs are needed to assist withdrawal of the pistons at high altitude because the pressure on the piston faces is not adequate to reliably move the pistons. The springs are chosen carefully so as to provide adequate force to withdraw the pistons, but not so much force that they prevent the pistons from sealing reliably to the filter.
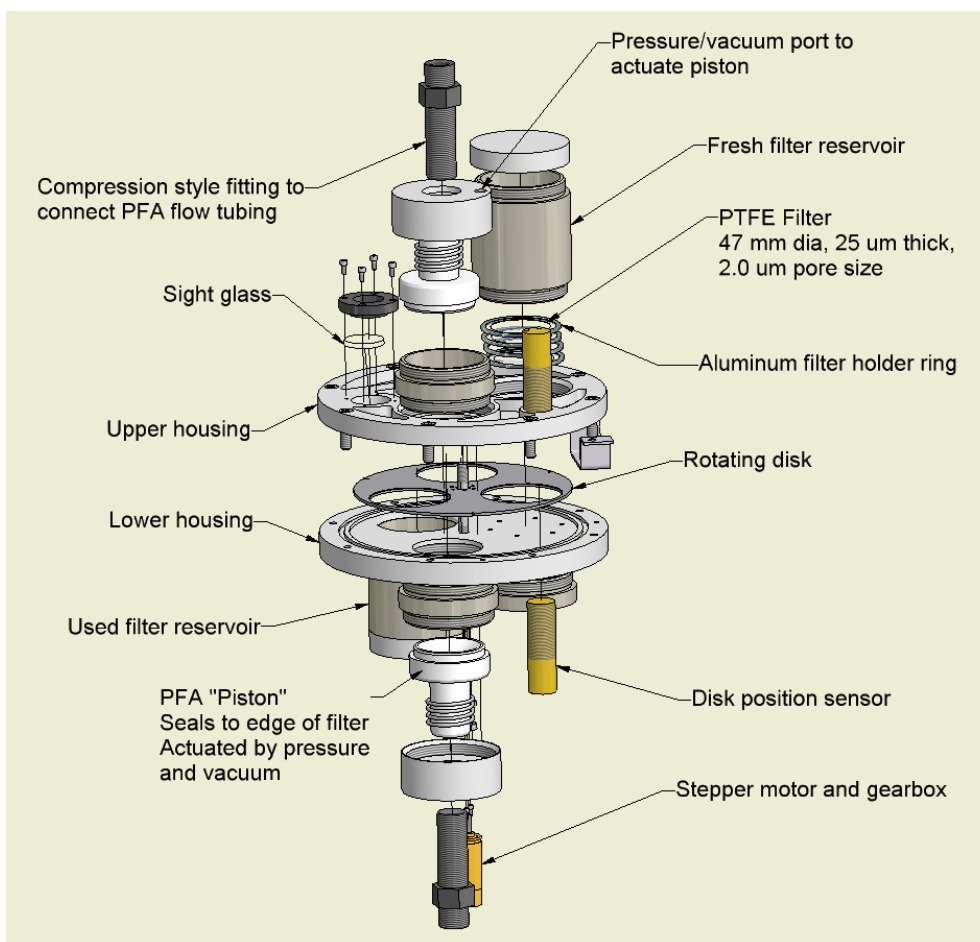
Figure 3-4: Schematic of the sealed, automated filter changer.

3.2.4 Zero acquisition

The instrument's zero absorption is determined by addition of a small quantity of NO to the air sample, as described previously [8]. Nitric oxide reacts rapidly with NO_3 to form NO_2 [53], whose absorption cross-section at 662 nm is nearly four orders of magnitude smaller than that of NO_3 [54].

$$NO + NO_3 \rightarrow 2NO_2 \tag{3-4}$$

$$k(298 \text{ K}) = 2.6 \times 10^{-11} \text{ cm}^3 \text{ molecule}^{-1} \text{ s}^{-1}$$

Addition of ~30 ppbv (parts per billion by volume) of NO just above the filter is sufficient to titrate NO_3 to >99 % completion prior to entry into the ambient channel (~0.25 s). There is a brief (0.2 s) purge of the NO addition line with zero air subsequent to the zero acquisition to prevent leakage of residual NO from this line into the sample stream during signal acquisition. Contamination of NO_2 in the NO mixture is small (<10^{-3} of total NO_x present as NO_2) and is undetectable as an absorption signal in either channel. Reaction of NO with ambient O_3 to produce NO_2 is too slow to produce a measurable signal on the ambient channel. However, on the heated channel, it does generate a small negative offset (equivalent to ≤0.3 pptv NO_3) because of the longer residence time and the increase in the rate

coefficient for this reaction with temperature. This offset is modelled from the residence time in the heated inlet and the measured concentration of ambient O_3 and then subtracted from the data.

The combination of 662 nm optical detection and titration with NO provides a highly specific detection scheme for NO_3 and in the case of thermal conversion to NO_3, N_2O_5 as well [8]. Prior to the 2004 deployments of the NO_3 CaRDS instruments, no evidence for any interfering absorber had been observed. During the New England Air Quality Study (NEAQS), we observed a small interference in the heated channel that correlated with the observed structure in peroxyacetylnitrate (PAN). This interference was typically 1 pptv, with maximum values of 2–4 pptv. It does not affect the interpretation of nocturnal results from this instrument, although it is of approximately the same order as N_2O_5 observed during the day. Its analysis has been described in a recent publication [55].

The NO titration allows periodic zero determination (every 0.5–5 min) without the need to scan the wavelength of the dye laser away from the peak of the NO_3 absorption spectrum. Variability in the background absorption of NO_2 and O_3, and to a much lesser extent water vapor, can produce small, spurious structure in the 662 nm absorption signal. During surface based sampling, the interpolation of the baseline variation between subsequent zero measurements is sufficient to track these changes; however, large instantaneous changes in O_3 and NO_2 are commonplace during aircraft sampling. Each 1 ppbv of O_3 or NO_2 produces a baseline shift equivalent to 0.1 and 0.15 pptv of NO_3, respectively. We corrected the instrument baseline for the measured variation in the concentrations of NO_2 and O_3 prior to analysis of the raw signals; the interference from water vapor was exceedingly small. By far the largest changes in the instrument baseline are due to Rayleigh scattering as the inlet pressure changed with aircraft altitude. Fortunately, these changes tended to be smooth and continuous, so that interpolation of the baseline between successive zero acquisitions produced no large, spurious signal offsets.

3.2.5   Sampling efficiency and measurement accuracy

There are a number of factors that govern the accuracy of the NO_3 and N_2O_5 measurements, but the most important is the inlet transmission efficiency, which is denoted by T_E in equation 3-3b. Therefore, this section mainly outlines improvements to the inlet system for NO_3 and N_2O_5 detection since our previously described prototype instrument [8, 51] had an inlet constructed of 1 in. (25.4 mm) diameter glass cells coated with halocarbon wax. The two channel 662 nm absorption measurement capability provides a method of accurately determining the wall loss rates for NO_3 in different types of inlet tubing and the transmission efficiency of various inlet components, (such as the filter and its housing) from a measurement of the same NO_3 and/or N_2O_5 sample flowed sequentially through the two ring-down cells. Synthetic NO_3 or N_2O_5 samples are prepared from a flow of zero air over crystalline N_2O_5 (synthesized by a standard method [56]) in a trap at $-78°C$. The sample is diluted twice

in zero air and heated, when desired, to convert N_2O_5 to NO_3, giving a sample with a concentration range of 10^9–10^{10} molecules cm^{-3} or roughly 40–400 pptv at atmospheric pressure.

(A) NO_3 accuracy

Figure 3-5 shows a measurement of the wall loss rate for NO_3 measured in 3/8 in. (9.5 mm) ID PFA tubing. The transmission between the two channels was fitted to an exponential decay as a function of the residence time, calculated as the plug flow time between the midpoints of the two ring-down cells. Plug flow is appropriate for a system in which the calculated rate constant for diffusion of NO_3 to the wall of the cylindrical tubing [57, 58] (k_d ~2 s^{-1}) is an order of magnitude faster than the observed NO_3 loss rate coefficient, and in which the 90° bends in the path between the two ring-down cells tend to mix the gas flow at the center with that at the walls. Repeated measurements gave a first order loss rate coefficient and associated uncertainty of k_{loss} = 0.2 ± 0.05 s^{-1}. When the instrument is deployed in the aircraft, the calculated residence time from the tip of the inlet to the midpoint of the ambient ring-down cell is ≤0.5 s (≤0.1 s in the fast flow section and ~0.4 s in the slow flow leading to the ambient side), giving a total loss of (10 ± 3) % for NO_3 to the walls of the tubing.
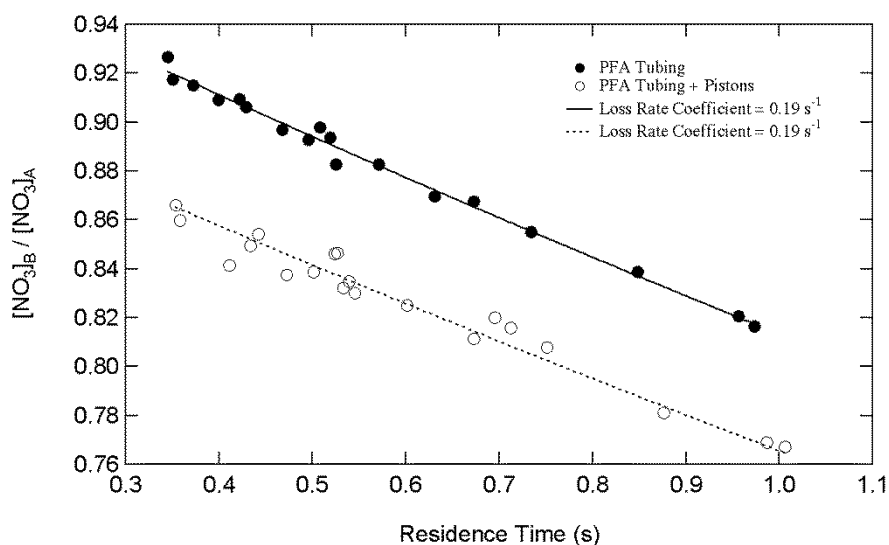
Figure 3-5: Measurement of the wall loss rate (upper trace, solid points) through 1/2 in. (12.7 mm) PFA tubing from exponential fit to the ratio of the NO_3 concentration measured in two channels against the mean residence time between them. Repeated measurements gave a net loss rate of 0.20 ± 0.05 s^{-1}. The lower trace (open circles) shows the additional loss due to insertion of the machined, PFA pistons that hold the filter in place. The loss rate is similar in this trace, but there is a constant offset indicating a point source loss for NO_3 in the flow system.

The lower trace in Figure 3-5 shows the measurement of the transmission through the tubing plus the custom-made pistons that hold the membrane filter in place (there is no filter present for the data in the figure). The pistons have a machined PFA surface rather than the molded surface present in the commercial PFA fittings and tubing in the rest of the inlet system. Although the loss rate coefficient

is similar with the pistons in place, the intercept at zero residence time is smaller, indicating that the pistons act as a point source loss for NO_3. Several measurements using different sets of pistons gave a net loss of (10 ± 5) %. Of the materials that were tested (including PFA, PTFE, Kel-f, etc.), machined PFA had the lowest surface losses, although the machining process clearly degrades the NO_3 transmission efficiency compared to commercial, molded components.

The other important loss for NO_3 is the Teflon membrane filters themselves. This loss has been measured by repeated insertion and removal of a filter into a flow of NO_3 in zero air and is (7 ± 2) % for clean filters. (Loss of N_2O_5 on clean filters is negligible.) Our previous measurement showed a decrease in the NO_3 transmission efficiency through the filters of up to 10 % per hour due to filter aging while sampling in ambient air. Thus, filter aging represents a potentially large uncertainty for the NO_3 concentration measurement because the aging rate may vary with the composition of the air mass. There are several diagnostics to check for the effects of filter aging while in the field, including discontinuities upon change of a filter in the measured concentrations of NO_3 and N_2O_5: the steady state lifetimes of these compounds (i.e. their concentrations divided by their production rate from the reaction of NO_2 with O_3) and the ratio of N_2O_5 to NO_3. For the majority (>90 %) of all filter changes on the aircraft, there was no evidence for filter aging effects, although in a few cases there were clear discontinuities across filter changes. Data showing such discontinuities have been either corrected for the estimated, time-dependent change in the transmission efficiency or else discarded from the data set. Based on the previously reported aging rate for the NO_3 transmission efficiency of 10 % per hour and the 7 % transmission efficiency for clean filters, the NO_3 filter transmission efficiency used for reduction of field data is (88 ± 7) %. The net transmission efficiency for NO_3 is the product of that for the inlet tubing, the filter housings and the filter, or (71 ± 13) %. The nearly 30 % loss of NO_3 radicals through the current inlet system illustrates the difficulties of sampling this reactive compound.

The inlet transmission efficiency was also verified by a second method, i.e. conversion of NO_3 to NO_2 via reaction equation 3-4, followed by pulsed CaRDS measurement of the resulting NO_2 concentration at 532 nm [48]. This method is currently being developed into an in-field calibration for NO_3 and N_2O_5. The net transmission measured from conversion to NO_2 was (71 ± 12) % and was constant for an inlet that had sampled ambient air over the course of 8 h. The error estimate on the NO_2 conversion test comes from the uncertainties in the cross-sections for NO_2 at 532 nm (6 %) [48], the NO_3 absorption cross-section at 662 nm (10 %) [49], and experimental scatter (3 %). Since the error in the two measurements of the transmission efficiency are comparable, the net transmission efficiency was taken as (70 ± 13) %. The resulting uncertainty due to inlet transmission in the measured NO_3 concentrations in equation 3-3 is 20 %.

The remaining uncertainty in the NO_3 measurement comes from the cross-section for absorption at 662 nm and the ratio of the length over which the air sample is present to the total length

of the optical cavity. We have used values for the temperature dependent cross-sections from Yokelson et al. [49].

$$\sigma(NO_3) = (4.56 - 0.00787 \times T[K]) \times 10^{-17} \text{ cm}^2 \text{ molecule}^{-1} \tag{3-5}$$

The stated uncertainty in the peak cross-section for NO_3 is 10 %. The ratio of distance between the mirrors to the length over which the absorber is present in the cavity, or R_L in equation 3-3b is defined by the lengths of the purge and sample volumes shown in Figure 3-1. This value was measured both from the physical dimensions of the cells and from the measured visible absorption in the Chappius bands due to known quantities of O_3, as described previously [8, 59]. The value for R_L determined from the physical cell dimensions was 1.22, while that determined from O_3 absorption was 1.16. The 5 % difference was presumably due to diffusion of O_3 into the orifices separating the purge and sample volumes. (Independent tests determined that it was not due to a limitation in the accuracy of the ring-down absorption measurement.) For NO_3 detection, the R_L value was assumed that the value of 1.22 is correct, since the more reactive NO_3 will be lost to the walls upon diffusion outside of the sample volume. However, an uncertainty of 5 % in this quantity was also assumed. Combining the cross-section uncertainty (10 %), the uncertainty in R_L (5 %) and the transmission efficiency (20 %) yields a net uncertainty in NO_3 of 25 %. The accuracy of the measured ambient NO_3 concentrations is dominated by the uncertainty in the inlet transmission efficiency.
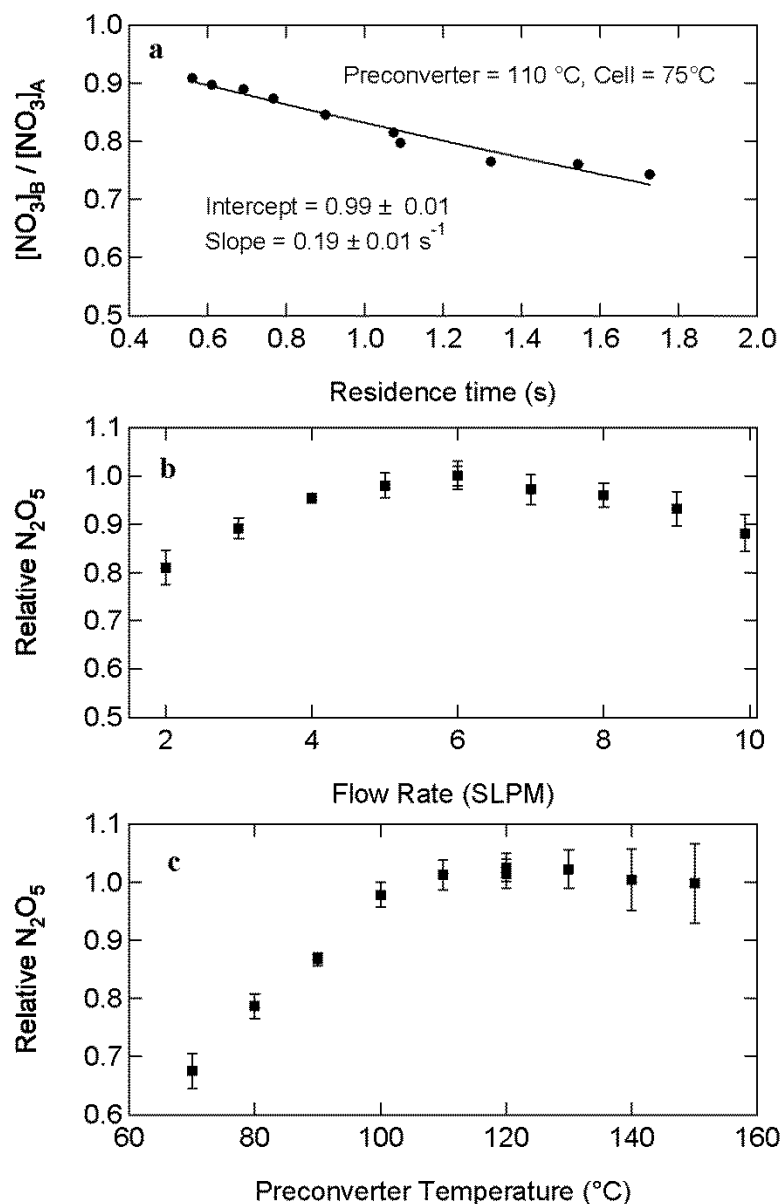
Figure 3-6: (a) Measurement of the NO₃ wall loss rate in the heated system at typical flows, converter, and measurement cell temperatures. (b, c) Measurement of the N₂O₅ conversion efficiency as a function of heated channel flow rate and preconverter temperature in the field using two different CaRDS instruments sampling from the same manifold. The reference instrument had a flow of 6 SLPM and a preconverter temperature of 120 °C. Variation of the flow and temperature on the second instrument showed that the conversion is not a strong function of the conditions over a flow range of 4–8 SLPM and preconverter temperature of 90–140 °C.

(B) N₂O₅ accuracy

The sampling efficiency for N_2O_5 depends on its transmission through the ambient temperature sections of the inlet prior to the split that divides the flow to the ambient and heated channels, the conversion efficiency for thermal dissociation of N_2O_5 to NO_3 and the loss rate for NO_3 in the heated sections of the inlet. The N_2O_5 wall loss rate is slow, and the conversion efficiency for thermal dissociation of N_2O_5 to NO_3 is essentially quantitative as long as the conditions of inlet temperature and

flow have been optimized. Therefore, the wall loss rate for NO_3 in the heated inlet is the most important contribution to the N_2O_5 sampling efficiency. Measurement of the heated wall loss rate coefficient for NO_3 was similar to that described above, except that the test section between the two ring-down cells consisted of the preconverter and reaction heater shown in Figure 3-1, and the second ring-down cell was heated. Figure 3-6(a) shows that the first order loss rate coefficient was the same as that measured at ambient temperature or 0.2 ± 0.05 s^{-1}. In the field instrument, the residence time through the heated sections of the flow system to the midpoint of the ring-down cell is 0.7 s, so that the net transmission efficiency for NO_3 in the heated portion of the inlet is (87 ± 3) %. A verification of this result via conversion of NO_3 to NO_2 as described above gave a transmission for NO_3 through this system of (93 ± 12) %. Measurement of NO_3 or $NO_3+ N_2O_5$ at 75°C depends upon the parameterization of the temperature dependence of the NO_3 absorption cross-sections given above. This cross-section is extrapolated from the temperature dependence measured below room temperature, and decreases by approximately 20 % between room temperature and 75°C. The high temperature cross-section found in the laboratory from conversion of NO_3 to NO_2 was independently varied by establishing a cross-section value of $(1.85 \pm 0.20) \times 10^{-17}$ cm^2 molecule^{-1}, in good agreement with the extrapolation. A recent calculation of the temperature dependence of the NO_3 absorption cross-section above room temperature [60] is also in agreement with the extrapolated ones based on Yokelson et al. data [49] and with the new measurements.

Optimization of the conditions of temperature and flow for the conversion of N_2O_5 to NO_3 came from tests similar to the wall loss rate measurement in the laboratory and from in-field comparison of the aircraft NO_3 and N_2O_5 CaRDS instrument to our second, ground-based instrument. Figure 3-6(b) and Figure 3-6(c) show the result of this optimization from the field data under cold conditions (T=264–266 K) and large NO_2 mixing ratio (~20 ppbv) where the predicted ratio of N_2O_5 to NO_3 was >1000:1. To test the efficiency of the N_2O_5 conversion, the conditions in the heated channel on one of the instruments were held constant at a flow of 6 SLPM (SLPM denotes standard liter per minute) and a preconverter temperature of 120°C, while the heated channel flow and temperature were varied in the other instrument. The figure shows that conversion of N_2O_5 is not a strong function of either temperature or flow under these conditions. There is wide latitude to set the flow between 4–8 SLPM and the preconverter temperature between 100 and 140°C while still maintaining an N_2O_5 signal within 90 % of its optimum value. Actual flows of 5–6 SLPM, preconverter temperature of 110–120°C, and reaction heater and measurement cell temperature of 70–75°C were used for the aircraft measurements during the NEAQS 2004 campaign. Although these tests show that conversion of N_2O_5 to NO_3 goes fully to its equilibrium value at the 70–75°C temperature of the heated ring-down cell, there is still a small fraction of N_2O_5 that remains undissociated at equilibrium at this temperature. This equilibrium necessitates an NO_2-dependent correction ranging from 0 %–5 % for NO_2 from 0–20 ppbv to the

47

measured sum of $NO_3 + N_2O_5$ in the heated channel (equilibrium constants from the NASA/JPL recommendation [53]). Typical in-flight corrections were less than 2 %.

Finally, in calculating the concentration of N_2O_5, it is important to accurately subtract the contribution from NO_3 to the signal in the heated channel, which can be comparable to or even larger than that due to N_2O_5 for summer conditions. Based on the losses, loss rates, and residence times outlined above, the net transmission of NO_3 through the entire flow system leading to the heated ringdown cell, including the tubing, filter, and filter housings, is (60 ± 15) %.

The measured N_2O_5 mixing ratio depends on the sum of NO_3 and N_2O_5, which is measured inside the heated channel (denoted SUM), the NO_3 mixing ratio derived from the ambient channel, the transmission efficiency for N_2O_5 (T_1 below), and the transmission efficiency for NO_3 in the heated inlet (T_2 below),

$$N_2O_5 = \frac{SUM - T_2[NO_3]}{T_1} \tag{3-6}$$

The estimated fractional uncertainty in the quantity of SUM is $\delta(SUM) = 15$ %, taken as the linear sum of a 10% uncertainty in the NO_3 cross-section and a 5 % uncertainty in R_L, as described above. The fractional uncertainty in the quantity $T_2[NO_3]$ can be taken only as the uncertainty in the transmission through the heated inlet since the uncertainties in this transmission efficiency are the same as those used to derive the concentration in the ambient channel. This quantity is $\delta(T_2) = 33$ %. The fractional uncertainty in T_1 is $\delta(T_1) = 13$ %. Propagating the errors in these quantities gives an expression for the uncertainty in the N_2O_5 measurement,

$$\delta(N_2O_5) = \left(\frac{(\delta(SUM) \, SUM)^2 + (\delta(T_2) \, T_2[NO_3])^2}{(SUM - T_2[NO_3])^2} + \partial(T_1)^2 \right)^{\frac{1}{2}} \tag{3-7}$$

Under conditions where $NO_3 \approx N_2O_5$, the uncertainty due to the NO_3 subtraction is the most important, while for $N_2O_5 \gg NO_3$, the uncertainty depends mainly on the efficiency of N_2O_5 conversion and sampling as described above. The range of values for $\delta(N_2O_5)$ from field data lies between 20 %–40 % for $N_2O_5 > 5$ pptv, but increases to unity for $N_2O_5 < 1$ pptv.

3.2.6 Detection sensitivities

The detection sensitivity of the CaRDS instrument can be calculated from the limit of equations 3-3a and 3-3b in which τ approaches τ_0 [61]

$$\alpha_{min} = \frac{\sqrt{2}}{c} \frac{\Delta\tau}{\tau_0^2} \tag{3-8}$$

$$[NO_3]_{min} = \alpha_{min} \frac{R_L}{\sigma T_E} \qquad (3\text{-}9)$$

Here $\Delta\tau$ is the smallest measurable change in τ_0, normally taken as the standard deviation in τ_0 from repeated measurements. Under laboratory conditions, $\tau_0 \approx 180$ µs and $\sigma(\tau) \approx 0.03$ µs [where $\sigma(\tau)$ has been taken as the standard deviation from repeated 1 s measurements], giving $\alpha_{min} = 4 \times 10^{-11}$ cm^{-1} Hz$^{-1/2}$. For a 662 nm NO$_3$ absorption cross-section of 2.2×10^{-17} cm^2 molecule^{-1}, R_L value of 1.22, and T_E value of 0.7, the corresponding detection limit for NO$_3$ is 0.1 pptv at 298 K and 1 atm. In the field, the limit is nearly always larger because there is a variable amount of noise on both channels that depends on the flow through the ring-down cells, possibly as a result of turbulence in the flow under conditions with modest temperature gradients not present in the laboratory. During summer conditions, actual detection sensitivities for NO$_3$ varied between 0.2–0.5 pptv (1σ), while under cold conditions at low altitude (i.e. higher ambient pressure), the sensitivity for NO$_3$ degrades to as much as 3 pptv. On the heated channel for detection of the sum of NO$_3$ and N$_2$O$_5$, the turbulent noise is always large at the optimal flow rate for N$_2$O$_5$ conversion. Although matching the index of refraction of the purge volume to that of the heated air sample by addition of He to the purge flow helps to suppress this noise, the actual detection sensitivity for the sum of NO$_3$ and N$_2$O$_5$ is a variable 0.5–2.0 pptv, with a typical value of approximately 1.0 pptv.

Figure 3-7 shows the Allan variance plots [62] for 800 s segments of NO$_3$ data from the laboratory and from the P-3 aircraft during a daytime flight (July 27, 2004). The laboratory data show a detection sensitivity of 0.13 pptv (one standard deviation, 1σ, from repeated 1 s measurements) at 1 s, but average to an optimal detection limit of 0.03 pptv for a 30 s average. The data shown in the figure were recorded at a total flow of 1–2 SLPM. Similar detection sensitivities have been observed under laboratory conditions at flow rates up to 16 LPM, although flow-dependent noise often degrades the detection sensitivity by a factor of two at this flow rate. The data from the aircraft are consistently noisier than the best case laboratory data and are also less amenable to signal averaging, with a 1 s detection sensitivity for this trace of 0.3 pptv and an optimal detection sensitivity of 0.15 pptv for a 10 s average. The Allan plots illustrate the degree to which averaging increases the instrument sensitivity under low signal conditions. However, the observed concentrations of NO$_3$ and N$_2$O$_5$ in the atmosphere, particularly from the aircraft, are so highly variable that signal averaging can result in a significant loss of information. Therefore, the 1 s sensitivities are the most appropriate measure of instrument performance.
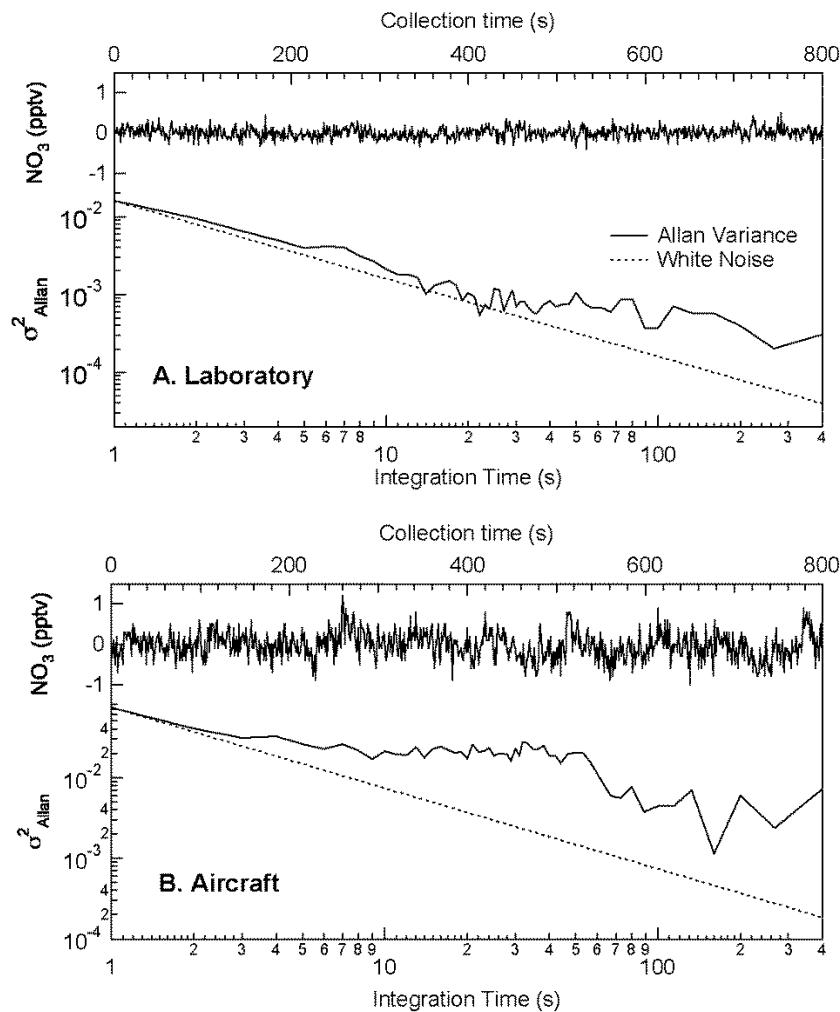
Figure 3-7: Allan variance plots of the instrument baseline in the laboratory (plot A) and from the aircraft during a daylight flight on July 27, 2004 (plot B). The laboratory data have a sensitivity of 0.13 pptv (1σ) at 1 s but average to a detection limit below 0.03 pptv at 30–40 s. The aircraft data are considerably noisier, with a 1 s sensitivity of 0.3 pptv and a detection limit at 10 s of averaging of 0.15 pptv.

3.3 Results and sample data

The NO_3 and N_2O_5 CaRDS instrument was deployed on the NOAA P-3 aircraft on March 30, 2004 for a flight to test instrument performance in advance of the planned deployment during the NEAQS field campaign in the summer of 2004. The results illustrate several interesting features of the instrument performance. Figure 3-8 shows a flight track for the test flight (upper left panel), a time series of the data and the altitude (lower panel), and a plot of the detection sensitivity versus altitude (upper right panel). The flight commenced just after the local sunset from MacDill Air Force Base in Tampa, FL, where the NOAA Aircraft Operation Center is located, and ran several level legs at increasing altitudes to approximately 7 km over the eastern Gulf of Mexico, returning at low altitude (~1 km) over populated areas in west central Florida. There was very little NO_3 or N_2O_5 at the higher altitude legs on this flight, although there was clear signal on the lower altitude legs over the Florida

peninsula, where the aircraft presumably sampled NO_x from anthropogenic sources. This was the first example of a measurement of NO_3 or N_2O_5 from an aircraft platform (to the best of my knowledge). The lack of signal on the higher altitude legs allowed for an assessment of the instrument sensitivity as a function of altitude from the statistics on the baseline, as shown in the upper right hand graph of Figure 3-8. Because the instrument sampled at a modest (<10 mbars) pressure drop from the ambient, external pressure, the background ring-down time constant, τ_0 increased monotonically with altitude. (Because of unfavorable mirror performance on the test flight, the τ_0 value at 1 atm was ~160 μs, rather than the more typical 180 μs for optimally clean mirrors.) Also, the turbulent flow noise described above tended to decrease with increasing altitude, presumably because the Reynolds number in the inlet decreases at constant volumetric flow.
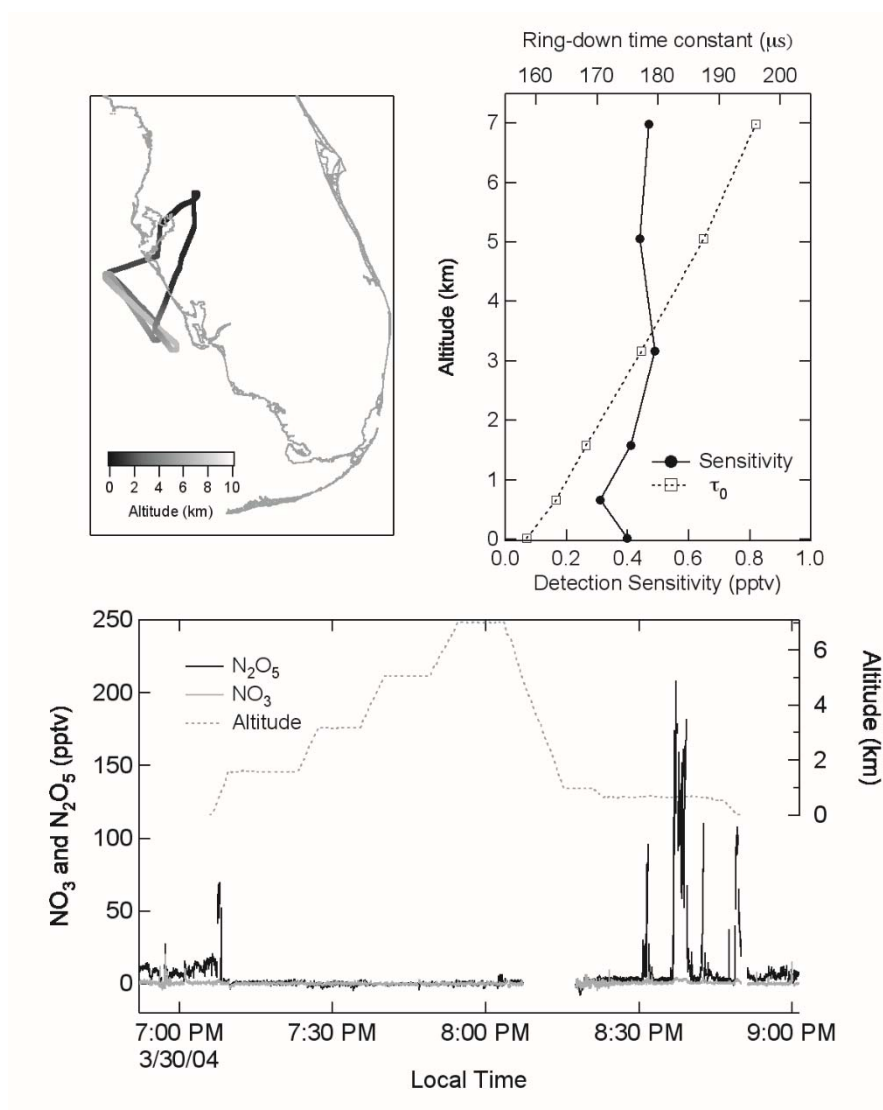
Figure 3-8: Results from the test flight of the CaRDS instrument on the NOAA P-3 in March, 2004. Upper left: flight track. Lower: time series of NO_3, N_2O_5, and altitude. Upper right: variation of the instrument detection sensitivity (lower axis) and ring-down time constant (top axis) with altitude. The increase in sensitivity due to the increasing ring-down time constant and reduced turbulent flow noise approximately cancels the decrease in ambient number density, leading to a nearly altitude independent sensitivity.

Both of these effects tended to increase the sensitivity of the instrument with respect to the absolute number density of absorbers. However, the decrease in the ambient number density with altitude approximately canceled these increases, and the sensitivity for NO_3 in mixing ratio units was approximately constant with altitude over a range of 0–7 km. This invariance with altitude suggested that the instrument would have worked equally well with an inlet controlled at a constant subambient temperature down to roughly 0.5 atm. It further suggested that with higher reflectivity mirrors, at the Rayleigh scattering limit, a pressure controlled inlet (or high altitude sampling) could yield a substantial increase in detection sensitivity.

3.4   Summary and future work

In this article (chapter 3) a pulsed, cavity ringdown spectrometer for in-situ detection of NO_3 and N_2O_5 from an aircraft is described. The instrument detects NO_3 in an ambient channel on its strong visible absorption band at 662 nm, and the sum of NO_3 and N_2O_5 in a separate, heated channel via the thermal conversion of N_2O_5 to NO_3. It is small enough for deployment on the NOAA P-3 aircraft and has performed reliably on that platform for one test flight in March of 2004 and for the duration of a six week field deployment in July-August 2004. At a time resolution of 1 s, the best case detection limits (1σ) for NO_3 and N_2O_5 are approximately 0.1 pptv, although actual detection limits encountered in the field were 0.2–0.5 pptv for NO_3 and 0.5–2 pptv for N_2O_5. Although cavity ring-down spectroscopy is an absolute, direct absorption method, the inlet transmission for NO_3 and the conversion efficiency of N_2O_5 to NO_3 are less than unity and add considerable uncertainty to the determination of their ambient concentrations. The estimated accuracy of the NO_3 measurement is 25 %, while the estimated N_2O_5 accuracy depends on the ratio of N_2O_5 to NO_3 but is generally in the range of 20 – 40 %.

There are a number of improvements to the instrument currently underway that should improve its sensitivity, accuracy, and versatility. The first is the incorporation of an additional 532 nm CaRDS measurement for NO_2 using a fraction of the 532 nm light used to pump the dye laser, as has been recently demonstrated for a ground-based instrument [48]. Detection of NO_2 not only provides information on an additional, related nitrogen oxide, but also provides a mean to calibrate the inlet transmission directly in the field from the conversion of NO_3 to NO_2 via reaction with NO [36]. Working on the reduction of the flow related noise underway, especially on the heated channel, to bring the field detection sensitivity closer to that achievable in the laboratory. Future planned deployments include experiments at a tall tower near our laboratories in Boulder, CO for vertical profiling of NO_3 and N_2O_5 and further air quality studies with the NOAA P-3.

4. Publication B:

Determination of inlet transmission and conversion efficiencies for in-situ measurements of the nocturnal nitrogen oxides, NO₃, N₂O₅ and NO₂, via pulsed cavity ring-down spectroscopy

Authors:

Hendrik Fuchs,[1,2] William P. Dube,[1,2] Steven J. Ciciora,[1] Steven S. Brown[1]

[1]*Earth System Research Laboratory, NOAA, Boulder, Colorado 80305, USA.*

[2]*Cooperative Institute for Research in the Environmental Sciences, University of Colorado, Boulder, Colorado 80309, USA.*

Abstract:

Pulsed cavity ring-down spectroscopy is a highly sensitive method for direct absorption spectroscopy that has been applied to in-situ detection of NO₃, N₂O₅ and NO₂ in the atmosphere from a variety of platforms, including ships, aircraft, and towers. In this paper (chapter 4), the development of schemes to significantly improve the accuracy of these measurements is reported. This includes the following: (1) an overall improvement in the inlet transmission efficiencies (92 ± 2 % for NO₃ and 97 ± 1 % for N₂O₅) achieved primarily through a reduction in the inlet residence time; and (2) the development of a calibration procedure that allows regular determination of these efficiencies in the field by addition of NO₃ or N₂O₅ to the inlet from a portable source followed by conversion of NO₃ to NO₂. In addition, the dependence of the instrument's sensitivity and accuracy to a variety of conditions encountered in the field, including variations in relative humidity, aerosol loading, and volatile organic compound (VOC) levels, was systematically investigated. The rate of degradation of N₂O₅ transmission efficiency on the inlet and filter system due to the accumulation of inorganic aerosol was determined, such that the frequency of filter changes required for accurate measurements could be defined. In the absence of aerosol, the presence of varying levels of relative humidity and reactive VOC were found to be unimportant factors in the instrument's performance. The 1σ accuracy of the NO₃, N₂O₅, and NO₂

measured with this instrument are -9/+12, -8/+11, ±6 %, respectively, where the - signs indicate that the actual value is low/high relative to the measurement. After improving the instrument the largest contribution to the overall uncertainty is due to the NO_3 absorption cross-section rather than the inlet transmission efficiency.

4.1 Introduction

The nitrate radical (NO_3) and dinitrogen pentoxide (N_2O_5) are key nocturnal forms of nitrogen oxides. NO_3 participates in the oxidation of pollutants during the night in the troposphere, [63-65] particularly of unsaturated hydrocarbons and sulfur compounds [66]. Hydrolysis of N_2O_5 on aerosol is one of the most important reactions in the conversion of nitrogen oxides to soluble nitrate (NO_3^-) in the troposphere [67]. NO_3 is formed in the reaction of nitrogen dioxide (NO_2) and ozone (O_3). Since it is easily photolyzed by visible light [10], appreciable levels of NO_3 can only accumulate in the dark. NO_3 is in a thermal equilibrium with N_2O_5, which is formed in the reaction of NO_2 and NO_3:

$$NO_2 + O_3 \rightarrow NO_3 + O_2 \quad (4\text{-}1)$$

$$NO_2 + NO_3 \leftrightarrow N_2O_5 \quad (4\text{-}2)$$

Early measurements of NO_3 were mostly performed by longpath differential optical absorption spectroscopy (DOAS) [9, 17, 18, 68]. Since the past decade, cavity ring-down spectroscopy (CaRDS) has been developed as a highly sensitive, in-situ method to detect NO_3 [30] and also the sum of NO_3 and N_2O_5 after the thermal decomposition of N_2O_5 to NO_3 in a heated inlet [1, 29, 31]. Detection limits of in the range of a few tenths of a pptv for NO_3 (pptv, parts per trillion per volume) at a high temporal resolution (in the range of seconds) can be reached for CaRDS. In contrast to the DOAS technique, CaRDS instruments sample air into a closed cavity, so that measured concentrations have to be corrected for losses of NO_3 on surfaces. This places a limitation on the accuracy of the measurement.

The NOAA CaRDS instruments for detection of NO_2, NO_3, and N_2O_5 [1, 48], have been successfully deployed in several aircraft and ship missions [69, 70] as well as at ground sites and at a tall tower [71]. This article reports the further developments of these instruments that have led to a significant improvement in their accuracy. The improvements include the following: changes in the instrument's NO_2 detection scheme to allow not only for monitoring of ambient NO_2 but also for periodic determination of the transmission efficiencies for NO_3 and N_2O_5 via their conversion to NO_2; changes to the inlet system to reduce the total residence time; and quantification of inlet transmission efficiencies through a series of laboratory tests. The latter involved a systematic investigation of the possible changes of the instrument's sensitivity and accuracy under a variety conditions representative of those encountered in the field.

4.2 Instrument overview

A description of the detection principle and operating characteristics of these instruments has been given elsewhere [1, 8, 48]; they are briefly summarized in the beginning of this section for completeness. CaRDS has become an established direct absorption technique to measure atmospheric trace gas concentrations [44, 72]. In the present case, a nanosecond scale laser pulse is coupled into a high-finesse cavity and the intensity of the light transmitted through the end mirror of the cavity is observed. The intensity [$I(t)$] decays as a single exponential with a time constant (τ). The detector's background signal is measured prior to the laser pulse and subtracted so that τ can be derived from a standard linear fit of the logarithmic signal:

$$I(t) = I_0 \exp(-t/\tau) \qquad (4\text{-}3)$$

The measurement of a trace gas concentration [A] is accomplished by comparing the fitted ring-down time constants in the presence (τ) and absence of the absorber (τ_0) using the absorption cross-section (σ_A) at the probing wavelength:

$$[A] = \frac{R_L}{c\,\sigma_A}\left(\frac{1}{\tau} - \frac{1}{\tau_0}\right) \qquad (4\text{-}4)$$

Here, c is the speed of the light and R_L is the ratio of the total cavity length to the length over which the absorber is present in the cavity. The background time constant (τ_0) is limited by the mirror reflectivity, Rayleigh and Mie scattering of the gas and aerosol present in the cavity, and absorption due to trace gases other than the target absorber.

Figure 4-1 shows the layout of the NOAA aircraft CaRDS instrument ARNOLD, which is capable of measuring NO_3, N_2O_5 and NO_2 concentrations simultaneously. The extinction of the sampled air at 662 nm is measured in two separate cavities. A 6 ns laser pulse (0.5 mJ pulse energy, 50 Hz repetition rate) at 662 nm is generated by a Nd:YAG (Big Sky Laser, ultra CFR) pumped dye laser (Dakota Technology, Northern Lights). The dye laser wavelength (line width 0.5 cm^{-1}) is tuned out of resonance with any of the weak water vapor absorption lines (line width $\sim$0.3 cm^{-1} at atmospheric pressure, [63]) that lie underneath the peak of the 80-cm^{-1}-wide NO_3 band centered near 662 nm. The laser light is coupled into the cavity (mirror reflectivity, 99.9995 %; transmission, ≤5 ppmv (parts per million by volume); curvature, 1 m; distance, 93 cm) after propagating through an optical isolator and a series of irises and lenses to minimize the spot size at the far end of the cavity. Light transmitted through the rear mirror is collected using an optical fiber and is imaged on to a small photomultiplier tube through a band-pass filter. Figure 4-2 shows an example ring-down trace recorded on a digital oscilloscope card at 16-bit resolution. The precision of the ring-down time constants gives the limit of

detection (2σ) of the instrument in terms of extinction coefficient to 1×10^{-10} cm^{-1}, similar to what has been reported previously [1].
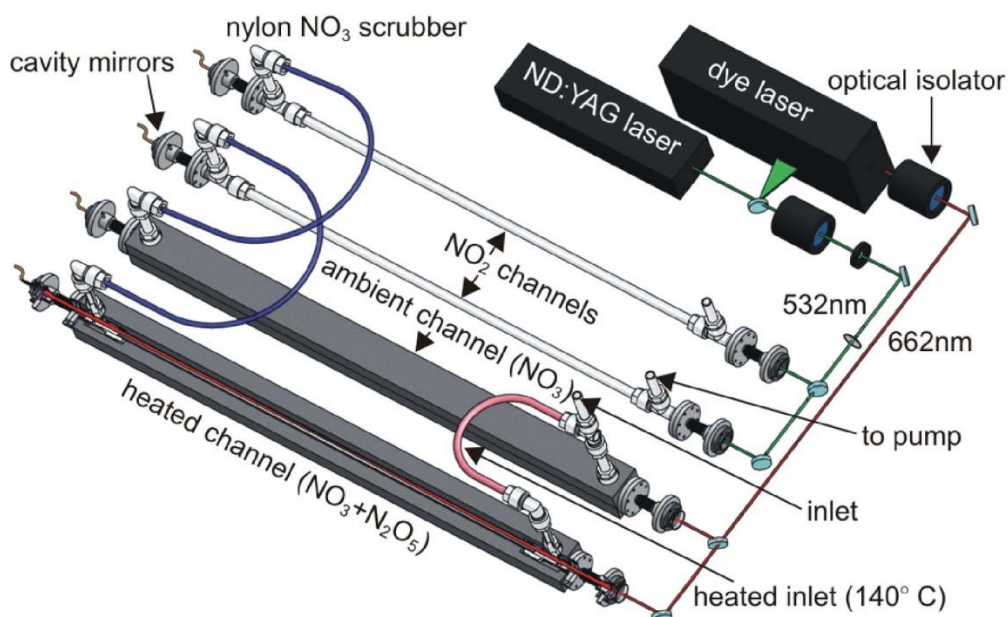
Figure 4-1: Schematic of the four-channel cavity ring-down instrument for measurements of ambient NO$_3$, N$_2$O$_5$, and NO$_2$ concentrations.

The measurement of the ring-down time constant without the absorber, which must be known to derive trace gas concentrations (equation 4-4), is accomplished by periodic addition of excess NO to the inlet to chemically destroy NO$_3$ via the reaction NO$_3$ + NO $\rightarrow$ 2NO$_2$. This zeroing method is highly specific to determine the extinction at 662 nm from all contributions other than NO$_3$ absorption. A 40 sccm (standard cubic centimeter per minute) flow of a mixture of 100 ppmv NO in nitrogen is added for 5 s every 3-5 min. This yields an NO mixing ratio of 0.5 ppmv in the sampled air, which is sufficient to completely titrate NO$_3$ in the system before it enters the cavities (NO$_3$ first-order loss rate coefficient 110 s^{-1}).
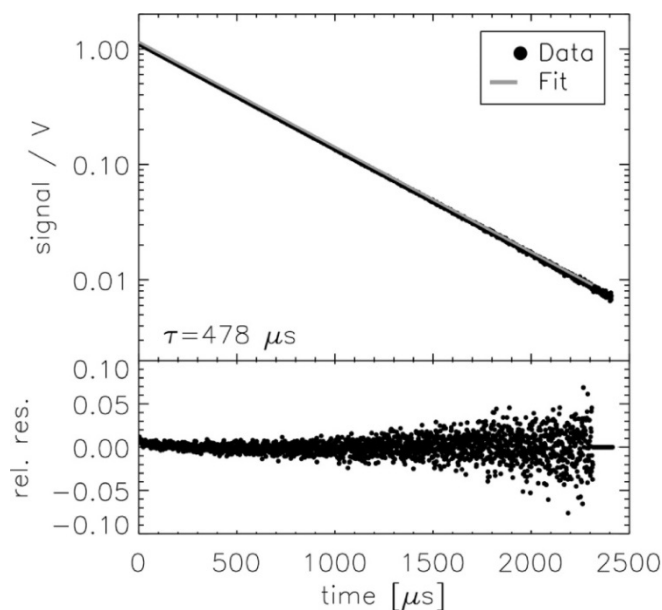
Figure 4-2: Example ring-down trace at 662 nm for 1-s integration time. The lower panel shows the relative residual to the fitted single-exponential decay with a ring-down time constant of 478 μs.
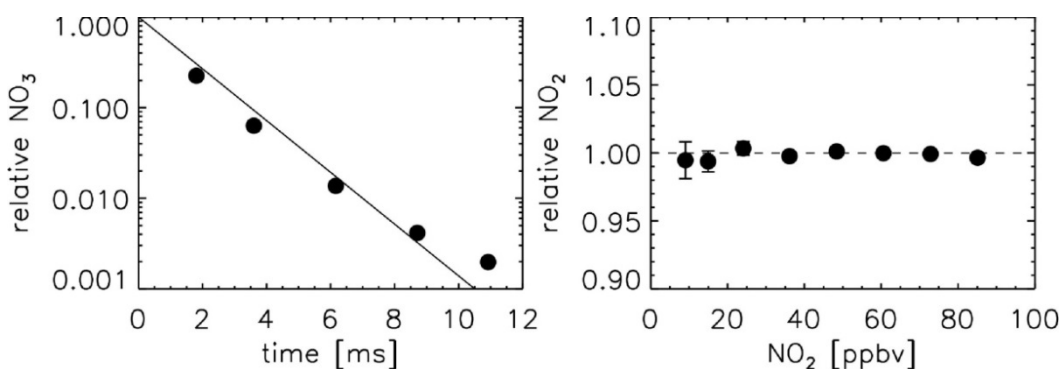
Figure 4-3: Left panel: relative NO_3 concentration vs residence time in 1/4-in. (6.4 mm) Nylon 11 tubing showing that this material is an effective scrubber for NO_3. Right panel: transmission of NO_2 through a 95-cm length of Nylon 11 tubing as a function of NO_2 mixing ratio. The average transmission is 99.8 (0.3%, amounting to a negligible loss for NO_2.

A key difference in the current instrument is a decreased residence time due largely to sampling at reduced pressure and due to using smaller diameter cavities and tubing (reduced from 3/8-in. (9.5 mm) to 1/4-in. (6.4 mm) internal diameter). The total flow through the instrument is 8 SLPM (SLPM denotes liter per minute at standard pressure and temperature) of ambient air, which is sampled through 0.3-0.4-m length of 1/8-in.-o.d. Teflon tubing that serves as restriction leading to a reduced pressure of ~350 hPa inside the instrument. The instrument can be operated under active pressure control (MKS type 640), in which a small fraction of the total flow is diverted directly to the pump downstream of the pressure restriction.

There are several advantages to operation at reduced pressure. First, the residence time through the inlet and optical cavities is shorter, minimizing the wall loss of NO_3 and N_2O_5. Second, the number density of other reactive trace gases and water vapor is reduced such that they are less likely to either react with NO_3 or adsorb to the walls of the inlet. Third, liquid water may evaporate at lower pressure and is less likely condensed on wall surfaces and aerosol where it could enhance wall and filter loss of NO_3 and N_2O_5. Fourth, Rayleigh scattering becomes smaller so that the ring-down time constant and therefore the effective optical path length is increased. This advantage is only important if the contribution of Rayleigh scatter to the overall light loss in the cavity is significant compared to the other losses such as the mirror transmission (e.g., for the instrument described here, losses due to both mirror reflectivity and Rayleigh scattering at 1 atm are both ~5 ppm per pass). The reduced pressure does not change the Reynolds number for given mass flow rate and therefore does not introduce additional turbulence, which can lead to optical noise in the measurement. However, the reduced pressure has the disadvantage of reduced number density of the target absorber so that 2σ limits of detection are slightly increased (NO_3, 0.6 pptv; N_2O_5, 2 pptv; NO_2, 200 pptv) compared to previously reported values [1, 48].

The sampled air passes through a Teflon filter (PTFE, 2 μm pore size, 25 μm thick) to remove particles that can significantly contribute to the extinction measured in the cavity. The filter is exchanged regularly (every 0.5-3 h) by a fully automated filter changer [1]. The sampled air is divided into two 4 SLPM flows downstream of the filter. One flow passes through a two-stage heater to thermally convert N_2O_5 to NO_3 (see below for details) and into a cavity maintained at 75°C. The other part of the sampled air enters the second cavity, which is maintained at ambient temperature using an actively cooled, aluminum manifold that surrounds the Teflon tubing. Turbulators (additional flow restrictions consisting of a short length of twisted, 1/4-in.-o.d. Teflon tubing inserted into the 3/8-in. tubing) are present in the tubing upstream of the cavities to ensure that the air is well mixed.

A second important difference from the previous versions of this instrument is the presence of two additional cavities downstream of each of the 662 nm cavities in which the extinction of the sampled air at 532 nm is measured, according to the method described by ref 17. A small part (5 %) of the ND:YAG laser output is split from the beam that pumps the dye laser and is coupled into these cavities (mirror reflectivity, 99.999 %). The geometrical design of the 532 nm cavities and the data acquisition are similar to that of the 662 nm cavities. These additional channels are used to measure atmospheric NO_2 concentrations and also to determine the NO_3 losses in the system as described in more detail below.

A 95 cm length of Nylon 11 tubing, which serves as a scrubber for NO_3, is placed between each 662 and 532 nm cavity. It is necessary to destroy the NO_3 between the cavities because its absorption cross-section at 532 nm is more than 1 order of magnitude larger than that of NO_2 [49]. Figure 4-3 (left panel) shows the loss of NO_3 on the Nylon tubing measured by observing the NO_3 extinction at 662 nm transmitted through various lengths of the Nylon tubing (first order loss rate, 90 ±10 s^{-1}). Thus, a 95 cm

length of Nylon tubing was found to remove NO_3 below the level where its optical extinction was detectable at 532 nm. The reaction of NO_3 with the Nylon surfaces does not lead to NO_2 production. This was checked by comparing the NO_2 measured in the two 532 nm cavities when NO_3 was scrubbed by Nylon upstream of one of the cavities and titrated via NO upstream of the other cavity. The difference between both NO_2 measurements were consistent with the increase of NO_2 from the titration of NO_3, whose concentration was measured in the 662 nm cavities. Loss of NO_2 on the NO_3 scrubber was checked by connecting the two NO_2 channels with a 95 cm length of Nylon tubing and comparing the measurements of NO_2 in dry zero air. Although this measurement was carried out in dry zero air, and so potentially neglects effects such as conversion of NO_2 to HONO on surfaces, recent field comparisons of this instrument to other NO_2 measurements under conditions of varying relative humidity have not revealed any humidity-dependent artifacts. Figure 4-3 (right panel) shows that loss of NO_2 is less than 0.3 % through the scrubber. Transmission of ozone (not shown here) was also quantitative to within 1 %.

As described previously [48], the determination of the τ_0 at 532 nm is accomplished by overflowing the inlet with zero air. Although this zero method for NO_2 is not as specific as the NO titration for NO_3, the only interference that we are aware of is optical extinction due to ozone (the ozone absorption cross-section is $\sim$50 times smaller than that of NO_2 at 532 nm [59]) Therefore, 532 nm extinction due to ozone absorption must be calculated from a separate ozone measurement and subtracted from the total extinction in order to determine the NO_2 concentration.

4.3 Instrument characterization

4.3.1 Effective Path Length R_L

The calculation of the absorber's concentration (equation 4-4) requires the knowledge of the ratio between the absorption path length and the distance between the mirrors, R_L. This ratio is reduced compared to the distance of the mirrors because the volumes adjacent to the mirrors are purged with a small flow of dry synthetic air (zero air) to keep them clean. An overall flow of 200 sccm of zero air is divided into nearly equal parts for each of the eight cavity mirrors using a single-flow controller and eight critical orifices. The ratio of the absorption path length and the mirror distance cannot be derived simply from the distance between the inlet and outlet of the sampled gas and the distance between the mirrors (ratio 1.24), because part of the sampled gas penetrates the purge volumes. Therefore, R_L was determined by the measurement of a known concentration of ozone, which was produced and measured (mixing ratio, 10-500 ppbv) by a standard ozone monitor. This was compared to the ozone absorption measured in each cavity by its visible optical absorption in the Chappius bands. The fitted slopes (1.14) were similar for all channels with an uncertainty of 3 % due to the ozone monitor (2 %) and the absorption cross-section (1 %).

4.3.2   Conversion of N_2O_5 to NO_3

The instrument has two channels in which the extinction of the sampled air at 662 nm is measured, one of which is heated to induce thermal decomposition of N_2O_5 to NO_3 in order to determine the sum of both trace gas concentrations. The conversion is achieved upstream of the cavity in a two-stage heater system consisting of heated 3/8 in. (9.5 mm) outer diameter (1/4 in. (6.4 mm) internal diameter) Teflon tubing. The first zone (length 31 cm) is kept at a temperature of 140°C (outside wall temperature) to heat the gas rapidly to temperatures that ensures that the equilibrium is shifted toward NO_3. The second zone (80°C, length 16 cm) serves as a relaxation zone to bring the gas temperature close to that inside the cavity in order to avoid temperature gradients and thereby reduce turbulent flow noise.

The sample volume inside the cavity of this channel is heated to a constant temperature of 75°C, which is sufficient to maintain the equilibrium between the two species on the side of NO_3 for typical atmospheric concentrations of NO_2. The ratio of NO_3 to N_2O_5 at this temperature depends linearly on the NO_2 mixing ratio in the sampled air. Measurements are corrected for this small equilibrium effect by calculating the fraction of $N_2O_5 + NO_3$ remaining as N_2O_5 (1 % per 10 ppbv NO_2 calculated from the equilibrium constant [44, 53, 72]).

The temperature of the heating zone 1 was optimized in laboratory experiments sampling air containing N_2O_5 from a calibration source (see below). The residence time of the sampled air in the heater and the heater temperature were systematically varied. The first was achieved by manipulating the flow rates in both channels simultaneously so that only the residence time in the heater and cavity was changed but not the overall flow conditions in the inlet and filter system upstream of the cavities. The residence time was calculated from the flow rate by assuming plug flow conditions.

The relative NO_3 absorption signal in the heated 662 nm channel as a function of residence time for different heater temperatures gives a measurement of the relative conversion efficiency of N_2O_5 in the system (Figure 4-4). It shows a distinct maximum as a function of residence time in the heater at a fixed heater temperature. In addition, this maximum increases and is shifted toward shorter residence times with higher heater temperature. This can be understood as a competition between thermal decomposition of N_2O_5, limited primarily by heat transfer rather than the unimolecular decomposition rate coefficient of N_2O_5, and NO_3 loss on Teflon surfaces at longer residence times.
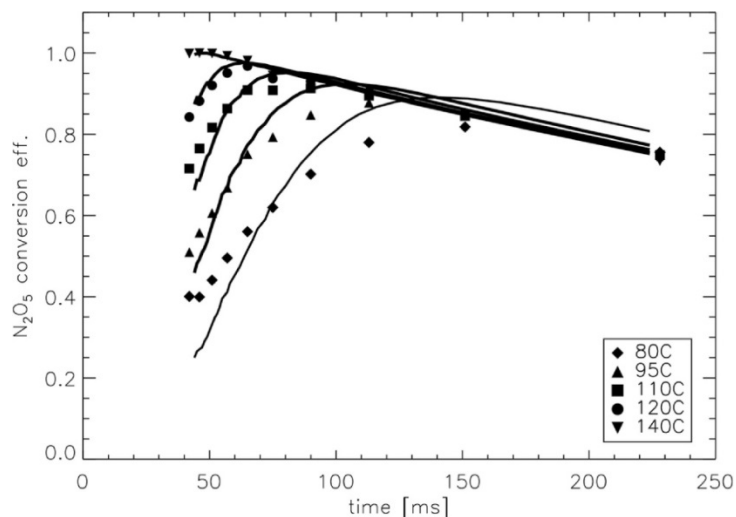
Figure 4-4: Measured dependence of N_2O_5 detection efficiency (i.e., the product of the conversion efficiency of N_2O_5 to NO_3 and the transmission efficiency of NO_3 through the inlet downstream of the N_2O_5 conversion) on the heater temperature and residence time (symbols). The residence time was varied by changing the flow rate. Measurements are compared with results of simple model calculations (solid lines, see text).

These results were confirmed qualitatively by model calculations (solid lines in Figure 4-4) that were constrained by an inlet temperature profile and included a first-order NO_3 wall loss ($k = 0.3 \pm 0.1$ s^{-1}; see below). Results are independent of the initial N_2O_5 mixing ratio at the tip of the inlet.

A temperature of 140°C of the converter and a flow rate of 4 SLPM lead to a maximum conversion efficiency. Together with the results of the absolute transmission efficiencies measurements for N_2O_5 of 98 % (see below), this configuration allows for optimum conversion of N_2O_5 to NO_3.

In contrast to the heated channel, the ambient channel used for the measurement of NO_3 is actively cooled to keep the gas temperature similar to ambient temperature. This suppresses unwanted thermal decomposition of N_2O_5 to NO_3 and prevents optical noise arising from thermal gradients within the ambient channel. However, under conditions of excessive heat load (e.g., aircraft sampling, in which the fuselage temperature may be higher than the ambient temperature outside the aircraft), the temperature of the NO_3 measurement channel may deviate from ambient. In this case, a factor is applied for the N_2O_5 thermal decomposition within the inlet. For aircraft measurements, in which the temperature gradients are most severe, the average value of this correction factor is 2 % but can be larger (e.g., 20 %) for large NO_x plumes (>25 ppbv).

4.3.3 Determination of inlet transmission efficiencies

NO_3 and N_2O_5 are reactive species. Therefore, losses in the inlet system and inside the cavity have to be quantified in order to correct concentrations measured inside the cavity to actual, ambient concentrations. The correction for NO_3 is straightforward because the NO_3 concentration is directly measured by its extinction at 662 nm:

$$[NO_3]_{amb} = \frac{[NO_3]_{meas}}{T_E(NO_3)}$$ (4-5)

$T_E(NO_3)$ is the transmission efficiency for NO_3 in the ambient channel.

In contrast, the heated channel measures the sum of N_2O_5 and NO_3. Only that part of the sum signal that refers to N_2O_5 must be corrected for the N_2O_5 losses by the N_2O_5 transmission efficiency $T_E(N_2O_5)$. It is therefore necessary to subtract the ambient NO_3 concentration prior to the N_2O_5 correction. However, the NO_3 transmission efficiency in the sum channel ($T_E'(NO_3)$) may differ from that of the ambient NO_3 channel ($T_E(NO_3)$):

$$[N_2O_5]_{amb} = \frac{1}{T_E(NO_3)}\left[\left([NO_3]+[N_2O_5]\right)_{meas} - T_E(NO_3)'[NO_3]_{amb}\right]$$ (4-6)

Thus, three different inlet transmission efficiencies (equation 4-5 and equation 4-6) have to be known to calculate the ambient N_2O_5 concentration from the two measured extinctions. These were determined via two different methods.

The first method was direct measurement of NO_3 and N_2O_5 losses on various components of the inlet system. First, reactive species are lost on the surface of the Teflon tubing. This can be described as a first-order loss process, since previous work has shown that the NO_3 loss scales with inlet residence time [1, 8]. Second, NO_3 and N_2O_5 are also lost on the filter, which acts as a fixed, point loss in the system. The loss in the latter was measured by comparing the NO_3 absorption from the NO_3 or N_2O_5 source sampled through the entire inlet including the filter system to that obtained by bypassing the filter system with a short piece of Teflon tubing. This yielded in a loss of NO_3 in the filter system of 5 ± 2 % and no significant loss of N_2O_5. Total loss on the filter and its housing are now considerably smaller than previously reported (10 ± 5 %, [1]), due largely to improvements in the machining process of the filter housing and reductions in the residence time.

The first-order loss rate of NO_3 on 3/8-in. (9.5 mm) outer diameter Teflon tubing was determined by measuring the NO_3 concentrations as a function of tubing length. A linear fit of the logarithmic extinction depending on the residence time in the additional tubing yielded in a loss rate of 0.3 ± 0.1 s^{-1} consistent with previous measurements in slightly larger diameter tubing (1/2-in. (12.7 mm) outer diameter, 0.2 ± 0.1 s^{-1} [1]). This results in a wall loss of NO_3 in the ambient channel of 3 ± 1 % at a residence time of 100 ms between the filter and the center of the cavity. Together with the NO_3 loss on the filter, the overall NO_3 transmission is 92 ± 2 %. Although this measurement was made in dry, particle-free air, the experiments described below show that the number is also applicable to ambient air that contains water vapor, aerosol, and other reactive trace gases.

In the case of N_2O_5, the only significant wall loss occurs subsequent to its conversion to NO_3 downstream of the heater, since N_2O_5 itself is less reactive toward Teflon surfaces. Thus, the N_2O_5

transmission efficiency is 97 ± 1 % at the given residence of 100 ms between the heater and the center of the cavity.
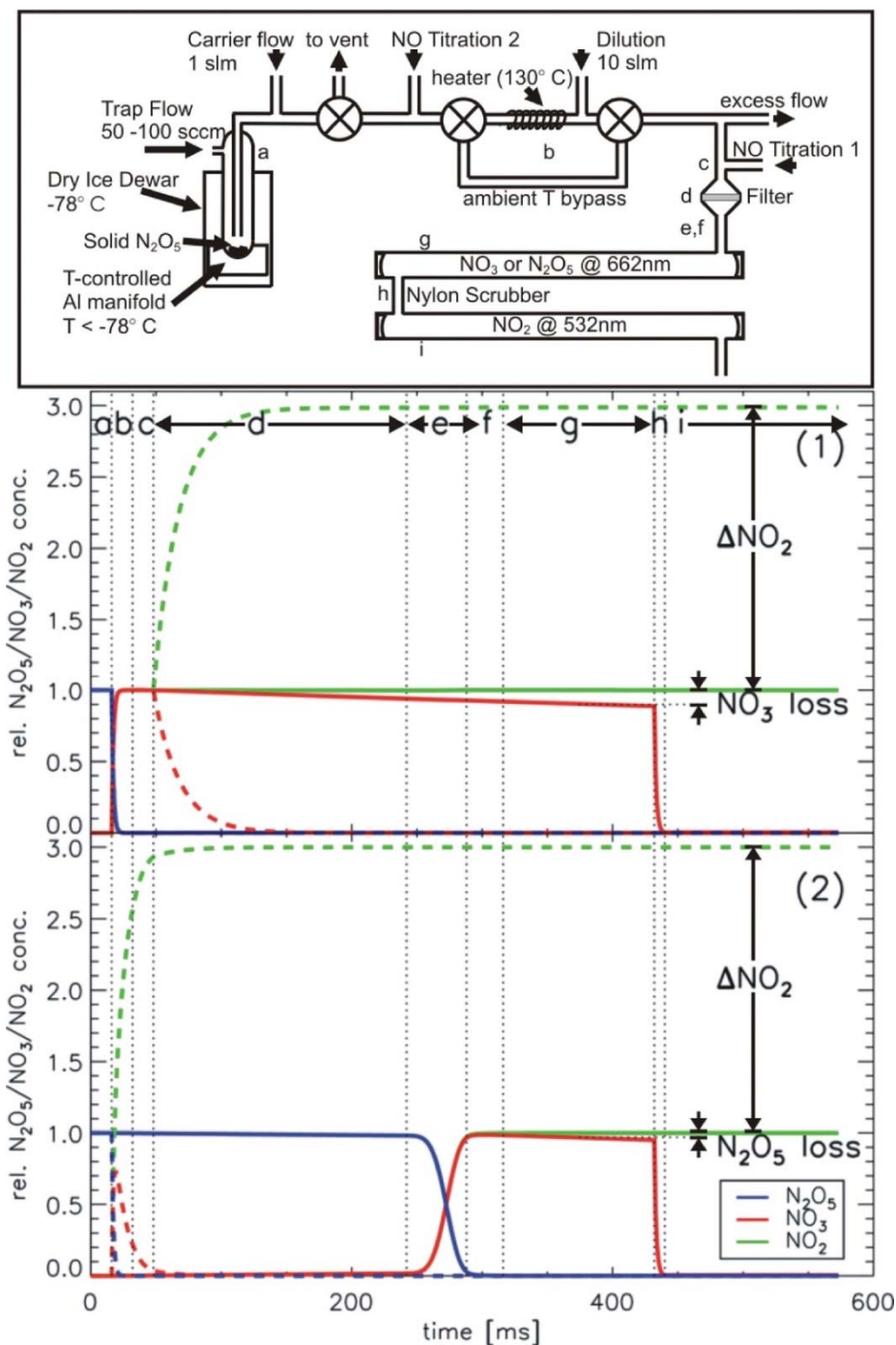
Figure 4-5: Schematic of the NO_3 and N_2O_5 source (upper panel) used to calibrate inlet transmission efficiency for NO_3 (1) and N_2O_5 (2). Graphs show the predicted time dependence of NO_3, N_2O_5, and NO_2 if the instrument (d, inlet system and filter; e/f, heater zone 1/2; g, NO_3 cavity; h, NO_3 scrubber; i, NO_2 cavity) samples from the N_2O_5 calibration source (a, cold source; b, heater; c, connection to the instrument). Dashed lines refer to the zeroing mode when excess NO is added upstream of the instrument. Heater zones e, f are present only for the N_2O_5 channel. The calibration heater b is bypassed for the N_2O_5 calibration but used for the corresponding zeroing mode (see text for details).

A second approach to determine inlet transmission efficiencies is via conversion of NO_3 or N_2O_5 to NO_2. We have used this method to develop a calibration suitable for use in both the laboratory and the field (Figure 4-5). The calibration system consists of a solid N_2O_5 sample kept at a constant temperature below -78°C (dry ice). This is accomplished by actively cooling the glass trap containing the crystalline N_2O_5 with a Peltier-cooled aluminum housing attached to a heat sink, all of which is immersed in a dry ice/2-propanol bath. A small flow of zero air (~50 sccm) is passed over the crystalline solid to produce a flow that is saturated with N_2O_5 at its vapor pressure at the chosen temperature. This flow is maintained in order to keep the output from this source more stable and can be diverted to a vent line during periods when calibration measurements are not being performed. A carrier flow of 1 SLPM ensures a rapid transport from the trap to the inlet of the instrument. The N_2O_5 is further diluted by ~10 SLPM of zero air just prior the instrument's inlet so that typical N_2O_5 mixing ratios used for the calibration measurements are ~1 ppbv. As shown in Figure 4-5, the flow from the N_2O_5 source can be directed through a heater at 130°C in order to deliver NO_3 instead of N_2O_5.

The N_2O_5 concentration supplied by the calibration source should be a constant determined by the vapor pressure of crystalline N_2O_5 at the set temperature of the trap. However, in practice, this is true only under ideal conditions; in general, the output of the N_2O_5 trap at a given temperature tends to vary somewhat with time and with the age of the sample. Therefore, rather than using the N_2O_5 (or NO_3) concentration supplied by the trap as an absolute standard for calibration purposes, the infield calibration scheme is a comparison of two measurements, one for NO_3 and one for NO_2 converted from NO_3 via reaction with NO.

Figure 4-5 shows a model calculation of relative NO_3, N_2O_5, and NO_2 concentrations as a function of time during the flow through the inlet for calibration of either NO_3 or N_2O_5 losses (distinguished by solid or dashed lines) including the different parts of the calibration source and the instrument (indicated by the dashed vertical lines).

The middle panel of Figure 4-5 describes the determination of the NO_3 transmission efficiency in either the heated or the ambient channels. The N_2O_5 from the source (a) is thermally decomposed to NO_3 and NO_2 (b) upstream of the inlet system of the instrument (c). First, NO_3 and NO_2 concentrations are measured in the 662 nm cavity (g) and the 532 nm cavity (i), respectively (solid lines). The concentration of NO_3 is reduced by losses on the filter, the filter housing (d), the Teflon tubing upstream of the cavity (e,f), and in the cavity itself (g). NO_3 is removed quantitatively on the Nylon tubing (h) between the two cavities. Second, NO_3 is titrated by excess NO added upstream of the inlet (c) (dashed lines), leading to the production of two NO_2 for every NO_3. The difference between the two NO_2 measurements (with and without NO titration) is twice the NO_3 concentration present at the tip of the inlet. The ratio between the NO_3 concentration measured in the calibration mode without NO titration and half of the difference of the two measured NO_2 concentrations, $\Delta[NO_2]$, gives the NO_3 transmission efficiency $T_E(NO_3)$:

$$T_{\mathrm{E}}(\mathrm{NO}_3) = \frac{[\mathrm{NO}_3]}{0.5\Delta[\mathrm{NO}_2]} \tag{4-7}$$

A similar calibration scheme can be applied to determine the $\mathrm{N}_2\mathrm{O}_5$ transmission and conversion efficiency (Figure 4-5 lower panel) using the calibration source in its $\mathrm{N}_2\mathrm{O}_5$ mode. First, $\mathrm{N}_2\mathrm{O}_5$ and NO_2 concentrations are measured in the two cavities (g, i). These are again compared to the NO_2 concentration, if $\mathrm{N}_2\mathrm{O}_5$ is converted to NO_2 upstream of the inlet system. Therefore, the $\mathrm{N}_2\mathrm{O}_5$ is directed through the heater within the calibration source (b), which was bypassed during the first measurement, to be converted to NO_3, which reacts with added excess NO to form NO_2 in a 2:1 ratio. The ratio of the measured $\mathrm{N}_2\mathrm{O}_5$ concentration and half of the difference of the two measured NO_2 concentrations gives the $\mathrm{N}_2\mathrm{O}_5$ transmission efficiency:

$$T_{\mathrm{E}}(\mathrm{N}_2\mathrm{O}_5) = \frac{[\mathrm{N}_2\mathrm{O}_5]}{0.5\Delta[\mathrm{NO}_2]} \tag{4-8}$$

The calibration resulted in a transmission efficiency of 90 ± 3 % for NO_3 in both the ambient and heated channels and of 98 ± 3 % for $\mathrm{N}_2\mathrm{O}_5$. The precision of these values us given by repeated measurements in the laboratory. These determinations are in agreement with the sum of the measurements of the losses on individual components of the inlet system described above.

The calibration source has been operated successfully in the field as well as the laboratory. For example, calibrations were carried out before and after each flight during the deployment of the aircraft instrument on the NOAA P-3 during the Texas Air Quality Study in August-October 2006 in Houston, TX. Measured transmission efficiencies for NO_3 were on average somewhat lower than those described here (84 %), but $\mathrm{N}_2\mathrm{O}_5$ conversion efficiencies were similar. The decreased NO_3 transmission efficiencies were consistent with the inlet residence times, which were somewhat longer with the inlet design used in that campaign than those described in this paper.

4.4 Sensitivity to aerosol, VOC, and water vapor

The sensitivity of the instrument against several possible loss processes that could result from sampling in ambient air was investigated (rather than dry, synthetic air), including water vapor, aerosols, and VOCs. All test experiments described in this section were performed by using the in-field calibration system as a source for either NO_3 or $\mathrm{N}_2\mathrm{O}_5$. Different contaminants were added to the dilution flow of the calibration system, and measured extinctions with and without the contaminants were compared.

Furthermore, the sensitivity of the $\mathrm{N}_2\mathrm{O}_5$ transmission efficiency to humidified air, which could introduce wall losses that are not accounted for by the investigations described in the previous section, was determined. The relative humidity of the air used for the dilution of $\mathrm{N}_2\mathrm{O}_5$ sampled from the calibration source was varied by mixing a flow of air saturated with water vapor that had been bubbled

through a liquid water sample with dry zero air. Relative humidity was measured by a standard capacitive hygrometer. N_2O_5 concentrations at different relative humidities (up to 95 % at room temperature (293 K)) were compared to the concentration in dry zero air. The concentration was invariant with relative humidity to within 0.7 %. This confirms that N_2O_5 hydrolysis on Teflon surfaces does not affect the N_2O_5 measurement. This might be partly due to the fact that the pressure in the system is significantly reduced so that the partial pressure of water vapor inside the instrument was smaller than that in the ambient air.

Accumulation of aerosol on the inlet filter could result in variable loss of N_2O_5 (or NO_3, depending on the aerosol type).
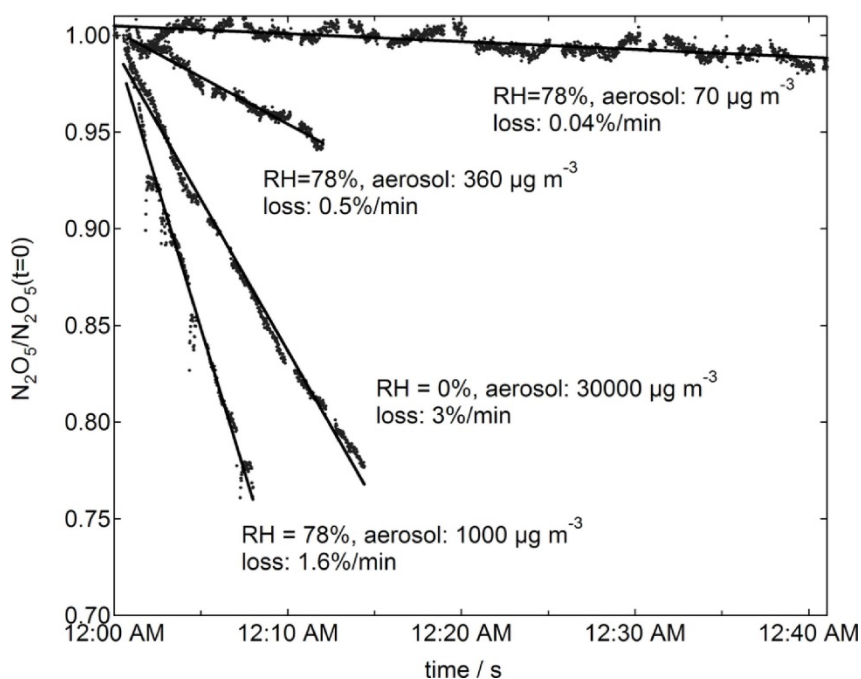
Figure 4-6: Measured N_2O_5 loss for sampling of inorganic aerosol $(NH_4)_2SO_4$ in humidified zero air (RH) 78 %) and dry zero air. The maximum of log-normal size distribution of aerosols is at a diameter of 100 nm.

To test the effect of this process, aerosols were added to the dilution flow of the calibration system. Zero air was humidified as described above to 78 % relative humidity at room temperature in three experiments and dry zero air was used in the other experiment. Ammonium sulfate aerosols were produced by a collision-type atomizer [73] from a 1 % solution in water. The size distribution was measured by a custom-designed differential mobility analyzer showing a center of the number distribution of ~100 nm in all experiments. The aerosol concentration was determined by a standard particle counter. Both measurements together were used to estimate the mass load that was applied to the instrument.

Figure 4-6 shows the time evolution of the measured N_2O_5 relative to the initial N_2O_5. A rapid decrease of the N_2O_5 signal in all experiments can be observed, indicating that aerosol accumulation on

the filter decreases the transmission efficiency. The measured N_2O_5 signal returned to its initial value when the filter in the inlet system was changed indicating that accumulation of aerosols on the filter, rather than on the wall of the Teflon tubing, was responsible for the additional loss of N_2O_5. Thus, regular filter changes are necessary to prevent degradation of the transmission efficiency for N_2O_5.

All mass loads used during these experiments were large relative to typical ambient conditions [67, 69, 70]. The loss was ~3 %/min on dry aerosol at a mass load of 30 000 μg m^{-3} and ~6-15 times faster with a comparable mass load at relative humidity of 78 % (Figure 4-6). At a typical mass load in polluted ambient air of ~20 μg m^{-3}, a decrease of 0.12 %/h is expected from a linear extrapolation for dry aerosol and a maximum of 2.0 %/h for humid conditions. It can be concluded from these measurements that a filter change interval of 1 h is sufficient to avoid N_2O_5 loss on the filter due to accumulation of aerosol under most conditions. However, the automatic filter changer system allows a change of filter more frequently if aerosol mass loadings are large. Alternatively, under conditions of low particle loading (e.g., remote locations or high altitude), the required interval for filter changes may be considerably longer than 1 h.

A similar test to that of N_2O_5 uptake on aerosols was performed to investigate a possible decrease of the transmission efficiency of NO_3 because of the interaction of NO_3 with organic aerosols. The experiment was performed in the same way as that for the inorganic aerosol, but aerosols were produced from an adipic acid solution in water (mass load, 150 μg m^{-3}; maximum aerosol diameter, 100 nm). However, no decrease of the instrument's transmission efficiency could be observed over a sampling period of 1 h.

Table 4-1 : Contribution to the 1σ accuracy of measured trace gas concentrations.

	N_2O_5 (%)	NO_3 (%)	NO_2 (%)
Cross-section	±4	±4	±3
R_L	±3	±3	±3
Inlet loss	±1	±2	na*
Filter aging	+3	+3	na*
Sum	-8, +11	-9, +12	±6

* not applicable

NO_3 is highly reactive toward many hydrocarbons [66]. We tested whether a degradation of the system's transmission efficiencies can be observed if a mixture of reactive hydrocarbons is sampled. A GC calibration standard (acetaldehyde 16.31 ppmv, ethanol 8.3 ppmv, *n*-pentane 7.89 ppmv, acetone 8.69 ppmv, and isoprene 7.21 ppmv) was diluted by a factor of 4000, resulting in a VOC mixing ratio

of 12 ppbv. No significant changes of the measured transmission efficiencies for NO_3 or N_2O_5 could be observed when this mixture was sampled over a period of 6 h. Thus, reactive VOC does not appear to adsorb on the Teflon surfaces to a large enough extent to significantly affect the transmission efficiency.

4.5 Accuracy of measurements

The accuracy of measurements achieved with this instrument is summarized in Table 4-1. In principle, the accuracy of N_2O_5 and NO_2 measurements also depend on the accuracy and the detection sensitivity with which NO_3 and O_3, respectively, is measured, because only the sum of both is detected in this instrument. An explicit expression for taking this into account is given by refs 11 and 17 using error propagation. Here, accuracies are given for measurements of single species.

The overall 1σ accuracy is determined by the uncertainties in the absorption cross-section (± 4 % [49, 60, 74]), path length ratio ($_{RL}$, ± 3 %), and transmission efficiencies (1% for N_2O_5, 2 % for NO_3).

Because some of the errors in this sum are likely to be systematic (e.g., the absorption cross-section and relative path length), we have added the contributions to the error linearly rather than in quadrature.

Although to our current understanding the decrease of transmission efficiencies due to the aging of the filter is small, if the filter in the inlet system is exchanged regularly, we add the standard deviation of the average of measured in-field calibrations during our last field mission (NO3Comp campaign in Jülich, Germany) as an upper limit of a possible filter aging. Filter aging adds a loss that would decrease the transmission efficiency. Therefore, this contribution to the accuracy is asymmetric and can only lead to an increased correction factor for NO_3 and N_2O_5 (+3 % for NO_3 and N_2O_5).

All contributions add up to an overall 1σ accuracy for N_2O_5 concentrations of -8, +11 %, for NO_3 concentrations of -9, +12 % and for NO_2 concentrations of ± 8 %, where the - signs indicate that the actual value is low/high relative to the measurement. NO_3 and N_2O_5 measurements are now approximately twice as accurate compared to previous reported values (± 25 % for NO_3 and ± 20 % for N_2O_5 [1]). The largest contribution to the error in the current instrument is now due to the uncertainty in the NO_3 cross-section itself rather than the inlet transmission efficiencies.

4.6 Summary

This article has described the further development of the NOAA pulsed cavity ring-down instrument used to measure simultaneously ambient NO_3, N_2O_5, and NO_2 concentrations with high sensitivity. The most important difference between previous descriptions of this instrument and that given in this paper include the following: (1) inclusion of four separate optical cavities, two each at 662 and 532 nm, with the 532 nm extinction measurements located immediately downstream in the sample flow from the 662 nm measurement; (2) reduction in the residence time of the sample air achieved by

operating at reduced pressure and in narrower diameter tubing; and (3) inclusion of a calibration for inlet transmission efficiencies based on production of either NO_3 or N_2O_5 from a stable source followed by titration of NO_3 to NO_2, which does not undergo significant loss in the instrument.

Possible losses of NO_3 and N_2O_5 were investigated via a series of laboratory tests. The overall NO_3 transmission efficiency was found to be 92 ± 2 % while the N_2O_5 conversion and transmission efficiency is 97 ± 1 %. Both values are in agreement with an independent determination of the transmission efficiencies using our in-field calibration system (90, 97 %, respectively). As a consequence, the accuracy has been significantly increased to -8, +11 % for N_2O_5 and -9, +12 % for NO_3.

Several systematic tests were performed to investigate possible changes of the transmission efficiencies against specific contaminations found in ambient air. Whereas gas-phase contaminations do not affect instrument performance, accumulation of aerosols on the filter can lead to a significant decrease of the transmission efficiency of N_2O_5. This emphasizes that a regular change of the filter with an interval of ~1 h is required to prevent that the transmission efficiency drops significantly with time for atmospherically relevant aerosol mass loads.

5. Publication C:

A sensitive and versatile detector for atmospheric NO₂ and NOₓ based on blue diode laser cavity ring-down spectroscopy

Authors:

Hendrik Fuchs,[1,2] William P. Dubé,[1,2] Brian M. Lerner,[1,2] Nicholas L. Wagner,[1] Eric J. Williams,[1,2] Steven S. Brown[1]

[1]*Earth System Research Laboratory, NOAA, Boulder, Colorado 80305, USA.*

[2]*Cooperative Institute for Research in the Environmental Sciences, University of Colorado, Boulder, Colorado 80309, USA.*

Abstract:

A sensitive, small detector was developed for atmospheric NO_2 and NO_x concentration measurements. NO_2 is directly detected by laser diode based cavity ring-down spectroscopy (CaRDS) at 404 nm. The sum of NO and NO_2 (=NO_x) is simultaneously measured in a second cavity by quantitative conversion of ambient NO to NO_2 in excess ozone. Interferences due to absorption by other trace gases at 404 nm, such as ozone and water vapor, are either negligible or small and are easily quantified. The limit of detection is 22 pptv (2σ precision) for NO_2 at 1 s time resolution. The conversion efficiency of NO to NO_2 is 99 % in excess O_3. The accuracy of the NO_2 measurement is mainly limited by the NO_2 absorption cross-section to ±3 %. Because of the formation of undetectable higher nitrogen oxides in subsequent reactions of NO_2 with ozone in the NO_x channel, the (1σ) accuracy of the NO_x measurement is increased to approximately ±5 % depending on the level of NO_x. The new instrument was designed to be easily deployed in the field with respect to size, weight and consumables. Measurements were validated against a photolysis/chemiluminescence detector during six days of sampling ambient air with collocated inlets. The data sets for NO_2, NO and NO_x exhibit high correlation and good agreement within the combined accuracies of both methods. Linear fits to the correlation data for all three species give similar slopes of 0.99 in ambient air.

5.1 Introduction

Nitrogen oxides, NO_x (=NO and NO_2), emitted from both natural (e.g. soil, lightning) and anthropogenic (e.g. combustion) sources, play a vital role in many aspects of atmospheric chemistry. For example, the cycling process between NO and NO_2 is the only known mechanism for ozone production within the troposphere and affects air quality and oxidant burdens on both regional and global scales [75]. Because of their importance, many direct and indirect techniques to measure both NO and NO_2 have been developed over the past decades. Nitric oxide (NO) is most commonly measured by its chemiluminescence (CLD) reaction in excess O_3 to produce electronically excited NO_2. The method is readily extended to NO_2 using a heated molybdenum surface or a photolytic converter to convert some fraction of NO_2 to NO [76, 77]. While CLD methods are available as both commercial and custom built, research grade instruments, they require toxic excess reagents (e.g. NO, O_3) and vacuum systems. Furthermore, the indirect NO_2 detection may be subject to interference from conversion of compounds other than NO_2 to NO in commercial instruments [78, 79]. It is thus less precise than the NO detection due to the requirement for subtraction of two signals, and requires careful calibration of the NO_2 conversion fraction. Direct detection methods for NO_2 via, for example, mid infrared tunable diode laser spectroscopy (TDLS) [80] and laser induced fluorescence (LIF) [81] have addressed concerns related to interference in the NO_2 to NO conversion process. During the past decade, cavity ring-down spectroscopy (CaRDS) and its related forms, cavity enhanced (CEAS) and attenuated phase shift spectroscopy (CAPS) have become powerful techniques to detect atmospheric trace gases [44] and have been applied to NO_2 detection [82-84]. The capability to also detect NO indirectly in such instruments by its conversion to NO_2 in excess O_3 has been suggested only recently for LIF [85] or CaRDS [86], although quantitative conversion has not been demonstrated for either case.

Here, we report the design and validation of an instrument for detection of NO_2 and total NO_x (=NO + NO_2) using a visible (404 nm) diode laser, based on the CaRDS technique (NOxCaRD). This instrument has several key advantages compared to those described in the recent literature [44, 82-84, 86] and is demonstrably superior to our previously reported, pulsed CaRDS instrument for NO_2 detection at 532 nm [48]. First, the light source is a simple, lightweight, low power, commercially available Fabry-Perot diode laser. The bandwidth of this source (0.5 nm) is sufficiently wide for passive coupling of the light source to an optical cavity without the need for a complicated scheme to match the laser frequency to the cavity resonances. Second, because NO_2 absorption is the dominant gas phase extinction at 404 nm, the method is not subject to interferences from ozone at ambient levels. This is particularly important because it allows quantitative conversion of NO to NO_2 with excess ozone such that the sum of both is detected as NO_2 in a second, parallel channel. Third, the instrument has reduced requirements for size, power, weight, and vacuum, especially compared to methods such as CLD, and no requirement for toxic reagents (the O_3 mixing ratio is much smaller (15 ppmv) compared to the requirement of CLDs (few percent)). Fourth, the limit of detection (LOD) is sufficient for NO_x

measurements even in remote regions (LOD(2σ) = 22 pptv in 1 s, 7 pptv in 10 s), and is better than that reported to date for other CaRDS instruments and comparable to other direct NO_2 methods (e.g. absorption detector: 40 pptv, 2σ, 10 s [87], fluorescence detector: 15 pptv, 2σ, 10 s [81]). Fifth, the instrument has a rapid time response (1 s), potentially enabling measurement from mobile platforms such as aircrafts. Lastly, the validation methods described herein demonstrate accuracy better than 3 % for simultaneous measurement of NO_2 and total NO_x over a wide dynamic range.

5.2 Experimental aspects

5.2.1 NO_2 detection by cavity ring-down spectroscopy

Cavity ring-down spectroscopy is a powerful, highly sensitive method to detect various atmospheric trace gases. A detailed description of its principle can be found elsewhere [44] and is only briefly described here. Light from a continuous wave (cw) diode laser (Power Technology, Fabry-Perot diode model IQμ series, 40 mW output power), aligned on the axis of a two-mirror optical cavity, is modulated on/off. After the buildup of light intensity in the cavity during the on-time, the time dependence of the light intensity transmitted through the end mirror is observed subsequently to rapidly turning off the laser. The time constant of the exponentially decreasing intensity gives a direct extinction measurement. The time constant with (τ) and without (τ_0) the absorber present in the cavity is used to calculate the number density of the absorber by

$$[\mathrm{NO}_2] = \frac{R_\mathrm{L}}{c\,\sigma_{\mathrm{NO}_2}}\left(\frac{1}{\tau} - \frac{1}{\tau_0}\right) \tag{5-1}$$

where, σ_{NO_2} is the absorption cross-section, c is the speed of the light, and R_L is the ratio of the total cavity length to the length over which the absorber is present in the cavity (see below).

A schematic overview of the optics and air sampling system is shown in Figure 5-1. The output of a diode laser with a center wavelength at 403.96 nm and a line width of 0.5 nm (full width half-maximum) is directly modulated by a square wave signal (on/off) at a repetition of 2 kHz with a duty cycle of 50 %. The laser shut off time (<1 μs) is much shorter than the observed time constants. The broadband laser output has been found to couple directly into the cavity without, for example, a requirement for active matching of any mode structure present in the laser output to the resonant frequencies of the cavity or a scheme to increase the cavity mode density [32, 88]. The cavity mirror reflectivity is 99.9965 % (total loss 35 parts per million per pass, ppm) as determined from ringdown time constants larger than 44 μs for a mirror separation of 95 cm in dry zero air at ambient pressure in Boulder, CO (1600 m ASL, p) 840 hPa). Extinction due to Rayleigh scattering at this pressure is 30 ppm/pass, comparable to mirror reflectivity, necessitating measurements of temperature and pressure in each cavity to track variation in the background ring-down time constant with the air sample number

density. Small purge flows (30 cm^3 per minute of zero air at each mirror) are used to maintain mirror cleanliness. Consequently, the ratio of the total length to the length over which the absorber is present, R_L in equation 5-1, is larger than unity. This value was measured as 1.14 in earlier experiments for an instrument with identical cavities [2].
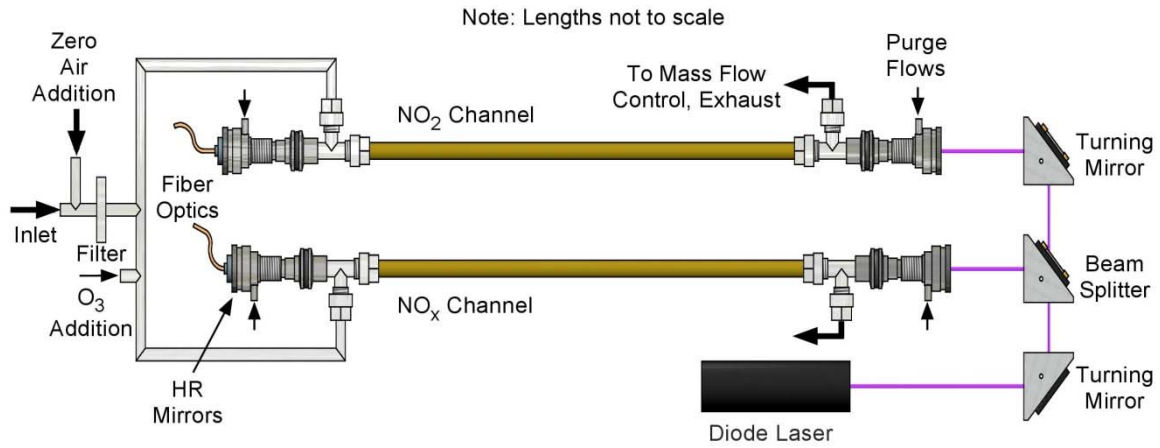
Figure 5-1: Schematic view of the two channel cavity ring-down instrument for atmospheric NO₂ and NOₓ measurements. NO₂ is directly detected in one channel and the sum of ambient NO₂ and NO is detected in the other by converting NO to NO₂ in excess O₃.

Air is sampled through Teflon lines (2 L per minute for each cavity) and filtered by a Teflon filter (1 μm pore size, but removes much smaller particles when used in gas, rather than liquid sampling) to remove optically active particles. Laser, turning optics and cavities are mounted in a cage system that is constructed from eight carbon fiber rods (outer diameter 12.8 mm, length 1 m) that have a small thermal expansion coefficient in order to minimize the sensitivity of the alignment to temperature changes of the environment. The ring-down time constant without the target absorber NO₂, τ_0 in equation 5-1, is measured in an excess flow of zero air for 5-10 s every 5-10 min. This frequency of zero measurements was found to be sufficient to track drifts in the zero ringdown time constant. Zero air time constants are linearly interpolated between two measurements in the data evaluation. Ring-down time traces are acquired with an oscilloscope card (14 bit, 2.5 MS/s sampling rate), and 1600 traces per second are averaged in order to achieve an overall time resolution of 1 s. The time constant is fitted to a single exponential decay with three parameters (time constant, amplitude, offset) by using general least-squares error fit (Levenberg-Marquardt) of the averaged ring-down trace, which offers no significant loss in accuracy compared to averaging fits of individual traces and is computationally more efficient [8]. The relative residual of the fit function is invariant with time to within 1 %.

5.2.2 Chemical conversion of NO for detection of NO$_x$

As shown in Figure 5-1, the instrument incorporates two separate cavities, one of which provides a measurement of total NO$_x$ subsequent to conversion of NO to NO$_2$ in excess O$_3$. The conversion is essentially quantitative.

$$NO + O_3 \rightarrow NO_2 + O_2 \tag{5-2}$$

Ozone is produced from O$_2$ photolysis at 185 nm by flowing 12 cm^3 per minute of oxygen over a low pressure discharge mercury lamp (mixing ratio is approximately 15 ppmv after mixing with the sampled air). The small but nonzero O$_3$ absorption at 404 nm reduces the ring-down constant by approximately 0.2 μs and provides a direct measure of the amount of added O$_3$ via periodic switching of the ozone flow to a vent line with a solenoid valve. The periodic switch also serves to compare ambient NO$_2$ measurements in the absence of added O$_3$ in both channels to define any small, intrinsic differences between them, such as dilution due to mirror purge flows. This is crucial if NO concentrations are small, because measurements of the two channels are subtracted to calculate the NO concentration.

A length of Teflon tubing (length 36 cm, i.d. 9.5mm) serves as reactor for the NO conversion, which is quantitative (>99 %) within the 0.9 s residence time of the reactor at 20°C [72]. A linear response over the entire atmospherically relevant range in NO (at least to several hundred ppbv) is expected because the reaction kinetics are pseudo-first order in large excess of ozone. Further oxidation of NO$_2$ to NO$_3$ and N$_2$O$_5$ is much slower and results in a maximum correction of 2 % to the NO$_x$ measurement as discussed below.

5.3 Results and discussion

5.3.1 NO$_2$ detection performance

The effective absorption cross-section for NO$_2$ at 404 nm was determined by sampling known NO$_2$ concentrations produced by quantitative conversion of ozone to NO$_2$ in excess NO and by reference to the existing, 532 nm NO$_2$ CaRDS instrument. The resulting value of 6.1×10^{-19} cm^2 is consistent with a calculation in which the laser line width, which was measured by a high resolution spectrograph, is convolved with several independent, high resolution measurements of the NO$_2$ absorption cross-section around 404 nm reported in literature (5.9×10^{-19} cm^2 [89]). The accuracy of this measurement of 3 % is given by the uncertainty of the ozone concentration which was measured and produced by a commercial ozone monitor/calibrator (Thermo Electron, model 49i, accuracy 2 %) and the uncertainty in the dilution of the ozone flow (1 %). Any uncertainty of the measurement of R_L (see above) is included in this accuracy, since the calibration procedure determines the ratio of σ/R_L directly, so that the choice of R_L is somewhat arbitrary (equation 5-1). The dependence of the absorption cross-section on temperature is small [89] and suggests at most a modest effect within the operational temperature

range of the instrument, i.e. a change of -2.2 % is expected between 293 and 260 K. The spectral output of the laser is stable on the time scale of measurements, and no drift of the center wavelength was observed over several months. The diode is also temperature stabilized at 25°C so that the temperature in the instrument does not affect the center wavelength. Even small changes in the diode temperature due to, e.g. the precision of the temperature control loop would only lead to negligible changes in the output since diode lasers at this wavelength are much less sensitive to temperature compared to, e.g. laser diodes with outputs at longer wavelengths.

The baseline precision of the NO_2, NO_x, and NO measurements was investigated by continuous sampling of zero air for a period of 12-16 h. Equivalent mixing ratios were calculated for conditions of 1013 hPa and 20°C. Figure 5-2 shows the 1σ precision for integration times between 1s and 10 min. The precision approximately follows a square root dependence up to an integration time of 1 min (i.e. 11 pptv at 1 s and 2 pptv at 1 min). The baseline does not show a long-term trend, indicating that the number and duration of the zero data acquisition scheme described above are sufficient. Figure 5-2 also shows the precision of NO detection while sampling a constant NO mixing ratio of 43 ppbv in zero air. The precision again follows approximately a square root dependence up to an integration time of 1min increasing the precision from 100 pptv (1 s) to 11 pptv (60 s). This high precision of measurements (<0.3 %) indicates the reliability of the NO conversion in addition to the low baseline noise. Acquisition of zero measurements in zero air makes this instrument vulnerable to interferences due to any other species contained in the sampled air that absorbs at 404 nm. To our knowledge, the only species that are of significant concern are water vapor and R-dicarbonyls. In reference [86] a large water vapor interference of a CaRDS instrument detecting NO_2 at 405 nm was reported, which is not consistent with the known spectroscopy of water vapor [90]. This possible interference was investigated carefully here. Zero air containing different levels of water vapor (relative humidity: 10-80 %) was sampled and the extinction measured. The result (Figure 5-3) clearly shows a linear decrease of the extinction with increasing water vapor rather than an increase due to absorption, contradictory to the results of reference [86]. The slope of the linear fit gives a cross-section difference between water vapor and dry air of 0.5 $\times 10^{-26}$ cm^2. This change is consistent with a Rayleigh scatter cross-section for water vapor that is approximately 70 % smaller than that of dry zero air (σ_{Ray}(air) = 1.61 $\times 10^{-26}$ cm^2) [91], in agreement with theoretical calculations and measurements [92]. Thus, only a well-understood correction is required to account for the difference in Rayleigh scattering between the dry zero air used for background measurements and humid, ambient air. For example, at 80 % RH (22°C), this correction is equivalent to 150 pptv NO_2. Water vapor variations for ambient air during ground-based sampling are typically on a time scale much longer than the repetition rate of CaRDS measurements and that of instruments measuring the water vapor so that this correction is unlikely to reduce the precision of NO_2 measurements.
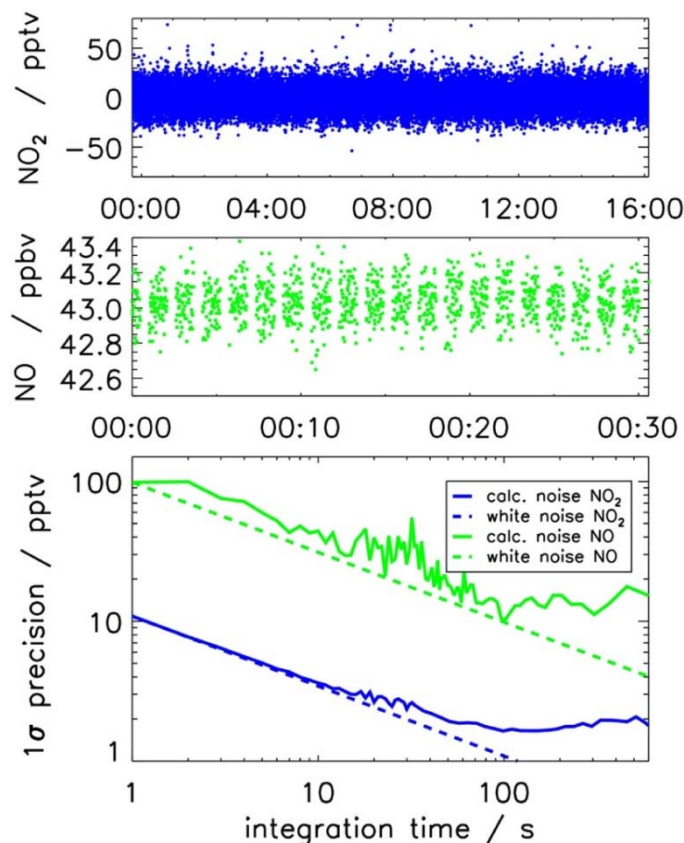
Figure 5-2: Dependence of 1σ precision on integration time (Allan deviation plot) from a 16 h period of measurement in zero air. The upper panel shows the time series of the equivalent NO_2 mixing ratio at 1013 hPa and 20 °C The middle panel shows a period of measurement of a constant NO mixing ratio of 43 ppbv. The dependence of the calculated 1σ precision on the integration time between 1 s and 10 min for the baseline measurement and sampling of NO is shown in the lower panel. The dashed line is the precision expected for purely random noise.

In contrast to CaRDS instruments that measure NO_2 from optical extinction at longer wavelengths, such as 532 nm, there is no significant interference from ozone absorption at 404 nm, because the ozone absorption cross-section is approximately 4×10^4 times smaller than that of NO_2 ($\sigma_{O_3} = (1.49 \pm 0.01) \times 10^{-23}$ cm^2). The absorption cross-section of O_3 was determined here experimentally by comparing the 404 nm and the 532 nm extinctions for various ozone concentrations. The measurement is within the range of the different literature values, although spectra differ from one another by more than an order of magnitude at this wavelength [93].

The only significant trace gas interference we are currently aware of is due to absorption of R-dicarbonyls, principally glyoxal and methyl glyoxal, whose absorption cross-sections are approximately ten times smaller than that of NO_2 at 404 nm [94, 95]. Glyoxal is a product of the photo-oxidation of VOCs. Glyoxal mixing ratios up to 1.85 ppbv (e.g. Mexico City) have been observed in highly polluted environments [96], although concentrations were less than 10 % of NO_2, thereby contributing an artifact that is less than 1 % of the reported NO_2 mixing ratio. In forested environments, smaller levels of up to 200 pptv have been observed [97], constituting an interference up to 20 pptv for NO_2.

All NO_2 detectors can exhibit interferences due to thermal decomposition of thermally labile species like N_2O_5, peroxyacyl nitrates (PANs) and pernitric acid (HO_2NO_2) in the inlet system. These interferences are minimized in this instrument by maintaining the temperature and pressure at near ambient conditions to minimize thermal decomposition of such labile species. For example, the optical head can be mounted in a weather-proof enclosure at the point of sampling to maintain it at ambient temperature. Field tests of this strategy have so far been successful under summer conditions with diurnal temperature variations of up to 20°C. Finally, conversion of NO to NO_2 in ambient ozone within the inlet system can comprise a small (typically about 2 % of ambient NO for a 1 s inlet residence time) but correctable artifact to the NO_2 measurement, as has been discussed for other NO_2 instruments in the recent literature [48].
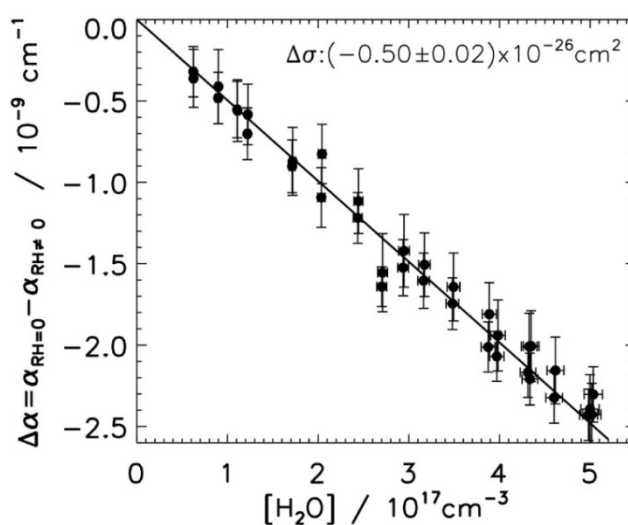
Figure 5-3: Dependence of the measured extinction at 404 nm on varying levels of water vapor added to a constant flow of zero air. The resulting decrease in extinction with increasing water vapor concentration is due to smaller Rayleigh scatter cross-section of water compared to zero air.

5.3.2   NO conversion efficiency

Because the rate constant for the conversion reaction 5-2 is strongly temperature dependent [72], the optimization of the sampling conditions (i.e., residence time, ozone concentration) to achieve a conversion efficiency >99 % at 20°C requires a small but straightforward correction at other temperatures based on the assumption of pseudo first order loss of NO in excess O_3. The efficiency of the NO to NO_2 conversion reaction in excess O_3 (equation 5-2) is also limited by the formation of higher nitrogen oxide species from further oxidation of NO_2:

$$NO_2 + O_3 \rightarrow NO_3 + O_2 \qquad\qquad (5\text{-}3)$$

$$NO_3 + NO_2 \leftrightarrow N_2O_5 \qquad\qquad (5\text{-}4)$$

The conversion efficiency was determined experimentally by sampling zero air that contained a constant NO concentration and varying the excess ozone concentration. The absorption cross-section of NO_3 and N_2O_5 are not significant [10, 98] at 404 nm so that these species are not detected. The measurement agrees well with results from numerical model calculations including reactions between, O_3, NO, NO_2, NO_3, and N_2O_5. Because the correction for production of NO_3 and N_2O_5 would be less than 1 % for the likely range of atmospheric sampling parameters, measurements are not explicitly corrected for this loss, but the additional uncertainty is reflected in the larger quoted accuracy for the NO measurement.

The reaction time was calculated from the same measurement for low ozone concentrations, where the formation of NO_3 and N_2O_5 is negligibly small, by fitting these data to a single exponential. This results in a reaction time of 1 s which is consistent with the residence time calculated from the assumption of plug flow in the reactor at the measured total flow rate. Tests of the stability of the conversion efficiency by comparison of CLD and CaRDS measurements of NO (where the latter is the difference of CaRDS NO_2 and NO_x measurements) generated upon repeated additions of an NO standard to zero air over a period of 16 h showed variability smaller than 1 % (2σ).

Under conditions where NO is absent, the loss of NO_2 on the NO_x channel due to oxidation by ozone is more rapid since it begins immediately after mixing of ozone into the sample air rather than subsequent to the conversion of NO. The loss rate is sensitive to temperature as well as to the NO_2 level, because of the increase of the $NO_2 + O_3$ reaction rate constant with increasing temperature. It rises by a factor of 2 within the temperature range of 0-35°C (operational temperature range of the instrument) and it changes by 25 % over a range of NO_2 mixing ratios from 0.1 to 160 ppbv. Our current approach is to neglect the dependence on the NO_2 concentration, which adds to the uncertainty of the NO_x measurement, but to apply a linear correction that depends on temperature derived from a fit of the dependence of the calculated loss rate on temperature.

5.3.3 Comparison of instruments

Measurements of the new CaRDS instrument were validated by comparison to measurements with a photolysis/chemiluminescence detector.

First, measurements were compared for artificial mixtures of NO_x in synthetic air with variable amounts of NO and NO_2. An NO standard (Scott Marin) was mixed into synthetic air producing variable NO concentrations. Various amounts of ozone were added to convert part of the NO to NO_2 to achieve NO_2 to NO_x ratios up to 95 %. Correlations of measurements for all three species are highly linear and exhibit similar slopes of 0.99 with a negligible intercept.

Variability of both NO and NO_2 during ambient measurements was largely due to local NO_x sources from passing cars and a nearby construction project at the measurement site. This variability

tested both the time response and dynamic range of the CaRDS NO_x instrument, with NO_2 mixing ratios from 0.1-120 ppbv and NO mixing ratios from below the detection limit (at nighttime) up to 300 ppbv (1 s time resolution). Figure 5-4 shows time series and correlation plots for ambient NO_2, NO_x, and NO. Data were averaged to 1 min time resolution (6300 points for NO_2 and NO_x, 4000 points for NO, as described below) to average over synchronization differences between instruments in rapidly varying plumes. During the first part of the comparison, the CaRDS instrument was configured with the NO_x channel in series with the NO_2 channel, leading to larger scatter in NO derived from the subtraction due to timing errors in the measurements at the 1 s time scale. NO data is not shown for this period. During the latter part of the comparison, the channels were configured in parallel, as shown in Figure 1, although there was still some scatter apparent in the data, due most likely to synchronization of the subtraction between the channels. Slopes, intercepts (unity and zero, respectively, to within fit errors) and correlation coefficients ($R^2 > 0.99$) for the instrument comparison are shown in the figure. Agreement between instruments was excellent, although there was considerably larger scatter in the NO data, likely arising from subtraction between imperfectly synchronized NO_2 and NO_x channels for the September, 2008 comparison.

Results from a separate experiment to test the performance of the NO measurement only, conducted in May 2009, are shown in Figure 5-5. This test included sampling of synthetic NO in zero air, during which the repeatability of the NO conversion was demonstrated, and additional measurements in ambient air. Figure 5-5 shows only the NO data from the ambient air test since the NO_2 channel of the CLD was not operating at this time. Sampling was conducted from a shared inlet, rather than co-located inlets, in order to better facilitate instrument comparison on a 1 s time scale. Correlation of the NO measurements was substantially improved, even at 1 s time resolution, indicating that one driver of variability of scatter in the previous measurement was the separation of inlets.

The comparisons of the 404 nm CaRDS to a standard, research grade instrument for NO_2 and total NO_x has demonstrated the potential of CaRDS for accurate, sensitive and rapid measurements of these compounds in a relatively simple instrument package. The direct measurement of NO_2 by this technique may represent an improvement over the indirect measurement utilized in CLD instruments. The indirect measurement of NO is less precise than the direct CLD measurement, but will be useful in polluted regions where sensitivity or precision below 0.1 ppbv is not as critical.
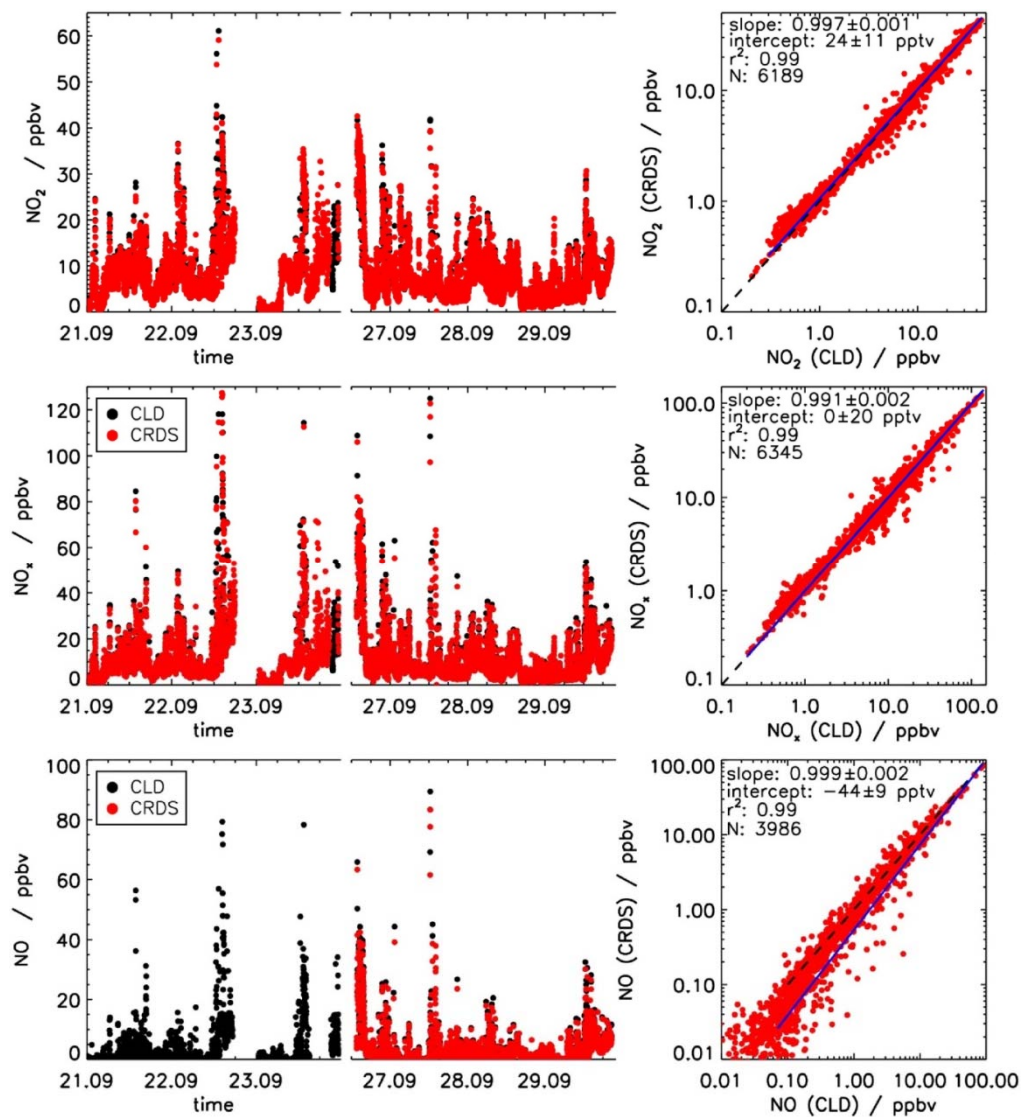
Figure 5-4: Time series and correlation between the 404 nm cavity ring-down instrument and the chemiluminescence detector for ambient NO₂, NO and NOₓ measurements in September 2008 for 1 min averaged data. Slope and intercept of linear fit (blue line) demonstrate good agreement between both measurements.
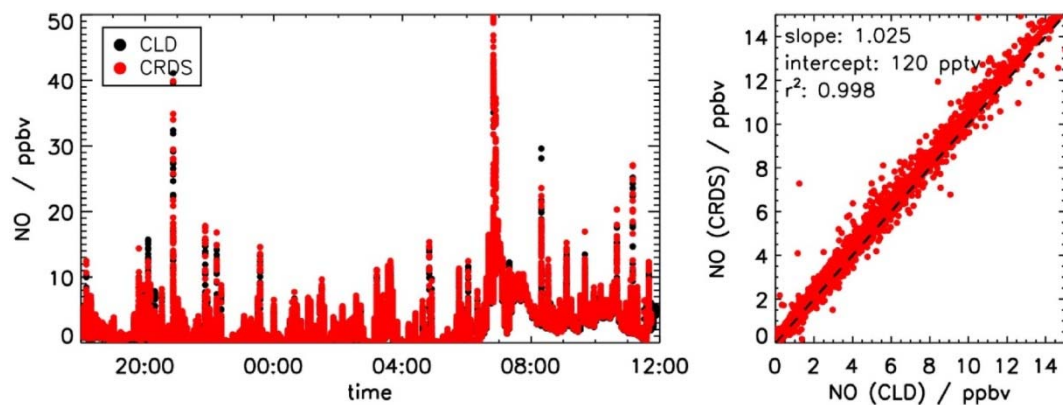
Figure 5-5: Comparison between measurements of the 404 nm cavity ring-down instrument and the chemiluminescence detector for ambient NO and NOₓ measurements in May 2009 for 1 s data.

6. Publication D:

Diode laser-based cavity ring-down instrument for NO₃, N₂O₅, NO, NO₂ and O₃ from aircraft

Authors:

Nicholas L. Wagner,[1,2] William P. Dubé,[1,2] Rebecca A. Washenfelder,[1,2] Cora J. Young,[1,2] Ilana B. Pollack,[1,2] Thomas B. Ryerson,[1] Steven S. Brown[1]

[1]*Earth System Research Laboratory, NOAA, Boulder, Colorado 80305, USA.*

[2]*Cooperative Institute for Research in the Environmental Sciences, University of Colorado, Boulder, Colorado 80309, USA.*

Abstract

This article presents a diode laser-based, cavity ring-down spectrometer for simultaneous in-situ measurements of four nitrogen oxide species, NO_3, N_2O_5, NO, NO_2, as well as O_3, designed for deployment on aircraft. The instrument measures NO_3 and NO_2 by optical extinction at 662 nm and 405 nm, respectively; N_2O_5 is measured by thermal conversion to NO_3, while NO and O_3 are measured by chemical conversion to NO_2. The instrument has several advantages over previous instruments developed by our group for measurement of NO_2, NO_3 and N_2O_5 alone, based on a pulsed Nd:YAG and dye laser. First, the use of TTL modulated diode lasers reduces the requirements for power and weight and eliminates hazardous materials. Second, detection of NO_2 at 405 nm is more sensitive than our previously reported 532 nm instrument, and does not have a measurable interference from O_3. Third, the instrument includes chemical conversion of NO and O_3 to NO_2 to provide measurements of total NO_x ($=NO+NO_2$) and O_x ($=NO_2+O_3$) on two separate channels; mixing ratios of NO and O_3 are determined by subtraction of NO_2. Finally, all five species are calibrated against a single standard based on 254 nm O_3 absorption to provide high accuracy. Disadvantages include an increased sensitivity to water vapor on the 662 nm NO_3 and N_2O_5 channels and a modest reduction in sensitivity

for these species compared to the pulsed laser instrument. The in-flight detection limit for both NO_3 and N_2O_5 is 3 pptv (2σ, 1 s) and for NO, NO_2 and O_3 is 140, 90, and 120 pptv (2σ, 1 s) respectively. Demonstrated performance of the instrument in a laboratory/ground based environment is better by approximately a factor of 2–3. The NO and NO_2 measurements are less precise than research-grade chemiluminescence instruments. However, the combination of these five species in a single instrument, calibrated to a single analytical standard, provides a complete and accurate picture of nighttime nitrogen oxide chemistry. The instrument performance is demonstrated using data acquired during a recent field campaign in California.

6.1 Introduction

The nitrate radical, NO_3 and its reservoir species, dinitrogen pentoxide (N_2O_5) are important trace gases in the nocturnal atmosphere [10]. NO_3 is formed by reaction of ozone with NO_2 (reaction equation 6-1) and reacts with NO_2 to reversibly form N_2O_5 (reaction equation 6-2).
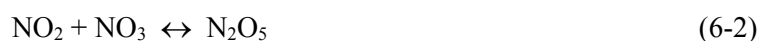
$$NO_2 + O_3 \ \rightarrow \ NO_3 + O_2 \tag{6-1}$$

$$NO_2 + NO_3 \ \leftrightarrow \ N_2O_5 \tag{6-2}$$

These species are typically present at very modest levels during daytime (less than 1 pptv) because NO_3 undergoes rapid photolysis and reaction with NO, which is present during the day and in close proximity to large NO_x emission sources during the night.

$$NO_2 + \ h\nu \ \rightarrow \ NO_2 + O \tag{6-3}$$

$$\rightarrow \ NO + O_2$$

$$NO_3 + NO \ \rightarrow \ 2NO_2 \tag{6-4}$$

The nitrate radical is a strong oxidant and is consumed by reactions with biogenic VOCs and sulfur compounds, and some classes of highly reactive anthropogenic VOCs [66]. N_2O_5 undergoes heterogeneous uptake to aerosol. Its hydrolysis leads either to non-photochemical conversion of NO_x to soluble nitrate via production of HNO_3 [99], or to activation of photolabile halogens through formation of nitryl chloride, $ClNO_2$ [6, 100]. Thus, NO_3 and N_2O_5 are intermediates in a number of important atmospheric chemical transformations, and understanding their atmospheric concentrations is an important topic of current research.

Much of the prior database for understanding these processes was based on measurements of NO_3 by differential optical absorption spectroscopy (DOAS) over a long, open path or by passive techniques using natural light sources [18, 19, 68]. Such measurements have been extremely useful in developing an understanding of the factors that govern nighttime chemistry. In-situ instruments add to

this database by enabling measurements from mobile platforms, such as aircraft and ships (e.g. [101]), and from tall towers (e.g. [71]). The in-situ measurements are valuable for characterizing the strong vertical gradients characteristic of the nocturnal boundary layer or for measurements within the residual daytime boundary layer.

Cavity ring-down spectroscopy (CaRDS) is a sensitive technique for in-situ measurement of atmospheric trace gases [44]. In-situ measurement of NO_3 was first developed approximately a decade ago and was based on CaRDS with either a pulsed dye laser [8] or extended cavity diode laser [30]. Thermal conversion of N_2O_5 to NO_3 in a second channel enabled direct measurement of the sum of the two compounds and measurement of N_2O_5 itself by difference. This development ultimately led to the deployment of a CaRDS instrument for NO_3 and N_2O_5 on aircraft [1]. Although the pulsed laser system used in this instrument had a relatively small footprint, such laser systems are in general somewhat cumbersome for field instruments because of their requirements for power and weight (30 kg and 0.5 kW). In addition, the use of toxic dyes and solvents requires hazardous materials that are not ideal for field environments, especially aircraft.

The aircraft instrument described above also incorporated measurements of NO_2 by pulsed laser CaRDS at 532 nm by taking advantage of the Nd:YAG laser second harmonic that was used to pump the dye laser [48]. These NO_2 measurements required active subtraction of an interference from ozone, but were otherwise accurate [102]. These CaRDS NO_2 measurements have recently been further developed using a diode laser with a center wavelength near 405 nm [3]. Because there is no significant interference from ozone at this wavelength, this approach is capable of simultaneous detection of NO via its conversion to NO_2 in excess ozone. We have also recently demonstrated the analogous conversion of O_3 to NO_2 in excess NO [103].

In this paper, we describe a single CaRDS instrument based on diode lasers that measures NO_3, N_2O_5, NO, NO_2, and O_3. Unlike the previous instruments from our group, this instrument uses a diode laser near the maximum in the NO_3 absorption spectrum at 662 nm for the measurement of NO_3 and N_2O_5 [1]. This is advantageous in terms of size, weight, power consumption, and elimination of toxic dyes. The main disadvantage to this approach is its increased sensitivity to water vapor. Implications of the water vapor sensitivity for aircraft measurements are described further below. A second diode laser centered near 405 nm is used for detection of NO_2 by CaRDS and of NO and O_3 by chemical conversion to NO_2. The NO_2 channel provides not only a direct measurement of this compound, but also a method for calibrating the NO_3 and N_2O_5 measurements via the conversion of these compounds to NO_2 in excess NO as described by Fuchs et al. [3]. The NO_2 measurement is itself calibrated against a standard based on ultraviolet absorption of ozone at 254 nm as described by Washenfelder et al. [103], providing a common analytical standard for all five species measured by this instrument.

The combination of these five trace gases provides a complete picture of the nighttime chemistry shown in reaction equation 6-1 through reaction equation 6-4. Measurements of NO_2 and O_3 provide the source for NO_3 formation. Direct measurement of NO_3 and N_2O_5 allow for understanding of their chemistry in the nighttime atmosphere. Measurement of NO characterizes the most important nighttime sink for NO_3 in near source regions (e.g., low altitude over urban areas). This paper describes the design and operation of this instrument, and its deployment on aircraft.

6.2 Instrument description

CaRDS is commonly used for sensitive detection of trace gases and has been described in several reviews [41, 104, 105]. CaRDS is a way to measure direct absorption with high sensitivity because the optical path length is enhanced by a high finesse cavity formed by a set of two highly reflective mirrors. A laser is directed into the cavity, the optical intensity builds in the cavity, and then the laser is turned off quickly compared with the decay of optical intensity in the cavity. The exponential decay of light intensity from the cavity is monitored by measuring the light transmitted through the back mirror. When an absorber is present, the exponential decay time constant is reduced, providing an absolute measurement of optical extinction, as given in equation 6-5.

$$\sigma[A] = \alpha = \frac{R_L}{c\sigma}\left(\frac{1}{\tau} - \frac{1}{\tau_0}\right) \tag{6-5}$$

Here, σ is the absorption cross-section corresponding to the absorber, averaged under the spectrum of the laser, $[A]$ is the concentration of the absorber, α is the optical extinction coefficient (units of inverse length), c is the speed of light, τ and τ_0 are the exponential decay constants with and without the absorber in the cavity and R_L is the ratio of the total length of the cavity to the length over which the absorber is present.

The instrument described here consists of two largely independent parts that share a common set of electronics, data acquisition, frame and optical mounting system. The first part is the measurement of NO_3 and N_2O_5 using a 662 nm diode laser. The second is the measurement of NO_2, NO, and O_3 using an additional 405 nm diode laser. The two parts of the instrument have separate inlets that are only connected together during automated calibrations, as described further below. A schematic of the instrument is shown in Figure 6-1 with NO_3/N_2O_5 measurement framed in red and the $NO/NO_2/O_3$ measurement framed in blue. A photo of the instrument is shown in the right panel of Figure 6-1.
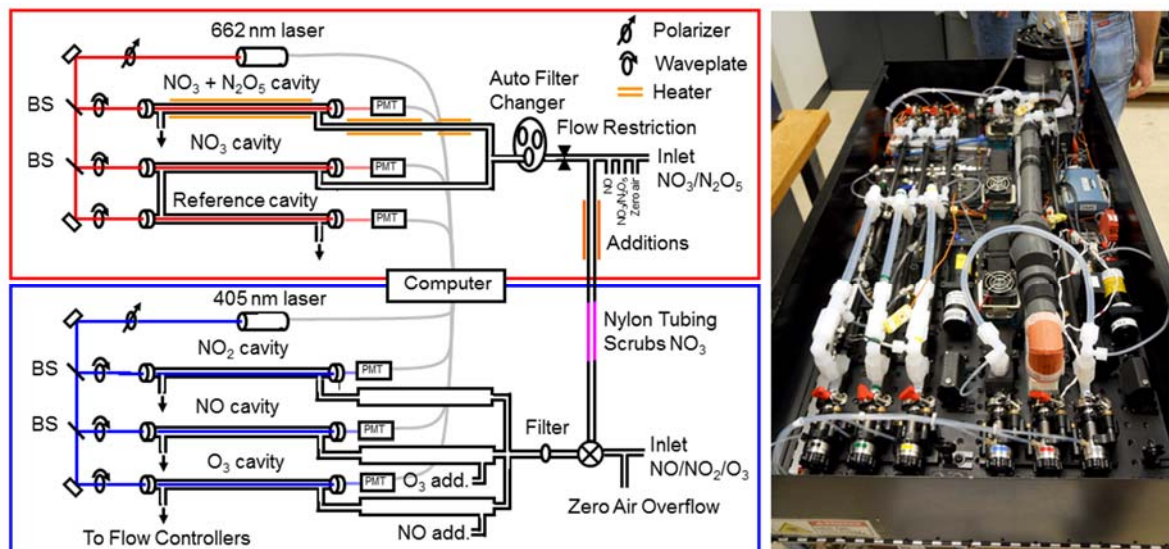
Figure 6-1: Instrument schematic. The upper part framed in red shows the NO₃ and N₂O₅ detection setup. The lower part framed in blue shows the NO, NO₂ and O₃ detection unit. BS denotes a beamsplitter. A photo of the optical bench instrument is shown on the right.

6.2.1 NO₃ and N₂O₅ measurement

Previous NO_3 and N_2O_5 instruments from our group were based on cavity ring-down spectroscopy using a pulsed dye laser and a Nd:YAG laser to pump the dye laser. Diode lasers, which are available at wavelengths near the 662 nm absorption maximum of the nitrate radical, are a suitable alternative that are smaller, lighter, lower in power consumption and do not require hazardous material. Like pulsed dye lasers, commercially available Fabry-Perot diode lasers are spectrally broad enough to couple passively to the mode structure of the optical cavity [3]. They are also spectrally narrow enough to provide a specific measurement for the nitrate radical. Ayers et al. [32] and Schuster et al. [106] have already demonstrated the use of similar diode lasers for detection of NO_3 and N_2O_5. The instrument described here is similar to these instruments aside from two distinct differences. First, our instrument uses an on-axis rather than an off-axis alignment to couple the laser to the optical cavity, similar to our 405 nm NO_2 detection scheme [3]. Since the nominal 0.5 nm width of the diode laser spectrum overlaps more than 2000 longitudinal modes of the 93 cm cavities, it couples passively without active control of the laser spectrum or cavity modes. On-axis coupling also allows for a more compact (i.e. smaller diameter) sample cell, decreasing sample residence time and simplifying the optical alignment. Second, this instrument incorporates an automated calibration for NO_3 and N_2O_5 against the NO_2 channels.

Light is provided by a continuous wave (cw) diode laser (Power Technology Inc., Fabry-Perot diode model IQµ series), with an output power of approximately 100 mW. The laser can be temperature tuned over a range of 15–33°C, corresponding to center wavelengths 659.1–662.7 nm, although individual laser diodes typically vary in tuning range. Upon request, the manufacturer selected a diode

with tuning range that includes the nitrate radical's absorption peak near 662 nm. The laser spectrum is typically composed of between 2–4 modes of the laser cavity. Each mode is separated by ~0.4 nm and has a width of ~0.3 nm. The intensity in each mode is determined by the temperature of the laser diode. Certain temperatures give output spectra that are dominated by 1, or at most 2, of these 0.3 nm modes. A compact spectrometer (Ocean Optics USB4000) is used to monitor the laser spectrum. The diode temperature is set to maximize the spectral overlap with the nitrate radical's absorption. The laser operates in cw mode and is modulated on and off by a 0–5 volt square wave input. The rise and fall time of the intensity is less than 30 ns, which is rapid on the time scale of the intensity decay from the optical cavity. The laser is optically isolated from the cavities in this on-axis alignment in order to prevent potentially damaging back reflections from entering the laser. The isolators consist of a single linear polarizer that is placed in front of the laser, and three separate quarter waveplates; one placed directly in front of each cavity. This design ensures that the polarization through the beamsplitters remains linear, so that the polarization sensitivity of the beamsplitters does not degrade the performance of the isolators.

The cavities consist of two 25.4 mm diameter, 1 m radius of curvature high-reflectivity dielectric mirrors. The mirrors are separated by 93 cm and mounted to an optical breadboard in a custom bellows mount that allows optical alignment and a flexible seal to the sample volume, from which the mirrors themselves are isolated. The cleanliness of the mirrors is maintained by a small purge flow, 25 sccm, of ultrapure air (zero air) over each mirror to separate the mirror surface from the sample flow. Light transmitted through the back mirror of the each cavity is collected by an optical fiber and detected on a photomultiplier tube (PMT) (Hamamatsu HC120-05M). A colored glass filter (Schott RG665) is used immediately before the PMT to reject stray light.

The ring-down traces are digitalized using 14-bit oscilloscope card (National Instruments PCI-6132) at a rate of 2.5×10^6 samples s^{-1}. A digital output of the oscilloscope card is used to modulate the laser intensity normally at 500 Hz, but this can be adjusted to increase the number of ring-down traces acquired or duration of each ring-down trace. The ring-down traces are transferred to a computer over the PCI bus and co-added in lots of 100. The number of ring-down traces in each lot can be adjusted to correspond with the laser modulation frequency and the desired measurement frequency. The co-added ring-down traces are then fit to a single exponential decay. The ring-down traces are fit using the techniques described by Everest and Atkinson [107]. Usually, the digital Fourier transform method is used; however the linear, LRS, and Levenberg-Marquardt methods are also available. When using the linear fitting method, the laser is turned off after every lot of 100 ring-down traces to measure the zero level of the PMTs. During ambient sampling, only the fit parameters are saved and ring-down traces are discarded after fitting.

The upper panel of Figure 6-2 shows a co-added ring-down trace acquired while sampling laboratory air at a cell pressure of 504.6 hPa. The *1/e* time constant for this ring-down trace is 217.98 ±

0.05 μs, where the error is the covariance of the fit parameter. The time constant is determined by the combination of Rayleigh scattering losses, mirror reflectivity, and cavity alignment. The mirror reflectivity is 99.999 %, or 10 ppm transmission. The lower panel in Figure 6-2 shows the fit residual as a percentage of the ring-down trace. Higher reflectivity mirrors (Advanced Thin Films, Inc.) with R = 99.9995 % (5 ppm transmission) have also been used in this instrument and give a ring-down time constant in excess of 400 μs at 500 hPa pressure. All of the performance characteristics described in this paper have been achieved with the lower reflectivity mirrors, which give a larger intensity throughput and allow a higher repetition rate. Instrument performance with the higher reflectivity mirrors is not substantially different. For the lower reflectivity mirrors, the laser is modulated at 500 Hz, and 0.2 s is needed to acquire 100 ringdown traces; thus the overall signal acquisition rate should be 5 Hz. However, due to overhead from transferring ring-down traces to the computer memory, fitting the ring-down traces, and auxiliary measurements, the actual data acquisition rate of the measurement is currently limited to 3 Hz.
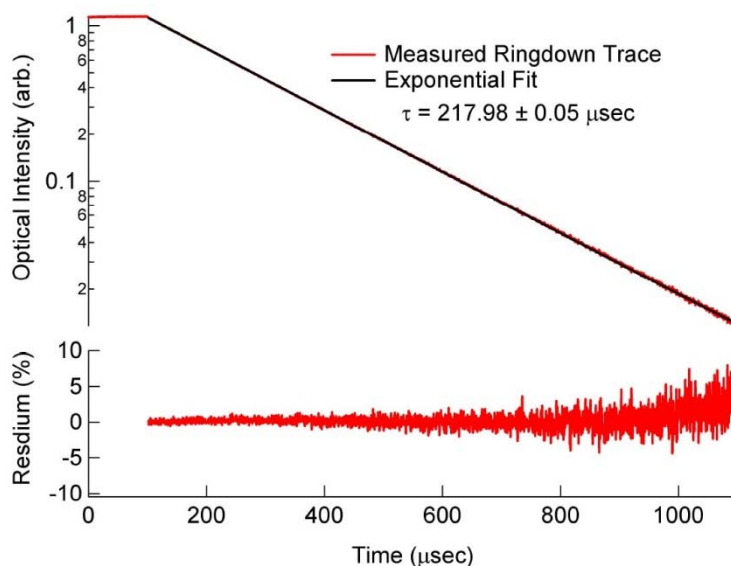
Figure 6-2: Upper panel: ring-down trace from one of the 662 nm cavities, along with the fit to the ring-down trace. The lower panel shows the fit residual as a percentage of the fit.

The sampling and inlet configuration for NO_3 and N_2O_5 is equivalent to that described by Fuchs et al. [2] (chapter 4) and is described only briefly here. Because NO_3 and N_2O_5 are reactive gases, the inlet is constructed from Teflon tubing and fittings. The shortest possible residence time is needed in order to minimize wall losses for NO_3, which has been shown previously to have a first order loss with respect to reactions on Teflon inlet walls of approximately 0.2 s^{-1} [1].

The inlet consists of several parts and is shown in Figure 6-1. The first is a short length of 4 mm inner diameter tubing to bring ambient air from outside into the aircraft or instrument enclosure. Following this there are addition points for NO used to determine the instrument zero, zero air used to overflow the inlet, and NO_3/N_2O_5 additions for calibration. Next, a short length of 1.6 mm inner

diameter tubing is used as a flow restriction to drop the pressure to approximately half of ambient. A Teflon membrane (Pall Corp. R2PJ047, 2 μm pore size, 25 μm thickness) is used in an automatic filter changer described by Dubé et al. [1] to remove aerosol from the sample flow. After the filter, the flow is split and delivered to each of the two sample cells by 0.64 cm inner diameter tubing. A 78 cm length of 7.9 mm inner diameter tubing along the axis of each cavity creates the sample cell. Flows are set using flow controllers positioned downstream of the sample cells. One cell remains at ambient temperature to measure the concentration of NO_3. The sample gas in the other channel is heated to convert N_2O_5 to NO_3 in order to detect the sum of NO_3 and N_2O_5. For this channel the gas flow is heated in three stages that are designed to rapidly bring the gas to a temperature sufficient to thermally dissociate N_2O_5 and then to hold it at a temperature where the equilibrium in reaction equation 6-1 is shifted mainly toward NO_3. For example, the conversion of N_2O_5 to NO_3 based on its equilibrium constant is greater than 98 % for ambient NO_2 levels less than 10 ppbv at 75°C. The first section is 6.4 mm inner diameter tubing, 40 cm long and held at 130°C. The second is 25 cm long and held at 80°C to reduce thermal gradients and minimize flow noise in the sample cell which is held at 75°C.

A third 662 nm channel is used to continuously monitor the optical extinction from species other than NO_3, such as NO_2, O_3 and water vapor. It consists of an optical cavity and sample cell downstream of the NO_3 sample cell. NO is continuously added to this sample cell in the same manner as the instrument zeroing described below.

The total flow through the inlet is controlled at a constant volumetric flow rate that is adjusted for conditions of a particular measurement campaign. Typical flows for recent aircraft measurements described below were 15 and 9 LPM (liters per minute) for the NO_3 and $NO_3+N_2O_5$ sample cells, respectively. As in our previously described instrument, the zero for the NO_3 measurement is determined by adding a small amount of NO to the inlet. In an excess of NO, NO_3 is rapidly converted via reaction equation 6-4 ($k = 2.6 \times 10^{-11}$ cm^3 $molecule^{-1}$ at 298 K) into NO_2, which has an absorption cross-section that is approximately 4×10^4 times smaller than that of NO_3 at 662 nm. This zero method does not influence optical extinction due to ambient levels of O_3, NO_2 or H_2O and is therefore highly specific for NO_3. A small flow of a 100 ppmv NO in N_2 mixture is added to the inlet flow to produce an NO concentration of $\sim 10^{12}$ molecules cm^{-3}, designed to give >99.9 % conversion of NO_3 to NO_2 before the flow enters the axis of the NO_3 measurement cell. The "zero of the instrument" is typically 5 s in duration and is measured at arbitrary intervals depending on requirements. During aircraft ascent and descent, when changes in pressure lead to rapid changes in background time constant due to Rayleigh scattering, the zero interval can be as short as once per minute. On level flight legs or for ground based measurements, a zero interval of 3–5 min is normally sufficient to track any changes in τ_0 due to cavity alignment or variable background absorbers.

6.2.2   NO, NO$_2$, and O$_3$ measurement

Measurement of NO$_2$ is integral to the NO$_3$ and N$_2$O$_5$ calibrations and measurements of inlet transmission. Measurement of NO$_2$ using a 405 nm diode laser improves its sensitivity compared to our previously described, 532 nm instrument [48, 102], since the NO$_2$ cross-section is approximately 4 times larger at 405 nm. Furthermore, the interference from ozone is essentially eliminated, since its absorption cross-section is approximately 4×10^4 times smaller than that of NO$_2$ at 405 nm. Both NO and O$_3$ can be measured by the same instrument via conversion to NO$_2$; conversion of NO to NO$_2$ in excess ozone has been described previously by [3], while conversion of O$_3$ to NO$_2$ in excess NO has been described by Washenfelder et al. [103].

A second diode laser centered at 405 nm (Power Technology Inc., Fabry-Perot diode model IQμ series) provides the light source for the CaRDS detection of NO$_2$. Unlike the 662 nm diode laser, this diode laser is not actively temperature tuned and is held at a constant 20°C. We have found the center wavelength to be stable over the lifetime of the laser by repeated checks against a calibrated grating spectrometer. The laser output power of 80 mW is divided into three equal parts using a 33 % beamsplitter and a 50 % beamsplitter. The three cavities are constructed in the same manner as the 662 nm cavities, except that a bandpass filter centered at 405 nm is used in front of the photomultiplier to reject stray light. The layout is shown schematically in Figure 6-1.

The data acquisition for the 405 nm channels is done in the same way as for the 662 nm channels using a second oscilloscope card to modulate the laser and acquire the ringdown down traces. The 405 nm mirrors have a reflectivity of 99.9965 % (35 ppmv transmission) and give typical background time constants of 40 μs at a pressure of 840 hPa. Because the time constants on the 405 nm cavities are shorter than the 662 nm cavities, the laser is modulated at four times the frequency, or 2 kHz. Ring-down traces are acquired in lots of 400 and co-added to achieve the same overall data acquisition rate (3 Hz) as the 662 nm side of the instrument. It is not required that both the 662 nm channels and the 405 nm channels acquire the ring-down traces in lots corresponding to equal acquisition time but doing so maximizes the total number of ring-down traces collected.

The NO, NO$_2$ and O$_3$ sample cells have a separate inlet from the NO$_3$/N$_2$O$_5$ measurement, and the inlet is simpler because the 405 nm cavities are operated at ambient pressure and the measured species are less reactive. The inlet and sample cells are constructed with Teflon tubing and fittings. Ambient air is drawn in through a length of 0.4 cm inner diameter tubing to a 1 μm pore size Teflon filter (Pall Corp. R2PL047) in a commercial, PFA Teflon mount (Savillex). The smaller pore-size filter ensures rejection of smaller size aerosol to which the 405 nm channels may in principle be more sensitive. Loss of NO, NO$_2$ and O$_3$ on these filters is negligible. There is no evidence for a signal due to aerosol extinction on the downstream side of these filters during sampling of ambient air. Following the filter, the flow is split into three equal parts and delivered to the sample cells. Before entering each

sample cell, there is a reactor consisting of a 33 cm length of 0.95 cm inner diameter tubing. The flow rate through each channel is controlled at 2.7 LPM (volumetric) to maintain a residence time of 0.6 s (plug flow) within each reactor while sampling from variable external pressures from the aircraft. On the first channel which is used for the NO_2 measurement, the purpose of the reactor is only to match the residence time of all three channels, so that NO_2 may be accurately subtracted from NO_x or O_x, as described below.

The second channel measures total NO_x via conversion of NO to NO_2 in excess O_3. A 12 sccm flow of 0.3 % ozone is added at the beginning of the reactor via a three way valve that allows switching of this ozone addition to a vent line. The ozone is generated by passing a flow of pure oxygen over a mercury-argon lamp (UVP 90-0004-01). The resulting ozone concentration in the sample cell is approximately 4×10^{14} (~16 ppmv at 1 atmosphere and 298 K) and is measured periodically from the change in optical extinction at 405 nm (~6×10^{-9} cm^{-1}) upon switching the ozone flow into and out of the sample cell. This measurement is checked less frequently using a commercial ozone monitoring instrument. The background extinction due to this added ozone changes the ring-down time constant by approximately 0.25 µs from its nominal value of 40 µs at atmospheric pressure (1013 hPa). The presence of this large excess ozone converts NO quantitatively to NO_2 via reaction equation 6-6.

$$O_3 + NO \rightarrow NO_2 + O_2 \tag{6-6}$$

$$k_{298} = 1.9 \times 10^{-14} \text{ cm}^3 \text{ molecule}^{-1} \text{ s}^{-1}$$

Conversion of NO to NO_2 under these reactor conditions is greater than 99 %. A small correction of 1–2 % is required to account for the further oxidation of NO_2 to higher oxides of nitrogen, NO_3 and N_2O_5, via reaction equations 6-1 and 6-2 [3]. The measured NO_x concentration is also corrected for the small dilution (~0.5 %) due to the addition of the O_3/O_2 flow.

The third channel measures total odd oxygen, $O_x = NO_2 + O_3$, via the analogous conversion of O_3 to NO_2 in excess NO. A small flow of NO from a standard mixture of NO in N_2 (Scott-Marin) is added at the beginning of the reactor to produce an excess concentration of NO identical to the excess O_3 concentration in the NO_x channel (i.e. 4×10^{14} molecules cm^{-3}). The excess NO quantitatively (greater than 99 %) converts O_3 in the ambient sample flow to NO_2 via reaction equation 6-6. There is no need for an additional correction for further oxidation of NO_2 on this channel since reaction equation 6-1 through reaction equation 6-2, to the small extent that they might occur without large, excess O_3, are effectively reversed by reaction of NO_3 with the excess NO (reaction equation 6-4). The excess NO added to this channel does contain an unavoidable contamination of NO_2, which can produce a large background signal. An $FeSO_4$ converter on the outlet of the standard cylinder reduces this NO_2 contamination considerably to a background level of 0.5–2 ppbv within the sample cell [103].

Maintaining a constant conversion efficiency of O_3 and NO to NO_2 is a potential challenge for sampling from an aircraft platform since the ambient pressure (and hence the reactant concentration and

reactor residence time) is variable with aircraft altitude. Flows on all three 405 nm channels are controlled at constant volumetric rates, rather than constant mass flow rates, to maintain constant residence time and reactant number density in each reactor. Addition of a constant, mass flow of the excess reactant with a well-defined mixing ratio to the variable, volumetric flow produces a constant number density in each reactor as the aircraft ascends and descends. For example, the number density of NO in the O_x sample cell is the product of mixing ratio of the NO standard cylinder (*MR*), the total number density in the sample cell (N_d) and the ratio of the volumetric flows (F_{vol}^{NO} and F_{vol}^{cell}) as shown in equation 6-7. Here, *P* is the pressure in the sample cell, P_0 is the standard pressure, *k* is Boltzmann's constant, *T* is the sample cell temperature, and F^{STD}_{NO} is the volumetric flow of the reactant at standard pressure and temperature which is directly proportional to the mass flow and independent of pressure.

$$[NO] = MR \times N_d \times \frac{F_{NO}^{vol}}{F_{cell}^{vol}} = MR \times \frac{P}{kT} \frac{F_{NO}^{STD}\left(\frac{P_0}{P}\right)}{F_{cell}^{vol}} \tag{6-7}$$

Because the flow through the sample cell is maintained at a constant volumetric rate, the only pressure dependences in equation 6-7 are the number density and the reactant volumetric flow, and they cancel each other. The result is a reactant number density that is independent of pressure. Thus, the conversion efficiencies outlined above do not vary with aircraft altitude.

The current scheme for acquiring a zero time constant for the 405 nm channels is identical to that used previously with our 532 nm CaRDS NO_2 instrument, namely to slightly overflow the inlet with zero air. The overflow is added through a concentric piece of Teflon tubing with an inner diameter slightly larger than the outer diameter of the inlet tubing and which extends slightly (2–4 cm) beyond the inlet tubing. Addition through this concentric inlet minimizes the pressure difference between the zero and signal measurements, which can be significant (1 hPa or greater) if the zero air overflow is added through a simple tee fitting. Such pressure differences between the zero and sample measurement change the Rayleigh scattering background, which must be corrected for after the measurement. An additional correction is needed to account for the difference in humidity between ambient air and the dry zero air used to overflow the inlet. The difference in the Rayleigh scattering cross-section of water vapor and air was measured at 405 nm by Fuchs et al. [3] to be 5×10^{-27} cm^2, leading to a maximum correction equivalent to 0.15 ppbv NO_2 at 80 % RH (22°C) . Actual water vapor corrections are typically smaller, however. The potential for an NO_2 impurity in the zero air limits the applicability of this zero scheme for sampling in remote environments, where ambient NO_x may be comparable to the NO_x impurity in commercial zero air. Chemiluminescence measurements at our laboratory showed the zero air (Scott-Marin Ultrazero) contains less than 10 pptv of NO_x. Zero measurements occurred every 3 min during ambient sampling and lasted 15 s to allow for the zero air to completely fill the sample cell.

The optical extinction due to excess O_3 on the NO_x channel, and the NO_2 impurity in the added NO on the O_x channel, are not affected by the addition of zero air to the inlet. Thus, no correction is required for these small, background optical extinctions.

6.3 Calibrations

Although cavity ring-down spectroscopy is, in principle, an absolute method, calibrations are required if either the inlet transmission efficiency for a particular trace gas is not unity, or if the effective absorption cross-section can vary as a function of sampling conditions (i.e. temperature, pressure, laser spectrum). The former is the case for NO_3 and N_2O_5, which are reactive trace gases whose transmission through the inlet system may vary. The latter is potentially the case for NO_2 (and by extension, NO and O_3 in this instrument) since its absorption cross-section varies with pressure, temperature, and laser spectrum. We have recently developed calibration standards for NO_3 and N_2O_5 based on their conversion to NO_2 [2] and for NO_2 based on conversion of standard additions of O_3, as described above [103]. The following sections outline these calibration schemes and their implementation in the current version of this aircraft instrument.
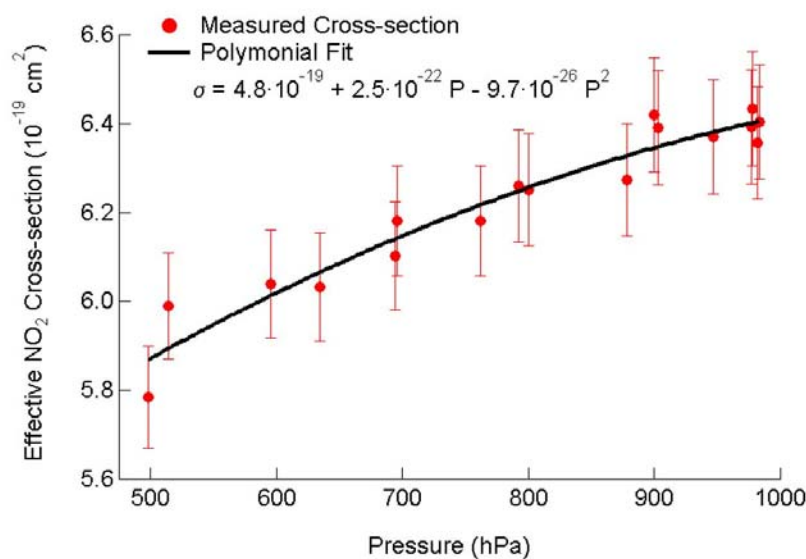
Figure 6-3: Pressure dependence of the effective NO_2 cross-section at 405 nm. The pressure-dependent cross-section is parameterized by 2nd order polynomial and used for calculating NO_2 concentration during aircraft sampling at variable altitudes and cell pressures. The pressure dependence may be due to the variation in the NO_2 cross-section itself, or to pressure dependence in R_l from equation 6-5. Here, the cross-section is fit to a pressure dependence assuming constant R_L of 1.15, though this choice is arbitrary.

6.3.1 NO₂ calibration

The 405 nm laser diodes provided by the manufacturer vary in center wavelength; hence, the effective cross-section for each laser must be calibrated by standard NO_2 additions. Standard concentrations of O_3 are generated and measured using a commercial ozone monitor, then quantitatively

converted to NO_2, which is measured on the CaRDS instrument, as described above. The calibrator contains its own NO cylinder and flow controllers for conversion of O_3 to NO_2 such that it delivers standard additions of NO_2 independent from the CaRDS instrument itself. The calibrator is also field portable and can be used for routine calibration on a daily basis. Typical calibration curves use a series of NO_2 mixing ratios between 0–200 ppbv, with the effective NO_2 cross-section determined as the slope of a plot of measured optical extinction against NO_2 concentration. The effective cross-section is the NO_2 cross-section integrated under the laser spectrum and divided by R_L, which is ratio of the cavity length to the length over which the absorber is present. The cell pressure in the 405 nm channels varies significantly with altitude, typically between 500–900 hPa over the altitude range of the NOAA P-3 aircraft and is typically 80–100 hPa below ambient pressure. Therefore, any pressure dependence in the effective cross-section for NO_2, or in the ratio of the cross-section to R_L in equation 6-5, will directly affect the measurement from aircraft. Literature spectra for NO_2 do indeed show a pressure dependence (e.g. [54]), but only for spectral features too fine to be resolved by the laser system in the CaRDS instrument. Nevertheless, the ratio of the effective NO_2 absorption cross-section to R_L, i.e. σ/R_L, shows a distinct pressure dependence, as shown in Figure 6-3. The value of σ/R_L decreases by approximately 6 % between 1000–500 hPa. The calibration curve in Figure 6-3 is the result of multiple determinations in the field on different days, which were reproducible at any given pressure to within ±2 %. For the purpose of calculating the NO_2 concentration, the cross-section is parameterized by a 2nd order polynomial. The measured pressure dependence of the effective cross-section may be due to a variation of the actual cross-section or a pressure dependence of R_L. Regardless of the source of the pressure dependence, the effective cross-section is still valid for determination of the NO_2 concentration.

6.3.2 NO_3 cross-section and water vapor sensitivity

The cross-section for NO_3 is determined using the absorption spectrum measured by Yokelson et al. [49] shown in Figure 6-4 and temperature-dependence determined by Osthoff et al. [74]. Although the absorption spectrum peaks at 2.17×10^{-17} cm^2 for 298 K, the effective cross-section in this instrument is a convolution of the measured cross-section and the laser spectrum and is therefore smaller than the peak absorption. Using a typical laser spectrum shown in Figure 6-4, the effective cross-section was 2.03×10^{-17} cm^2, a reduction of 7 %. One drawback of the 662 nm diode laser used in this instrument is that the intensity in different modes, and thus its spectral output, is not stable on the time scale of hours. Based on several measured laser spectra, this instability leads to a variation of 1.5 % in the effective NO_3 cross-section. The cross-sections measured by Yokelson et al. [49] and Osthoff et al. [74] are accurate to ±4 %. In this instrument the variability of spectrum increases the inaccuracy of the effective cross-section to ±6 %. The laser spectrum is currently measured infrequently (e.g. once per flight) using a small grating spectrometer (Ocean Optics, USB4000) but will be incorporated into routine data acquisition in the future. The NO_3 cross-section is temperature dependent, as described previously, such that the effective cross-section for the heated channel is 1.68×10^{-17} cm^2 molecule^{-1} at 348 K.
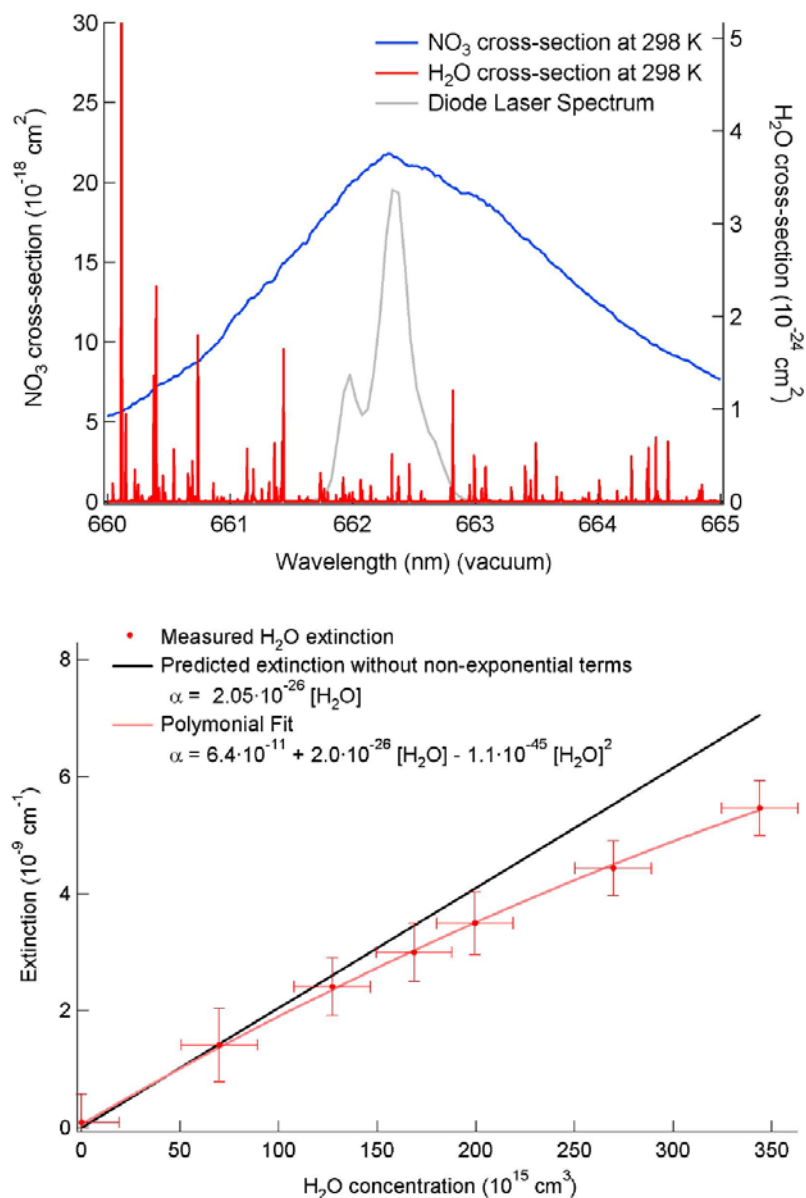
Figure 6-4: The right panel shows the NO₃ (blue) and water vapor (red) absorption spectrum around 662 nm. A typical laser spectrum is also shown. The left panel shows the measured water sensitivity along with predicted sensitivity neglecting the non-exponential terms. The measured sensitivity is fit to a 2ⁿᵈ order polynomial and used to correct the field data.

Water vapor has an absorption in the 662 nm region of the spectrum. The potential for water vapor interference with NO_3 measurements is well known from broadband optical measurements of NO_3 (e.g. [19, 108]). The water vapor spectrum at 20°C from the HITRAN database [90] is shown in red on Figure 6-4 along with the nitrate radical absorption spectrum (blue) and typical diode laser spectrum (gray). Our previous, pulsed dye laser instrument had a narrow bandwidth which effectively resolved this water vapor spectrum, and could be tuned off resonance with the discrete water vapor lines while still being tuned effectively to the maximum in the NO_3 absorption spectrum. The output of the

diode laser, by contrast, unavoidably overlaps multiple water vapor lines, making the instrument much more sensitive to this interference. Furthermore, because the water vapor absorption spectrum consists of several peaks under the laser bandwidth, the variation in absorption cross-section can lead to non-exponential ring-down traces.

The measured sensitivity to water vapor is shown in Figure 6-4 (lower panel). The extinction is not linear with respect to water concentration *because* the ring-down transients become slightly non-exponential at higher optical extinctions because of the mismatch between the discrete, water vapor lines and the broadband laser source [45]. However, the data can be corrected by using the fitted polynomial as an effective concentration-dependent cross-section as shown in equation 6-8.

$$\tau_{corrected} = \left(\frac{1}{\tau} + \frac{f([H_2O])c}{R_L} \right)^{-1} \tag{6-8}$$

$\tau_{corrected}$ is the exponential decay time constant that would be measured in the absence of water vapor. τ is the measured exponential decay constant. $f([H_2O])$ is the fitted polynomial sensitivity and requires an independent measurement of the water vapor mixing ratio. The linear term in the polynomial fit corresponds to the water vapor cross-section when averaged over the laser spectrum and agrees well with the value calculated using the water vapor cross-section obtained from the HITRAN database, 2.05×10^{-26} cm^2. This linear absorption is insensitive to the presence of added NO, and will therefore only interfere with the measurement of NO_3 and N_2O_5, if the water vapor mixing ratio changes rapidly on the time scale of the instrument zero frequency. Such variations can, in principle, be corrected by the reference channel, though in practice the active correction described here proved as useful as a reference channel. For ground based measurements, simple interpolation between zeros would normally be sufficient. However, for aircraft sampling, which may rapidly traverse regions of higher or lower absolute humidity (e.g. on vertical profiles), the interferences must be actively corrected via equation 6-8. A worst-case change in relative humidity of 0 to 100 %, or 3.5×10^{17} cm^{-3} (2.9 % mixing ratio at 20°C and 505 hPa in the sample cells), would result in an additional extinction of 7×10^{-9} cm^{-1}, or the equivalent of 30 pptv of NO_3/N_2O_5. In practice, we have never observed variations in background extinction that are this extreme; however active correction remains a necessity.

When the water vapor concentration is approximately constant between the zero and the signal measurement, there is an additional, small error due to fitting the slightly non-exponential ring-down transients in the presence of water vapor as though they were single exponentials to retrieve concentrations of NO_3 or N_2O_5. This effect produces a measurement error of less than 0.2 % for either compound.

Although much smaller, both NO_2 and NO_3 have some variation in the cross-section under the laser spectrum like water vapor. We have not observed non-exponential ring down traces from either

NO$_2$ or NO$_3$. For NO$_2$ the exponential character of the ring-down trace is further confirmed by the linear extinction as a function of the NO$_2$ concentration during calibrations.

6.3.3   NO$_3$ and N$_2$O$_5$ inlet transmission

Wall loss of NO$_3$ on the Teflon surfaces of the inlet and measurement cells is the most significant source of uncertainty for CaRDS measurement of NO$_3$ and N$_2$O$_5$ [1]. Characterization of the NO$_3$ and N$_2$O$_5$ transmission efficiency has been described by Fuchs et al. [2]. The following provides a short description of the method and the changes that are specific to the current instrument design. The calibration scheme for NO$_3$ is based on its chemical conversion to NO$_2$ with excess NO by reaction equation 6-4, the same as used for zeroing the 662 nm channels. The resulting NO$_2$ has negligible inlet loss and can be measured by CaRDS at 405 nm to provide a standard for the 662 nm NO$_3$ measurement. N$_2$O$_5$ transmission efficiency can be measured similarly by chemical and thermal conversion of N$_2$O$_5$ to NO$_2$. During transmission efficiency measurement the inlet is overflowed with zero air to avoid interference from ambient O$_3$ and NO.

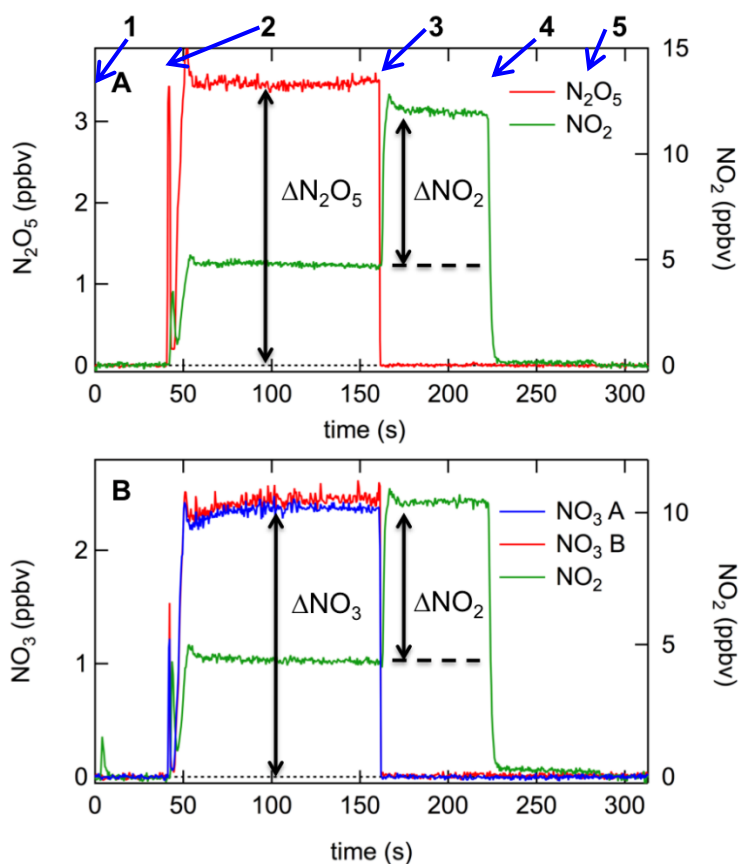Each   measurement   of   NO$_3$ transmission   efficiency   has   five   steps   shown   in

Figure 6-5. First, the zero of the instrument is measured as discussed above. Second, the NO$_3$ source is added to the tip of the NO$_3$/N$_2$O$_5$ inlet and the mixing ratio NO$_3$ is measured in 662 nm

channels. The amount of NO_2 coming from the source directly is measured in the NO_2 channel. As described above, for ambient sampling, the inlet for the NO_2, NO_x and O_x channels is separate from the NO_3 and N_2O_5 inlet; however, during the transmission measurements the NO_2 channel must be connected to the NO_3/N_2O_5 inlet. This connection is made via the three-way valve shown in Figure 6-1, which switches the instrument between sampling and calibration mode. Unlike the previously described pulsed laser instrument, in which the NO_3 and NO_2 measurements were in series, they are in parallel in this instrument, such that measurements of NO_3 or N_2O_5 occur simultaneously with that of NO_2. The third step of the transmission efficiency measurement is to add NO_3 and NO simultaneously to the NO_3/N_2O_5 inlet. The reaction of NO_3 and NO quantitatively converts NO_3 into NO_2 producing two molecules of NO_2 for each molecule of NO_3 added to the inlet. During this step the NO_2 channel measures NO_2 from three sources: NO_2 coming directly from the N_2O calibration source, NO_2 produced by the reaction of NO_3 and NO, and the NO_2 impurity present in the NO addition. The fourth step is to shut off the NO_3/N_2O_5 addition from the calibration source, but leave the NO flow present to measure the NO_2 impurity present in this NO. The fourth step accounts for this contamination. The fifth step is a second zero measurement, with no addition of either NO or NO_3/N_2O_5.

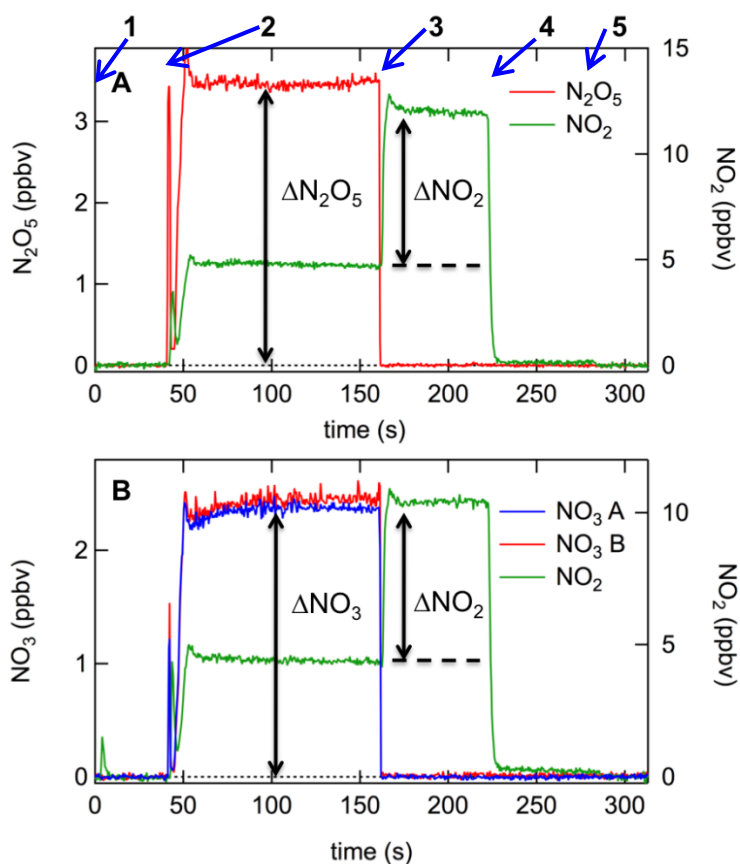*Figure 6-5: Example calibration sequences for (A) N_2O_5 and (B) NO_3. For the N_2O_5 calibration, the N_2O_5 source is added directly to the inlet, while for the NO_3 calibration it first passes through a heater to convert it primarily to*

97

NO₃. The sequence of the calibration, indicated by the numbers across the top, includes (1) zero measurement; (2) addition of N₂O₅/NO₃ source; (3) titration of the NO₃/N₂O₅ source with excess NO to convert it to 2×NO₂; (4) N₂O₅/NO₃ source switched off, NO titration on to determine NO₂ content of the added NO; and (5) NO titration turned off. The calibration is given by equation 6-9 and is effectively the ratio of 2Δ (N₂O₅)/ΔNO₂ (or 2ΔNO₃/ΔNO₂) marked in the figure, where ΔNO₂ is corrected for the small additional NO₂ in the added NO source given by the difference between equation 6-9 and equation 6-10 in the sequence above. For the data shown in the figure, the N₂O₅ transmission is 99 %. The NO₃ calibrations factors are shown for the ambient channel – NO₃, (A) – and the heated channel – NO₃ (B), and are 87% and 85 %, respectively.

Note: Error in the published plot. Blue arrows indicate the start time of each portion of the calibration sequence.

The N_2O_5 transmission efficiency can be measured by a similar five step procedure with the addition of N_2O_5 to the inlet instead of NO_3; however, during the third step a heater is used to convert the N_2O_5 into NO_3 which is then converted to NO_2 by reaction with NO. This heater is along the connection between the NO_3/N_2O_5 inlet and the NO_2 sample cell and is followed by a short section of nylon tubing which acts as an NO_3 scrubber, as described in Fuchs et al. [2]. In this configuration, the scrubber serves to remove NO_3 from the flow produced by thermal decomposition of N_2O_5 when the NO addition is off during step 2, so that the NO_2 channel measures only the NO_2 arising from thermal dissociation of N_2O_5 and not any optical extinction from NO_3. It also prevents recombination of NO_3 with NO_2 in the NO_2 sample cell. (Both the heater and scrubber are necessary for the NO_3 transmission measurement as well, because our source cannot produce pure NO_3. It is unavoidably contaminated with N_2O_5.) During addition of NO, all NO_3 produced in the heater between the inlet and the NO_2 sample cell is converted to 2×NO_2, which is not affected by the scrubber. Calibration samples of N_2O_5 or NO_3 are generated by passing a small flow of zero air over a sample of solid N_2O_5 stored in a trap at −78°C (dry ice). The source produces N_2O_5 with less than 2 % NO_3 or, if switched through an additional heater mounted in the calibration box, greater than 90 % NO_3.

The transmission efficiency can be calculated using the measurements taken during each of the five steps. Equation 6-9 then gives the expression for the transmission efficiency as the ratio between measured NO_3 during step 2 in the 662 nm channel and 1/2 the NO_2 generated from the conversion in reaction equation 6-4.

$$T_e = \frac{2 \times [NO_3]}{[NO_3]_{source+NO} - [NO_2]_{source} - [NO_2]_{NO}} \tag{6-9}$$

Here, $[NO_2]_{source+NO}$ is the NO_2 concentration when both the NO_3 and NO are added to the inlet during step 3, and $[NO_2]_{source}$ and $[NO_2]_{NO}$ are the NO_2 concentrations when the NO_3 and NO are added to the inlet separately, during steps 2 and 4 respectively.

To relate ambient concentrations with those measured in the sample cells, three separate transmission efficiencies are required: (1) the transmission of N_2O_5 through the heated inlet, T_e (N_2O_5), which is the combination of the transmission efficiency for N_2O_5 itself, the conversion efficiency to

NO_3, and the transmission of NO_3 through the heated inlet; (2) the transmission of NO_3 through the ambient channel, $T_e^{ambient}(NO_3)$; and (3) the transmission of NO_3 through the heated channel, T_e^{heated} (NO_3) [1, 2]. For the NO_3 channel only the inlet transmission of NO_3 is needed to determine the ambient NO_3 concentration, equation 6-10. However, because N_2O_5 is converted to NO_3 in the inlet and consequently lost to the walls, the inlet transmission of both NO_3 and N_2O_5 is needed to calculate the ambient N_2O_5 concentration, equation 6-11.

$$[NO_3]_{amb} = \frac{[NO_3]_{cell}}{T_e^{amb}(NO_3)} \tag{6-10}$$

$$[N_2O_5]_{amb} = \frac{([NO_3]+[N_2O_5])_{cell} - T_e^{heated}(NO_3)[NO_3]_{amb}}{T_e(N_2O_5)} \tag{6-11}$$

$[NO_3]_{amb}$ and $[N_2O_5]_{amb}$ are the ambient concentration of NO_3 and N_2O_5. $[NO_3]_{cell}$ and $([NO_3] + [N_2O_5])_{cell}$ are the concentrations measured in the sample cells.
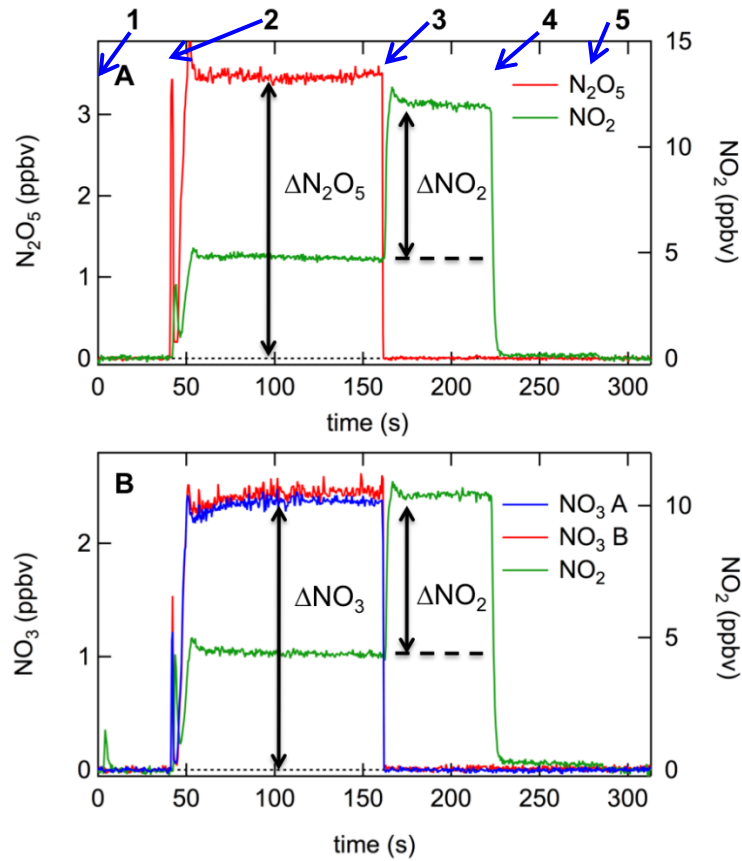

Figure 6-5 illustrates the scheme for an example calibration. Panel (A) shows the N_2O_5 transmission measurement, while panel (B) shows the NO_3 transmission measurements in both the ambient and heated measurement cells, which is done simultaneously by addition of NO_3 to both channels. In field calibrations during CalNex showed no dependence of NO_3 transmission efficiency on

NO_3 mixing ratio over the range 0.3–4.3 ppbv, although calibrations on any given day were normally performed at a single concentration.

6.4 Detection limits, accuracy, and sample data

Figure 6-6 shows a representative measurement of the NO_3 and N_2O_5 instrument baseline precision in our laboratory while sampling zero air. The Allan variance plot gives a detection limit under ~1 pptv (2σ) in 1 s for both species. For NO_3, this sensitivity is comparable to, but slightly worse than that reported by Dubé et al. [1] (e.g. 0.5 pptv, 1 s, 2σ) using the Nd:YAG/dye laser instrument. For N_2O_5, the sensitivity is slightly improved over the pulsed laser version (e.g. 2 pptv, 1 s, 2σ), although the improvement derives more from reduction in the optical noise associated with the fast flow in the heated channel than with any change in the optical system itself. The reduction in precision compared to the previously reported, pulsed laser instrument is due to a combination of factors, including reduced performance from the composite optical bench and cavity ring-down mirrors experience during the CalNex field intensive, and is not due solely to the introduction of diode lasers. Due to environmental effects (e.g. vibrations on the aircraft) and variations in the ambient air (e.g. temperature gradients), the precision of the instrument is reduced while sampling ambient air in flight. The in-flight detection limits are determined from daytime measurements during CalNex when the ambient mixing ratios of both NO_3 and N_2O_5 were below the laboratory detection limits and were 3 pptv (2σ) in 1 s for both NO_3 and N_2O_5.

The laboratory detection limits for the NO_2 and O_3 measurements have been reported in a separate publication [103] and are 46 pptv and 56 pptv (1 s, 2σ) respectively. Our previously reported, ground based NO_x instrument [3] exhibits a better precision of 22 pptv (1s, 2σ). In-flight baseline precision can be determined during zero measurements, which are 10–15 s in duration. For NO, NO_2, and O_3 the in-flight detection limits were 140 pptv, 90 pptv, and 120 pptv, respectively. These detection limits are the average precision of 140 zero measurements from an 8 h flight on 3 June 2010. During some time periods, the aircraft measurements of NO, NO_2 and O_3 also suffer from an optical instability in flight that leads to drifts on the order of 0.1–0.3 ppbv in flight. The longer-term baseline instability is most likely related to the mechanical stability of the optical cavity alignments on these channels. Investigation into the source of this instability and potential solutions is ongoing, although it could be addressed by simply increasing the frequency of zero measurements from the current 5 min interval. We anticipate improvements, primarily in the data acquisition software, to improve the precision of the NO_x and O_3 channels on the aircraft instrument.
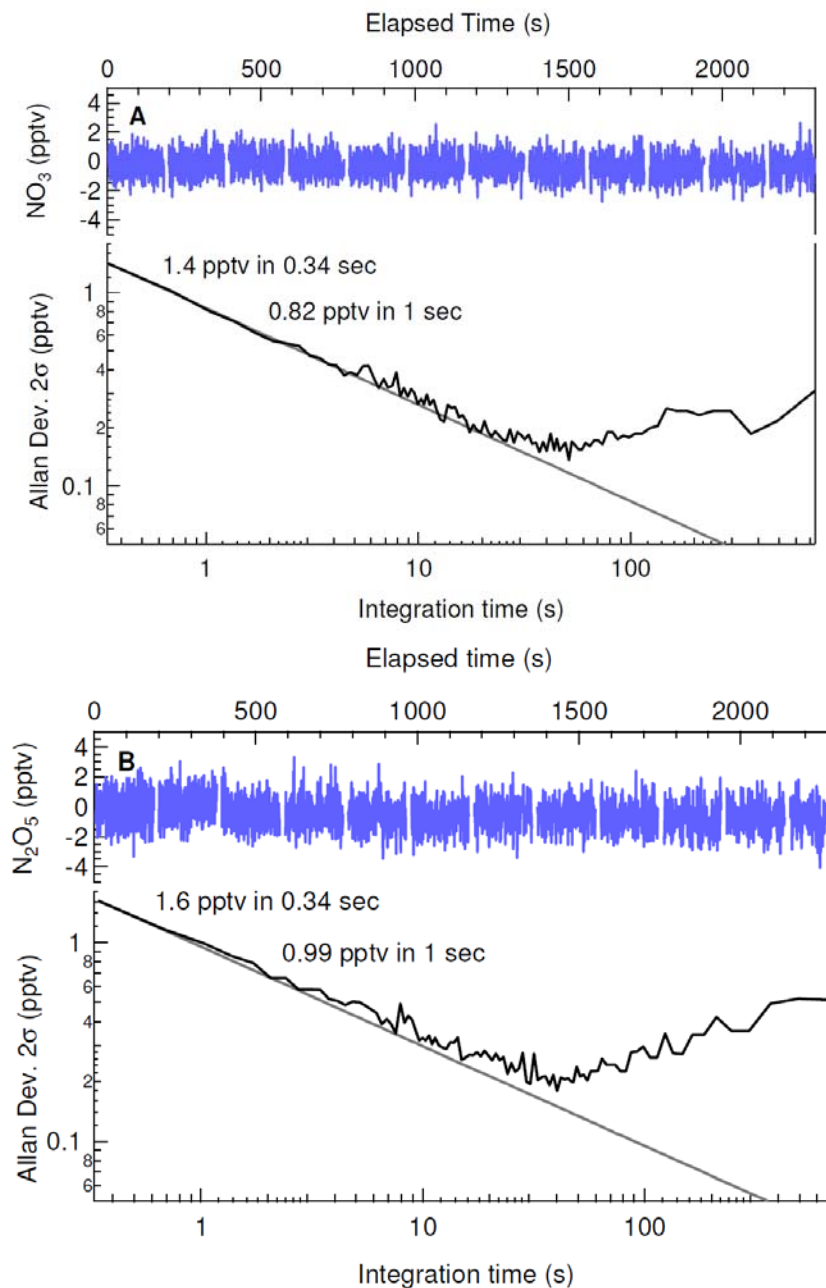
Figure 6-6: Allan variance plots for the NO₃ (upper) and N₂O₅ (lower) measurements when sampling synthetic zero air. Both channels have a 2 σ precision better than 1 pptv in 1 s.

The accuracy of the NO_3 and N_2O_5 measurements were described in detail by Fuchs et al. [2], are unchanged by modifications described here. The N_2O_5 accuracy ranges from −8 % to +11 % (1σ). The major uncertainties contributing to the accuracy are uncertainty in the cross-section, R_l, inlet loss and filter aging. Because the filter aging can only decrease the measured mixing ratios, it only contributes to the upper limit of the accuracy. The same factors contribute to the accuracy of the NO_3 measurement (−9 %, +12 %, 1σ). However, the inlet loss of NO_3 is more uncertain leading to a decreased accuracy compared with N_2O_5.

For measurements of NO, NO_2 and O_3, the accuracy is dominated by uncertainty of the effective cross-section which is directly related to the ±2 % accuracy of the UV ozone monitor used to measure the cross-section as describe in section 6.3.1. There is additional uncertainty (±1 %) in the dilution associated with the NO addition required to convert the O_3 to NO_2. The total accuracy for each of three measurements is ±3 % (1σ).
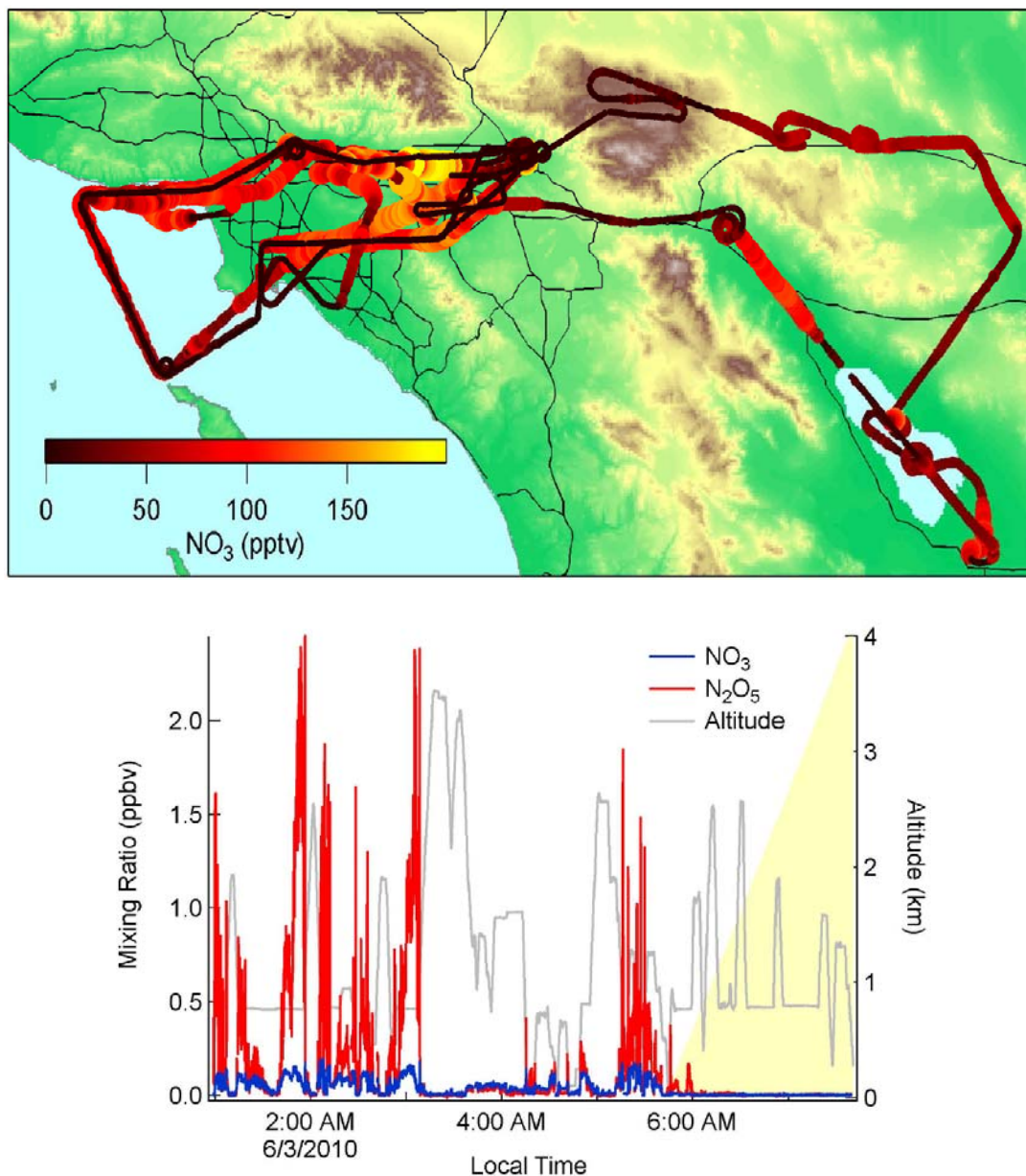
Figure 6-7: Sample NO_3 and N_2O_5 data from the flight on 3 June 2010. The upper panel shows the flight track in the Los Angeles basin. The lower panel shows the NO_3 (blue) and N_2O_5 (red) mixing ratios measured during the flight along with the aircraft altitude in gray. The yellow background indicates the time of sunrise.

This aircraft instrument was deployed during the CalNex campaign in California on the NOAA P-3 aircraft and took measurements on 25 research flights. An example of the performance and utility of this instrument is shown in Figure 6-7, which shows data from a flight in the Los Angeles basin on

3 June 2010. The flight track is shown on the left panel of the figure. This flight includes a series of vertical profiles over the ocean and the urban area of the Los Angeles basin. The flight began in late evening and landed 2 hours after sunrise. The second panel shows the measured NO_3 and N_2O_5 concentrations during the flight along with altitude. The yellow background indicates the solar elevation angle and time of sunrise. The mixing ratios of NO_3 and N_2O_5 vary strongly with altitude, consistent with the previous measurements of vertical stratification within the nighttime atmosphere [101].
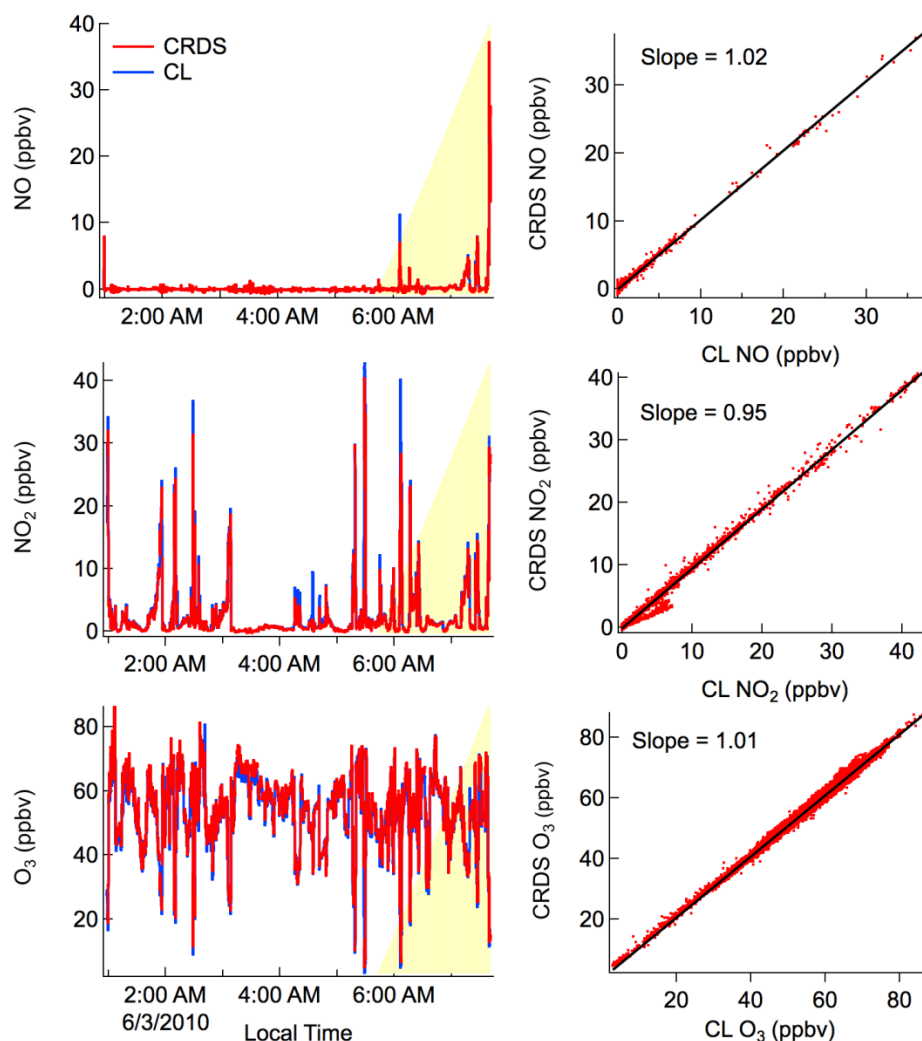
Figure 6-8: The left panels show sample NO (upper panels), NO₂ (middle panels) and O₃ (lower panels) mixing ratio from both the CaRDS instrument in red and the chemiluminescence (CL) measurements in blue for the 3 June flight. The right panels show the correlations of the two measurements for each species. There was a small population of points on this flight for which there was a deviation on the NO₂ measurement, likely related to the zero measurement on one or the other instruments. These deviations were not observed on other CalNex flights.

The NO, NO_2 and O_3 data for the same flight are shown in the left panels of Figure 6-8. Very little NO was encountered during darkness on this flight since the majority of the sampled air masses were distant from direct NO_x emission sources. Several NO_2 plumes were encountered throughout the night, many of which showed distinct anticorrelations with O_3 due to titration and subsequent nighttime

chemistry within these plumes. After sunrise, the NO_x containing plumes showed measurable levels of NO, which peaked near 30 ppbv during landing at Ontario airport.

The standard P-3 instrument for measurement of ambient NO, NO_2 and O_3 is a custom-built, high-precision, research grade chemiluminescence (CL) instrument [77, 109, 110]. The NO_2 channel of the CL instrument has recently undergone substantial improvement to the photolysis system for conversion of NO_2 to NO and modifications of inlet and sample flow path for improved time response of all channels [111]. The right three panels of Figure 6-8 show the scatter plots comparing NO, NO_2, and O_3 measurements from the 405 nm CaRDS instrument with those from the CL instrument at 1 s time resolution. The instruments agree to within 3% for NO, 5% for NO_2, and 1 % for O_3 measurements, which is within the summed accuracy of both instruments for each species. Correlation among all measurements was excellent, with R^2 values ≥ 0.99. Much of the scatter in the correlation plots is the result of synchronization between the instruments when transecting NO_x plumes with sharp edges. Although CaRDS is lower in precision than the CL instrument and is subject to some baseline instability as described above, the comparisons in Figure 6-8 demonstrate that it is accurate, at least at larger NO_x and O_3 values.

One common diagnostic used to understand the nighttime reactivity of NO_3 and N_2O_5 is their steady state atmospheric lifetime [11]. The steady state lifetime of a species can be determined from its rate of production and its concentration, defined in equation 6-12 and equation 6-13 for NO_3 and N_2O_5 [44].

$$\tau_{SS}(NO_3) = \frac{[NO_3]}{k_1[O_3][NO_2]} \approx \left(k_{NO_3} + k_{N_2O_5}K_{eq}[NO_2]\right)^{-1} \tag{6-12}$$

$$\tau_{SS}(N_2O_5) = \frac{[N_2O_5]}{k_1[O_3][NO_2]} \approx \left(k_{N_2O_5} + \frac{k_{NO_3}}{K_{eq}[NO_2]}\right)^{-1} \tag{6-13}$$

Here τ_{SS} (NO_3) and τ_{SS} (N_2O_5) are the steady state lifetimes and k_1 is the rate constant for reaction equation 6-1. When the steady state approximation is valid the lifetimes can be used to determine the pseudo first-order loss rate of NO_3 and N_2O_5, k_{NO_3} and $k_{N_2O_5}$. K_{eq} is the equilibrium constant for reaction equation 6-2.

In past field campaigns, this analysis would require data from at least two separate instruments. Figure 6-8 demonstrates the advantage of the combined measurements of nighttime nitrogen oxides (NO_2, NO_3 and N_2O_5) and O_3 into a single instrument. Figure 6-9 shows the steady state lifetimes for the flight of 3 June. The lifetimes of NO_3 range from 0–1.5 h and lifetimes up to 3 h are observed for N_2O_5. Thus, the combination of NO_2, O_3 with NO_3 and N_2O_5, all tied to a single analytical standard, provides a complete and accurate representation of nighttime nitrogen oxide chemistry.
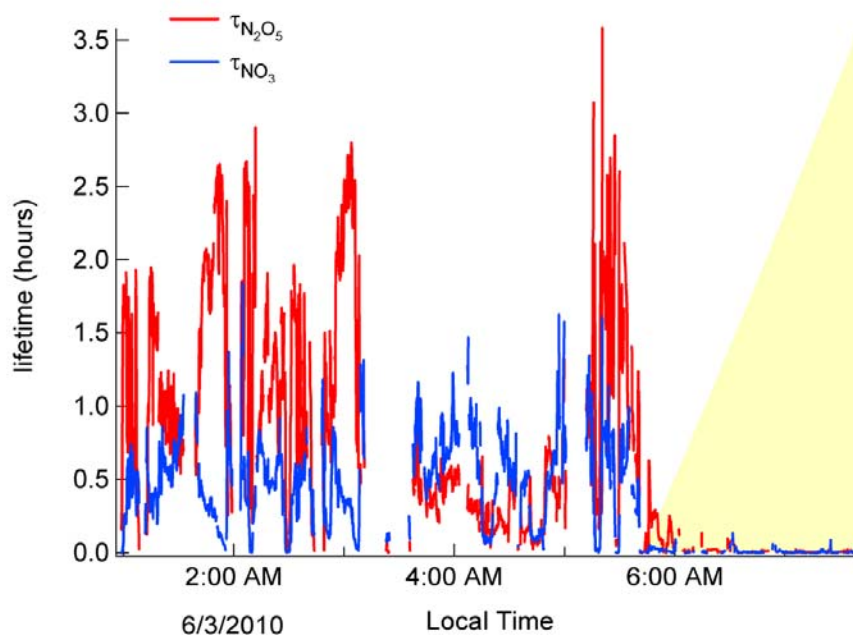
Figure 6-9: The lifetimes of NO₃ (blue) and N₂O₅ (red) for the 3 June flight. The lifetimes were calculated using concentrations measured by a single instrument.

6.5 Conclusions

The article has described an aircraft instrument for atmospheric measurements of NO_3, N_2O_5, NO, NO_2, and O_3 by cavity ring-down spectroscopy. NO_3 and NO_2 are measured directly using a diode lasers with center wavelengths of 662 nm and 405 nm. N_2O_5 is thermally converted to NO_3 for measurement and NO and O_3 are chemically converted to NO_2 and measured. Each channel is regularly calibrated in the field by a scheme linking the cross-sections of each measured species to the O_3 cross-section at 254 nm. The inlet transmission of NO_3 and N_2O_5 is also measured regularly in the field. The performance of the instrument was demonstrated during its first deployment on the NOAA P-3 in California during a 2010 field intensive.

7. Publication E:

A measurement of total reactive nitrogen, NO_y, together with NO_2, NO, and O_3 via cavity ring-down spectroscopy

Authors:

Robert J. Wild,[1,2] Peter M. Edwards,[1,2] William P. Dubé,[1,2] Karsten Baumann,[3] Eric S. Edgerton,[3] Patricia K. Quinn,[4] James M. Roberts,[2] Andrew W. Rollins,[1,2] Patrick R. Veres,[1,2] Carsten Warneke,[1,2] Eric J. Williams,[2] Bin Yuan,[1,2] Steven S. Brown[1]

[1]*Cooperative Institute for Research in the Environmental Sciences, University of Colorado, Boulder, Colorado 80309, USA.*

[2]*Earth System Research Laboratory, NOAA, Boulder, Colorado 80305, USA.*

[3]*Atmospheric Research and Analysis, Inc., Cary, North Carolina 27513, USA.*

[4]*Pacific Marine Environmental Laboratory, National Oceanic and Atmospheric Administration, Seattle, Washington 98115, USA.*

Abstract:

We present a sensitive, compact detector that measures total reactive nitrogen (NO_y), as well as NO_2, NO, and O_3. In all channels, NO_2 is directly detected by laser diode based cavity ringdown spectroscopy (CaRDS) at 405 nm. Ambient O_3 is converted to NO_2 in excess NO for the O_3 measurement channel. Likewise, ambient NO is converted to NO_2 in excess O_3. Ambient NO_y is thermally dissociated at ~700°C to form NO_2 or NO in a heated quartz inlet. Any NO present in ambient air or formed from thermal dissociation of other reactive nitrogen compounds is converted to NO_2 in excess O_3 after the thermal converter. We measured thermal dissociation profiles for six of the major NO_y components and compared ambient measurements with other instruments during field campaigns in Utah and Alabama. Alabama measurements were made in a rural location with high biogenic emissions, and Utah

measurements were made in the wintertime in unusual conditions that form high ozone levels from emissions related to oil and gas production. The NO_y comparison in Alabama, to an accepted standard measurement method (a molybdenum catalytic converter/chemiluminescence instrument), agreed to within 12 %, which we define as an upper limit to the accuracy of the NO_y channel. The 1σ precision is <30 pptv at 1 s and <4 pptv at 1 min time resolution for all measurement channels. The accuracy is 3 % for the NO_2 and O_3 channels and 5 % for the NO channel. The precision and accuracy of this instrument make it a versatile alternative to standard chemiluminescence-based NO_y instruments.

7.1 Introduction

Reactive nitrogen compounds play a central role in atmospheric chemistry. Nitrogen oxides ($NO_x \equiv NO + NO_2$) strongly affect the oxidative capacity of the atmosphere through the catalytic cycle that produces ozone (O_3) in the lower atmosphere. Total reactive nitrogen (NO_y) includes NO_x and all its reservoirs:

$$NO_y \equiv NO + NO_2 + NO_3 + 2N_2O_5 + HNO_3 + HONO + HO_2NO_2 + PAN \text{ (peroxy acetyl}$$
$$\text{nitrates)} + \text{aerosol nitrates} + \text{organic nitrates}$$
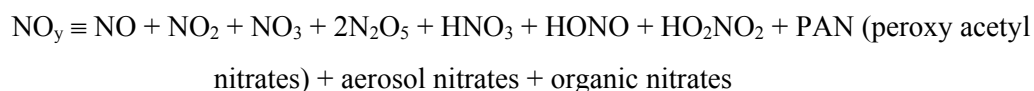
Knowledge of the abundance of this chemical family, as well as NO, NO_2, and the related compound O_3, is a useful indicator of total nitrogen emissions, air mass age, competition between different chemical processes, and the efficiency of ozone production associated with particular emission sources. Standard measurements of NO_y rely on catalytic decomposition of NO_y to NO, followed by NO detection using chemiluminescence [112, 113]. The most commonly used materials for conversion are gold and molybdenum. However, catalytic converters are prone to deterioration, affecting conversion efficiencies. As a result, they require calibrations at least every few days and must be reconditioned, or cleaned, every few months of continuous operation, although the latter depends on the history of exposure [112-114]. Additionally, the chemical processes involved in the catalytic conversion are not fully understood [115]. Inlet design can also play a major role, as some NO_y species, notably HNO_3, can suffer significant losses on non-heated inlet surfaces [113, 116].

In this paper, we report a new method for detection of NO_y as part of a compact system that measures NO, NO_2, NO_y, and O_3 based on cavity ring-down spectroscopy (CaRDS). Similar to direct absorption spectroscopy, CaRDS is an absolute measurement of trace gas concentration, with an accuracy inherently limited only by knowledge of the absorption cross-section and potential interfering absorbers. For the instrument described here, small species-dependent corrections must be made only for sampling losses, conversion efficiencies, and dilution actors. Furthermore, the instrument has lower power, size, weight, and vacuum requirements than a chemiluminescence-based instrument while approaching its sensitivity, precision, and time response. In the NO_y CaRDS instrument we describe

here, NO_y and its components are converted into NO_2 by thermal decomposition (TD) in a fused silica inlet (henceforth referred to as quartz following convention), followed by the addition of ozone to convert NO to NO_2. The successful use of TD has been demonstrated for various individual NO_y compounds (N_2O_5 [1], peroxy nitrates [117, 118], HONO [119], $ClNO_2$ [120], alkyl nitrates, and HNO_3 [118, 121]), but the combination of thermal dissociation plus ozone has not, to our knowledge, been demonstrated previously for measurement of total NO_y. It represents an analytical simplification for NO_y measurements over methods that only detect NO_2 through thermal dissociation, since it does not require the summation of separate measurements. We combine this with existing techniques for measuring NO, NO_2, and O_3, allowing all four of these important and related species to be measured simultaneously with precision, accuracy, and time response sufficient for their measurement in ambient air across a range of environments and measurement platforms, including measurements from moving vehicles.
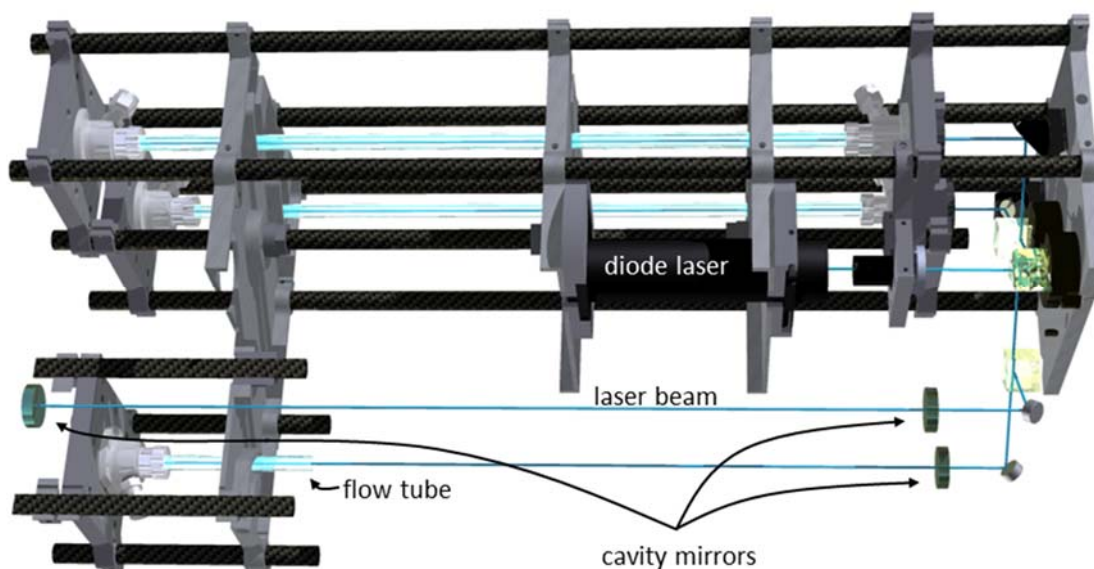
Figure 7-1: Schematic of the custom cage system that houses all the optical components. A large section has been cut out for ease of illustration. The laser is shown in blue, and the optics have been left in place. The combination of aluminum plates and carbon fiber rods give the system high mechanical rigidity, helping to achieve a measurement precision of a few pptv on a minute time scale.

7.2 Experiment

The instrument is based on in-situ detection of NO_2 via cavity ring-down spectroscopy [3, 84, 122-124]. The working principle of CaRDS, as well as the conversion of O_3 and NO to NO_2, has been described in detail in previous papers [3, 103] and will only be summarized here with emphasis on the design improvements. Sampling is done by pulling ambient air through Teflon inlet lines or our NO_y converter, and data are acquired in 1 s intervals. An 80 mW laser diode centered at 405 nm and modulated with a 2 kHz square wave provides light for the four measurement channels. A Faraday

optical isolator provides protection from optical feedback into the laser. When the light is modulated off, the intensity inside the optical cavities decreases exponentially as measured by four photomultiplier tubes that detect the light intensity transmitted through the rear mirrors. The exponential decays are co-added and fitted once per second to extract the time constant with (τ) and without (τ_0) the absorber present. The number density of the absorber is then given by

$$[NO_2] = \frac{R_L}{c\sigma_{NO_2}}\left(\frac{1}{\tau} - \frac{1}{\tau_0}\right)$$ (7-1)

where c is the speed of light and σ_{NO_2} is the NO2 absorption cross-section. Previous 405 nm CaRDS instruments from this group have included purge volumes adjacent to the mirrors to maintain their cleanliness. Purge volumes require a multiplicative factor, $R_L = d / l$ in equation 7-1, where d is the mirror separation and l is the length over which the sample is present. This factor may have had a dependence on pressure that introduces uncertainties into the measurement [4]. The instrument described here does not currently include mirror purge volumes, which simplifies the calibrations and eliminates a possible source of error. However, the elimination of the purge volumes can lead to degradation in mirror reflectivity under some circumstances. Since the sampled air is in direct contact with the mirrors, some compounds can condense onto the mirrors, causing a decrease of the time constants. This has been observed in an environment with high relative humidity and required drying of the sampled air. We have also encountered mirror degradation in the NOy channel under conditions of extremely large hydrocarbon concentration in ambient air, to be discussed below.

The optical system is mounted in a custom designed cage system with 1/2 in. (12.7 mm) carbon fiber rods providing stability against mechanical and thermal stress. A schematic of the cage system can be seen in Figure 7-1. To increase stability and compactness over previous designs, the distance between cavity mirrors has been reduced from 1 m to 50 cm. We reuse the cavity mirrors with 1 m radius of curvature and have found a minimal loss of sensitivity. The corresponding ring down time constant (τ_0), determined by a combination of mirror reflectivity and Rayleigh scattering losses at ambient pressure, is approximately 30 µs, with a precision (1σ, 1s) of 6 ns.

The instrument as a whole is compact and requires low power and maintenance. It measures approximately 110 cm high with a 50 by 70 cm footprint and consumes 300 W of power at its peak. It weighs 95 kg, which includes the sample pump, a zero air generator, and the data acquisition system. The data acquisition system, however, has not been designed for low weight and currently contributes 15 kg, a figure which could be substantially reduced. The instrument also requires a cylinder of O2 and a cylinder of NO (2000 ppm in nitrogen). These additions can be contained in 1.2 L cylinders mounted directly in the instrument rack and last for 4 days of continuous operation. Standard 30 L cylinders would provide >120 days of continuous operation.

NO_2 concentrations are directly determined in all channels using equation 7-1, whereas NO, O_3, and NO_y are quantitatively converted to NO_2 prior to measurement. Atmospheric NO is converted to NO_2 via reaction with excess O_3, created by flowing O_2 over a Hg Pen-Ray lamp (185 nm). As described in detail by Fuchs et al. [3], the added O_3 results in a small percentage (<1 %) of NO_2 conversion to NO_3, which subsequently reacts with NO_2 to form N_2O_5. Similarly, O_3 is converted to NO_2 via the same reaction by the addition of excess NO as described by Washenfelder et al. [103], but without the N_2O_5 interference because $NO + NO_3 \rightarrow 2NO_2$.

Conversion of the NO_y species is performed via gas-phase thermal dissociation in a quartz inlet, chosen for its high melting point and because it is relatively unreactive [121]. Figure 7-2 depicts a conceptual drawing of the NO_y converter. During normal operations, the front half of a quartz tube is heated such that the sample air reaches a temperature of approximately 700°C. The inset shows a typical temperature profile of the gas in the heater (set to heat the gas to 750°C), measured by insertion of a thermocouple probe in the gas flow during ambient air sampling. For a 1.5 SLPM flow, the plug flow residence time in the heated section is approximately 48 ms. The Reynolds number is <1000 for the given range of temperatures, well in the laminar flow regime. The metal shell ends in a cone-shaped nozzle to ensure that the quartz is heated to the inlet end in order to minimize losses of HNO_3, which can be significant on colder surfaces, especially quartz [116]. After the heated section, NO_y components have been converted to NO_2 (and possibly some NO), which can be transported to the CaRDS measurement cell through an arbitrary length of Teflon tubing without significant losses. Since the converter itself functions as the inlet, we anticipate particulate sampling with high efficiency and include particulate nitrate in our NO_y budget [125]. Particulate nitrate entering the converter should evaporate rapidly, eliminating inertial loss normally associated with particulate sampling. However, we have not attempted to determine a characteristic cut point (a size at which particles are no longer transmitted effectively) for the converter as a whole. The thermal conversion process likely produces mainly NO_2, although some compounds, such as HONO, may dissociate to NO [119]. A small fraction of the NO_2 may also be reduced to NO by reaction with atomic oxygen in the converter [121]. Finally, the thermal converter is not designed to convert NO to NO_2. Any NO in the air sample after the heating and cooling process is converted to NO_2 via addition of excess O_3 just prior to the CaRDS measurement cell, as in the NO_x channel. The O_3 is generated from the same Pen-Ray ultraviolet lamp source and split evenly between the two channels using a pair of critical orifices to divide the flow.

To zero the instrument (i.e. to measure τ_0 in equation 7-1), we flush the sample tube by overflowing the inlets with air from which all NO_x and O_3 has been removed (zero air) that is generated in-situ (or supplied by a cylinder when necessary). We overflow using an annular inlet (i.e. with zero air added through a large diameter tube that surrounds and extends just beyond the sample inlet) for the NO, NO_2, and O_3 channels, and a simple tee fitting, shown in Figure 7-2, is used for the separate NO_y inlet.
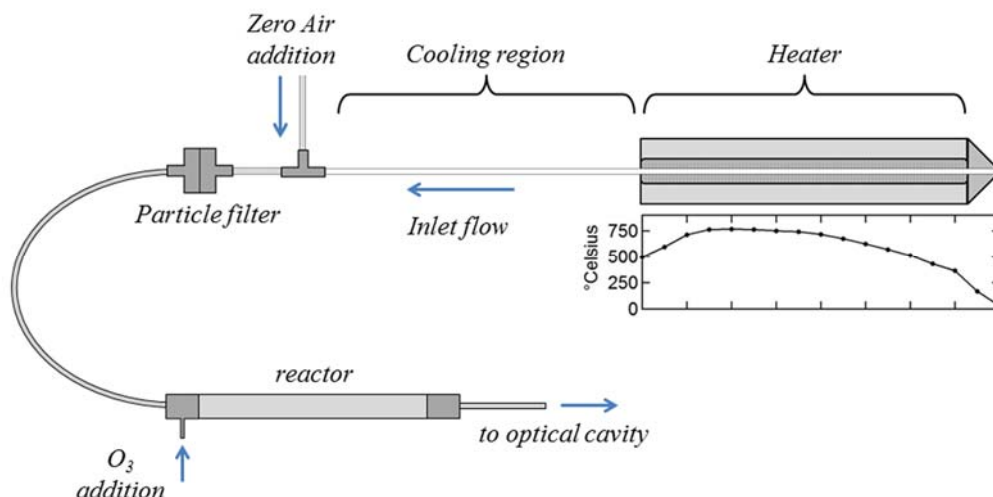
Figure 7-2: Diagram of the NO$_y$ converter. The heated section consists of nichrome wire wrapped around a quartz tube. It is thermally insulated with fiberglass insulation and encased in a metal shell ending in a cone, protecting the quartz and conducting heat to the tip. A profile of air temperature as a function of position inside the heater with a flow of 1.5 standard liters per minute at atmospheric pressure is shown (with set point higher than normal operation). The total residence time in the heated section is about 48 ms. The zero air addition is used for a periodic measurement of τ_0. Just before the optical cavity, excess O$_3$ is added to convert any NO to NO$_2$.

The overflow during the zeroing process creates a pressure change of <0.2 hPa (0.03 %) for the annular inlet and a change of 4 hPa (0.5 %) in the NO$_y$ inlet. The changes in pressure for the NO$_y$ zeroing changes the Rayleigh scattering of the air sample, requiring a correction of approximately 60 pptv equivalent NO$_2$, which is based on well-known Rayleigh cross-sections and is accurate to well within 3 pptv. We zero the channels every 7 min during mobile platform operations but increase this time to 15 min for stationary settings (a zero takes between 30 and 90 s, depending on the length of the inlet).

7.3   Results and discussion

7.3.1   Laboratory tests

To illustrate the conversion of the various NO$_y$ components, we show measured temperature profiles of the signal from several NO$_y$ species in Figure 7-3. Many of these conversions have been previously demonstrated with heated quartz [117, 119-121], and we have repeated tests for the compounds that were readily available. For most samples, the output concentration was uncalibrated and scaled to unity in Figure 7-3, but a leveling off at high temperature strongly suggests unit conversion. We did not explicitly test conversion of the nitrate radical, NO$_3$, but expect full conversion at the operating temperature [126]. We directly compared our measurements of HNO$_3$ and PAN to that of a heated Mo catalytic converter and saw full conversion at our operating temperature of 700°C. The alkyl nitrates (a mix of methyl, ethyl, i-propyl, n-propyl, ipentyl, and i-butyl nitrate from a calibration cylinder) show a rapid conversion to NO$_2$ up to 300°C, then a slower increase up to 800°C, where we

see full conversion to within the cylinder specifications (±10 %). The slower conversion at higher temperature differs from previously reported temperature profiles for organic nitrates [121] and may be due to the temperature profile specific to our inlet. Since our design goal is total rather than speciated NO_y, the behavior of organic nitrates at intermediate temperatures does not significantly affect the performance of the total NO_y measurement.
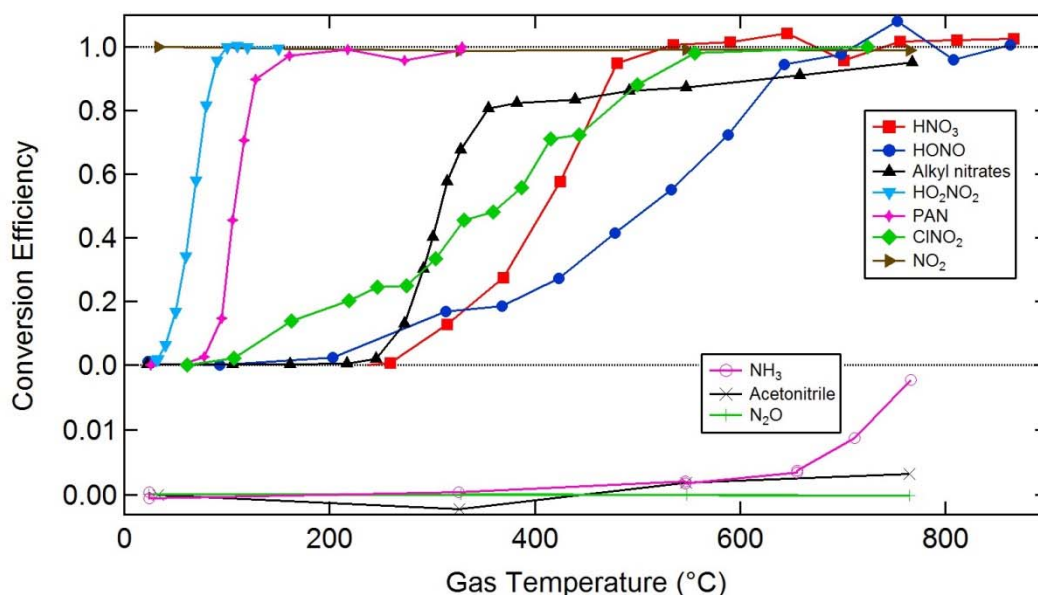
Figure 7-3: (Upper plot) Temperature profiles of several of the most abundant components of NO_y. HNO_3 and alkyl nitrates were compared to a known standard, and the other compounds are scaled to unity at high temperatures. (Lower plot) Temperature profiles from known quantities of possible interference compounds. NH_3 in dry air resulted in the only measurable interference of <1 % at 700°C. The interference was less than 0.1 % for air with a relative humidity of 10 % or greater.

Some nitrogen-containing gases that are not products of NO_x oxidation and therefore not components of NO_y as traditionally defined could conceivably be converted to NO_x at high temperatures. If they are present at mixing ratios comparable to or larger than NO_y in the atmosphere, as can be the case for NH_3, N_2O, and nitriles, these compounds could represent a significant interference for an NO_y measurement based on thermal conversion to NO_2. We sampled known standards of NH_3, N_2O, and acetonitrile with the thermal converter, as shown in the lower plot of Figure 7-3. Ammonia resulted in the only nonzero interference, reaching about 1 % conversion at our working sample temperature of 700°C. However, this interference was only present in dry air from a cylinder (<1 ppmv water vapor mixing ratio). A relative humidity of 10 % was enough to suppress the NH_3 conversion to NO_2 to below 0.1 %, such that it can be considered a negligible interference in nearly all field situations. Like Day et al., we do not expect to be sensitive to aromatic nitro compounds [121]. Furthermore, they are not typically expected to be a large fraction of NO_y. Reports of particle bound nitro-PAHs in Los Angeles, for example, have an equivalent gas phase concentration <0.1 pptv [127].

Other interferences to NO_2 detection using 405 nm CaRDS have been described before. A water vapor interference results from the change in Rayleigh scattering, which was measured by Fuchs et al. [3] and results in a small correction to our data. Absorbing gases other than NO_2, such as α-dicarbonyls, are a direct interference but constitute a small percentage of NO_x in most scenarios [3]. However, since these compounds require a higher dissociation temperature than our NO_y converter provides, they only represent an error in the NO_2 baseline. The subtractive measurements of NO, O_3, and NO_z ($\equiv NO_y -$ NO_x) are therefore unaffected by α-dicarbonyls. Direct absorption by ambient O_3 in the NO and NO_2 channels represents a negligible interference because the absorption cross-section of O_3 at 405 nm is 1.5×10^{-23} cm^2 (~4×10^4 times smaller than that of NO_2) [3, 128]. For 50 ppbv of O_3, the optical extinction is 1.9×10^{-11} cm^{-1}, or equivalent to approximately 1 pptv of NO_2. The optical extinction due to the added 30 ppmv O_3 in the NO_x and NO_y channels is measurable, but this signal is constant across instrument zeroing and thus does not contribute to the measurement. However, it provides a convenient means to measure the added O_3 by switching the O_3 addition on and off during periods of zero air sampling.

The NO_2 calibrations of the four channels have also been described in previous papers [3, 103]. O_3 is measured by a commercial UV absorption O_3 instrument and then quantitatively converted to NO_2 in excess NO. The NO_2 is then measured by CaRDS in the four channels. This provides four measurements of the effective absorption cross-section, σ_{NO_2}, which differ by less than 2 % between the channels. The day-today variability of these measurements is less than 1 %. Figure 7-4 shows a typical plot showing the relation between integration time and 1σ precision (Allan deviation plot) for the four channels during sampling of zero air. The dashed lines indicate the expected square root relationship for statistically random noise. All channels follow a nearly statistical noise distribution out to 100 s integration time, resulting in a minimum detection limit of a few parts per trillion volume. The uncertainties of the NO_2 measurement in the four channels are due to calibration uncertainties and result in a 3 % uncertainty in the base measurement. 16 Conversion of NO_2 to N_2O_5 in the two channels that add excess O_3 (NO_x and NO_y) increases the uncertainty of NO_x measurements up to 5 %.
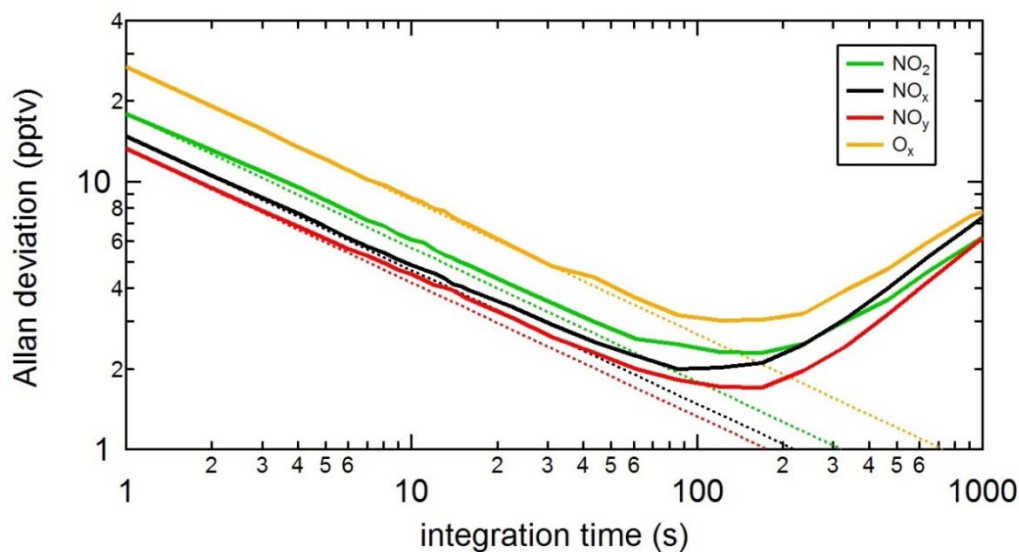
Figure 7-4: Dependence of 1σ precision on integration time (Allan deviation plots) for the four channels measuring NO$_2$ in zero air under laboratory conditions. The dashed lines show the expected trend for statistically random noise. The uncertainty of the NO$_y$ measurement must include the conversion efficiency uncertainties for the different O$_y$ compounds. The comparisons to known concentrations (HNO$_3$, PAN, and alkyl nitrates) showed full conversion to within the uncertainty of the standards (approximately 10 %, from the uncertainty in conversion efficiency of the Mo converter and the alkyl nitrate cylinder mixing ratio). But for the other compounds, quantitative conversion was implied by the temperature profile, and uncertainties are unavailable. We derive a total uncertainty empirically by comparison of the thermal dissociation CaRDS instrument to a standard NO$_y$ instrument under field conditions. The results of this comparison, discussed below, suggest a limiting uncertainty in the NO$_y$ measurement of 12 %.

7.3.2   Field comparisons

The new NO$_y$ detection scheme was quantitatively tested during two field comparisons in 2013. One was the Uintah Basin Winter Ozone Study (UBWOS) 2013, during which our measurement was compared to the sum of the separately measured NO$_y$ components. The other comparison occurred during the Southeast Oxidant and Aerosol Study (SOAS), where our total NO$_y$ measurement was directly compared to total NO$_y$ measured with a standard Mo catalytic converter.

The UBWOS 2013 campaign was a four-week study in the Uintah Basin of Utah in February and March. The area is host to extensive oil and gas operations and regularly experiences strong temperature inversions. This results in very high ozone events as well as elevated levels of NO$_z$ ($\equiv$ NO$_y$ − NO$_x$, averaging about 12 ppbv over the campaign), making it an ideal field test for the NO$_y$ converter. In addition to our measurement of total NO$_y$ and NO$_x$, two chemical ionization mass spectrometers measured concentrations of HNO$_3$, ClNO$_2$, HONO, and PAN [39, 129]. A particle-into-liquid sampler measured particle phase inorganic nitrate, and a separate cavity ring-down system measured NO$_3$ and N$_2$O$_5$ [1].
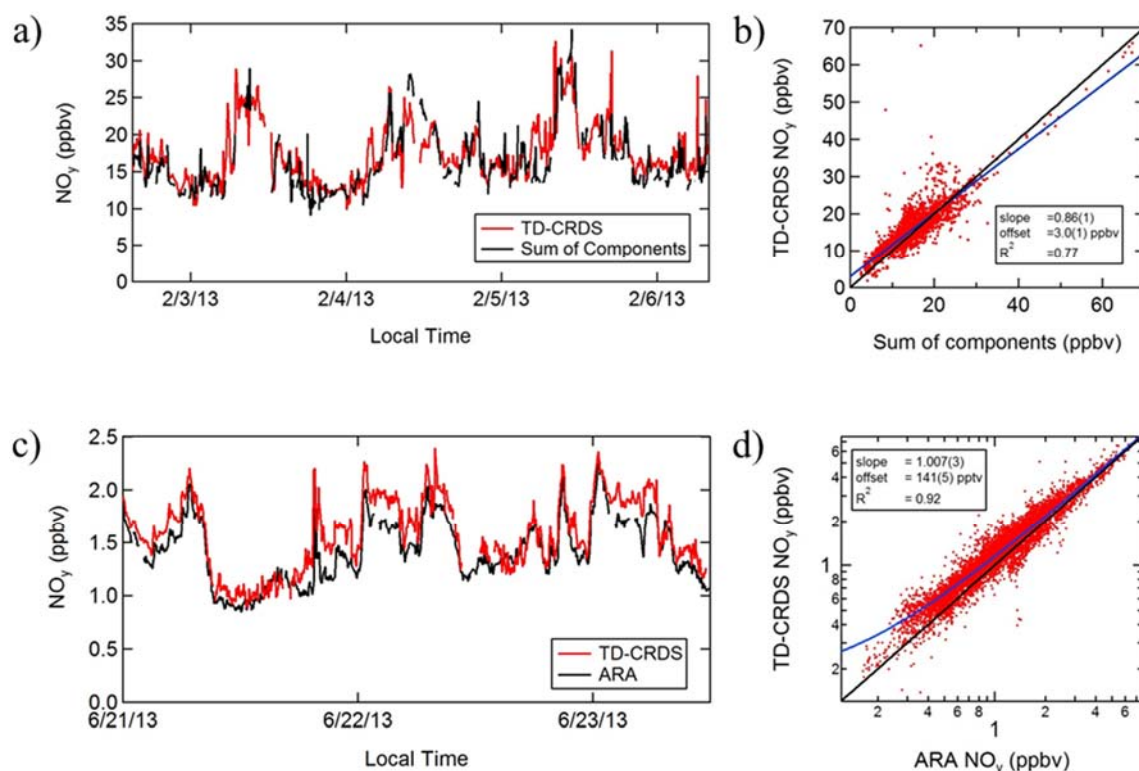
Figure 7-5: (a) A representative time series showing several days of measurement comparing the total NO_y as measured by our instrument with the sum of NO_y components during the February/March UBWOS field campaign, during which NO_x contributed 28 % to NO_y. (b) Correlation plot of NO_y to the sum of components for the entire campaign. (c) A time series comparing the total NO_y measured by TD to total NO_y measured by a Mo catalytic converter used by Atmospheric Research and Analysis, Inc. (ARA) during the June/July SOAS field campaign, during which NO_x contributed 43 % to NO_y. (d) Correlation plot for the two methods for the entire campaign. All data shown are 5 min averages.

During this campaign we observed degradation of the mirror reflectivity to unworkable values over the course of 5 min time scales when sampling behind the heated inlet and without purge volumes in place. The cause of this degradation was not clear, but it may have been the result of production of condensable gases from hydrocarbon degradation occurring in the NO_y converter. Measured hydrocarbon mixing ratios were anomalously large, in excess of 0.5 ppmv on average and frequently several parts per million, due to the location of the sampling site in a natural gas extraction field [130]. Installation of a hydrocarbon scrubber tube downstream of the NO_y converter prevented mirror reflectivity degradation without apparent influence on measured NO_y, increasing response time by a mere 150 ms[1]. We observed

---

[1] This hydrocarbon scrubber is the same as the one used in the Thermo Electron Corporation's Model 43C-TLE SO_2 instrument. Documentation can be found at www.thermo.com/eThermo/CMA/PDFs/Product/productPDF_20982.pdf

the scrubber to be required for measurements during this campaign, though subsequent trials, including another campaign in the Uintah Basin in 2014, did not require use of the scrubber. In the upper part of Figure 7-5, we show the comparison between our total NO_y measurement and the sum of the NO_y components as measured by different instruments (not including organic nitrates), for which NO_x represents a 28 % contribution to NO_y. Figure 7-5 shows a representative time series over a few days. In Figure 7-5b we plot the correlation between the NO_y measurement and the sum of the components over the whole campaign. The data presented are 5 min averages because inlets had small differences in location (several meters separation) at the field site, and because of frequent transient high-NO_x spikes that were inhomogeneously mixed. On average, the new NO_y instrument measured 0.9 ppbv (6 %) higher NO_y than the sum of components. This difference may be due to organic nitrates, for which data are not available in 2013, or simply from the combined uncertainties of the individual measurements.

The SOAS campaign was a six-week study in central Alabama in June and July of 2013. The site is co-located with a SEARCH network monitoring station maintained by Atmospheric Research and Analysis, Inc. (ARA), which collects long-term measurements of a suite of gases, including total NO_y. The ARA NO_y measurement is performed using a standard Mo catalytic converter that converts NO_y to NO, followed by chemiluminescent detection of NO. The SOAS campaign thus provided an opportunity for direct comparison between the TD-CaRDS NO_y and a more conventional NO_y instrument. The inlets were separated by about 110 m horizontally and 15 m vertically, with the ARA inlet positioned a few meters above ground. Although mirror purge volumes were also not used for this campaign, a hydrocarbon scrubber as in the UBWOS campaign was not required. However, the high humidity of air sampled during summertime in Alabama required drying the sample air with a cold trap for all the channels (after the converter for the NO_y channel) in order to avoid signal degradation due to water vapor condensation on the mirrors. This modification is similar to that used on commercial CaRDS instruments that measure NO_2 alone [124]. The cold trap reduced the relative humidity to <15 % but did not measurably influence the transmission of NO_2.

The lower part of Figure 7-5 shows a comparison of the two measurements. In this case, the average NO_x contribution to NO_y was 43 % during the SOAS campaign. High concentration spikes tended to show poorer agreement, most likely due to the separation between the inlets. In Figure 7-5c, we plot a time series of the two instruments spanning 2 days with low occurrences of large concentration spikes. In Figure 7-5d, we show a correlation plot of all the data from the campaign. The slope is equal to unity to within our 5 % measurement uncertainty, but there is an average offset of about 140 pptv. This offset may be caused by variation in the sensitivity to specific components of NO_y, such as coarse aerosol nitrate, between the two instruments, a real difference in ambient NO_y due to the separation of the inlets, a systematic error between the two instruments, or a combination of these. Nevertheless, the observed offset provides an upper limit for our NO_y measurement uncertainty relative to an accepted standard

measurement method. Taking the difference between the two measurements, dividing it by our measurement, and averaging the result over the whole campaign results in a 12 % upper limit uncertainty estimate for our NO_y measurement.

7.4 Conclusions

In summary, we have described a compact CaRDS instrument measuring NO, NO_2, O_3, and total NO_y. Although we encountered potential artifacts due to response of the mirrors to relative humidity and extreme VOC concentrations, the instrument in its current form is robust, able to operate essentially unattended for days to weeks at a time. We have further demonstrated a new technique for measuring NO_y using thermal decomposition to NO_2 in a heated quartz inlet, followed by conversion of NO to NO_2 in excess O_3.

Temperature profiles of individual components are consistent with unit conversion efficiency for every NO_y component measured, and there is no significant interference from other reduced nitrogen compounds. Instrument performance has been demonstrated with comparisons at two ground sites. These field tests show agreement both with the sum of NO_y components measured by separate, independent instruments and with a measurement of total NO_y by a standard molybdenum catalytic converter to within <1 % correlation and an absolute offset of 140 pptv. The latter comparison allows us to empirically define an upper limit on the NO_y measurement uncertainty of 12 %, although the uncertainty may depend on the relative concentrations of NO_y components. The instrument performance was equivalent while sampling from within a moving vehicle (instrumented van) and is likely to be appropriate for aircraft sampling based on our previous experience [4].

Future work will involve investigation of methods to prevent mirror degradation without the need for drying the sample air or scrubbing it of hydrocarbons. Designs are currently being tested for smaller purge volumes that require smaller path length corrections than our previously reported instruments, or for testing other methods to make the mirrors less susceptible to condensation effects. The current instrument, while smaller than previously reported versions, can be further reduced in size and weight to allow for more versatile deployments on mobile platforms.

8. Discussion

The author's main contributions in the development of CaRDS instruments for airborne detection of nitrogen oxides are in six areas: instrument rack design, automated filter changer, low loss inlet design and flow control, optical cage design, clamped/nudged mirror mounts, and purge system improvements. These areas are discussed in detail in this chapter.

8.1 Instrument rack design

The rack design for an airborne instrument is often overlooked. While the main purpose of the rack is to provide physical support for the instrument components, it can also play a role in, for example, vibration isolation. Improvement of rack design can also save mass, which is important in airborne applications where mass is typically highly restricted. Improved rack design can also save cost.

8.1.1 Welded steel instrument rack as replacement for standard aluminum

The traditional instrument rack design is based on riveted and/or bolted aluminum extrusions, plates, and other standard structural parts. This standard rack design is typically used for NASA's airborne instruments. An example of a riveted design is shown to the right in Figure 8-1. The riveted aluminum racks are comparatively expensive and can still be rather heavy. While high-strength aluminum is the established standard material for airborne applications, high-strength 4130 alloy steel was considered instead as a superior instrument rack fabrication material in the NOAA applications presented in this thesis. The specific strength (strength per unit mass) of different steel alloys can be as high, or higher, than that of aluminum. Finite element analyses (Figure 8-2) showed that a frame made from welded 4130 alloy chrome-moly steel could result in higher strength, lower weight (30 % mass reduction), and lower cost than an aluminum rack that is riveted or bolted together. It can also provide better vibration isolation, which will be discussed in subsequent sections.

Extensive finite element analyses (FEA) were performed for the welded steel design for comparison with the traditional riveted aluminum design. Figure 8-2 illustrates the FEA displacement under 7 G loading for the welded steel rack. In all aspects of the finite element analysis and structural analysis, the welded steel design performed equal or better than the riveted aluminum design. FEA simulations and structural analyses on the welded steel instrument racks were submitted to a Federal Aviation Administration (FAA) Designated Engineering Representative (DER) for certification approval. The certification was necessary to use them on research aircrafts, such as the NOAA P-3, the NOAA Twin Otter, the NASA DC-8, and the NCAR C-130.

Welded steel racks were used in numerous field missions [2, 4, 6, 7, 103, 131], as well as the latest mission using the NOAA Twin Otter aircraft (Figure 2-6c and Figure 8-2).
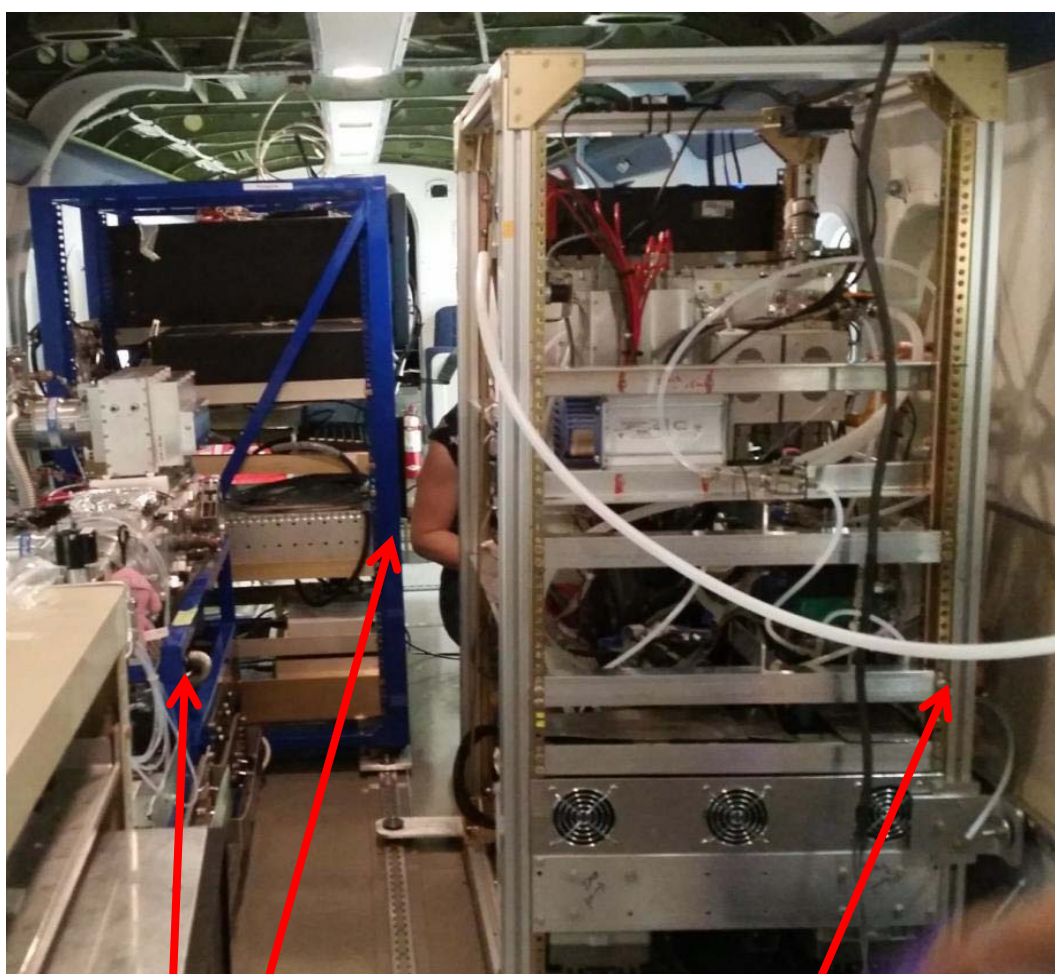
Welded steel instrument racks.

Traditional riveted aluminum
instrument rack.

Figure 8-1: Traditional riveted aluminum instrument rack to the right, and two welded steel racks to the left (in blue) on the NOAA Twin Otter airplane on the latest field mission, the Utah Winter Fine Particulate Study (UWFPS) 2017.
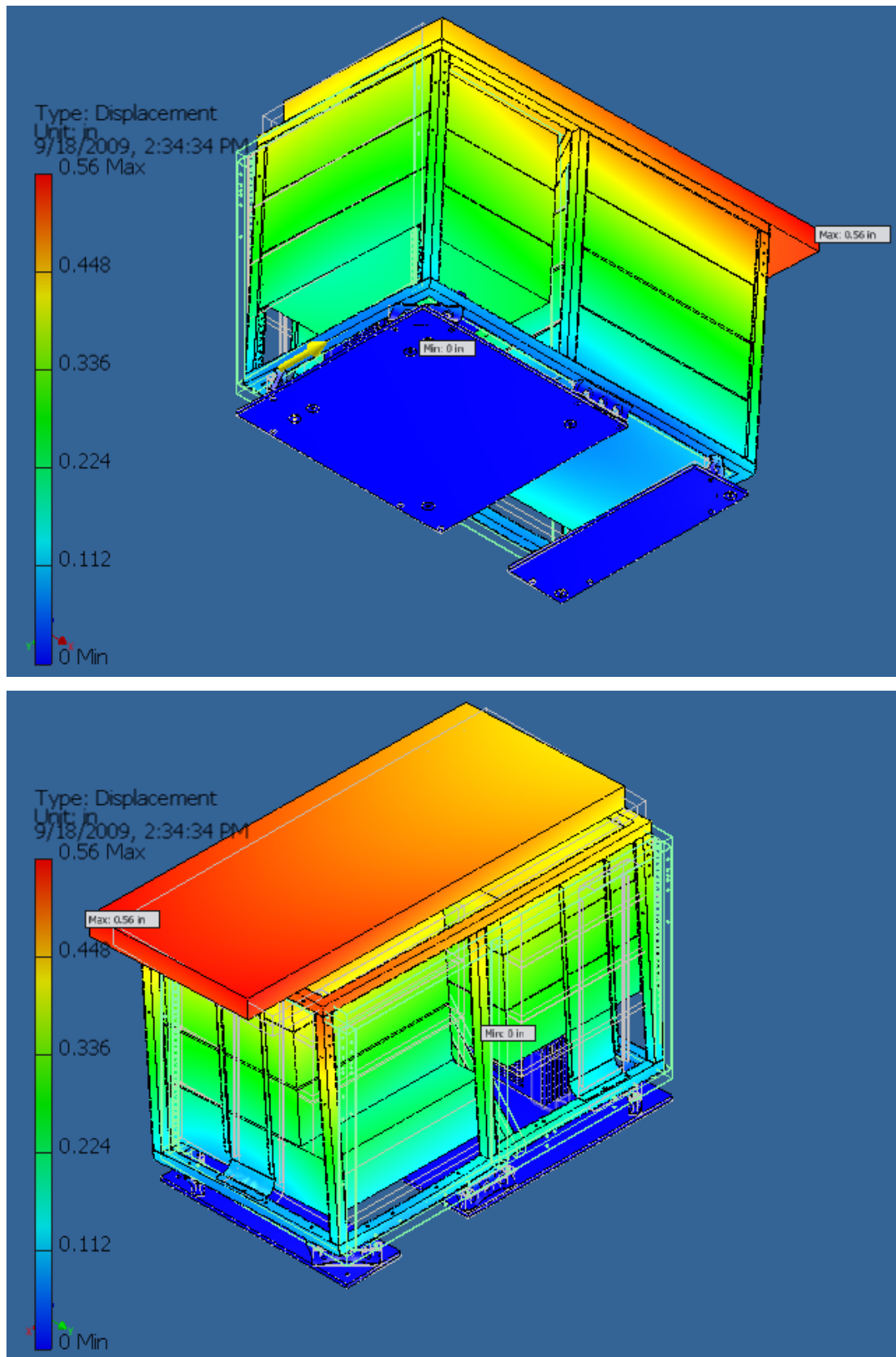
Figure 8-2: Finite Element Analysis of the welded steel instrument rack design. The illustrations display the displacement during a simulated 7G acceleration load.

8.1.2 Vibration isolation

Vibration is always a concern on a mobile platform, particularly on propeller-driven aircrafts. Hence, one of the main focuses for the first deployment of a CaRDS instrument was vibration isolation. Early experience with field deployments of CaRDS systems on a ship had shown that they are rather robust with respect to vibration [1]. Thus, the approach to manage CaRDs instrument vibration in aircraft deployment was less rigorous than initially anticipated. The decision was made to <u>not</u> vibration isolate the optical table in the ARNOLD instrument from the rack and the support systems. Instead, the optical table was purposely coupled to the rack and other non-vibrating support equipment (such as the computer, gas bottles, and flow controllers). The much larger mass caused the optical components to be better vibration isolated from the aircraft and from the vibration isolators. Vibrations that leaked by the wire-rope vibration isolators were attenuated to a degree, by the purposefully supple support frame. Moreover, the instruments and support equipment helped "soak up" and damp the leakage vibration before it reached the optical table and the most vibration-sensitive CaRDS components on the optical table. This approach proved successful as there were virtually no vibration-related issues during the deployment of the instrument. The instrument sensitivity, as measured by the precision of the ringdown time constant, was identical for the aircraft on the ground without engines running and during flights (see [1]).

Over a decade later, the approach to vibration isolation is still the same. Vibration isolation of the entire instrument rack, rather than just the optical components within the rack, has now become the norm for airborne CaRDS instruments.

8.1.3 Benefits of the new rack design

Improved instrument access

- 4130 steel frame members are ~2× the strength and ~3× the modulus of aluminum frame members, resulting in much smaller size of steel frame members of equivalent strength and stiffness.

- The slender steel frame members significantly improve physical access to the individual components installed in the rack, much improving the ease of maintenance and repair of instruments.

Installation advantages

- The smaller steel frame members reduce the outer dimensions of the equivalent capacity rack.

- The smaller overall dimensions, coupled with inset welded instrument mounting rails, allow the 4130 steel racks to be installed on the aircraft fully populated with instruments. This greatly hastens the aircraft integration process and reduces the time required for installation (by more than a factor of 20) for the same capacity steel instrument rack.

Cost savings

- The fabrication cost of a welded 4130 steel rack is approximately 1/5th of the cost of a riveted aluminum rack of the same capacity (US$ 2,500 vs. US$ 12,500 in the year 2017).

8.2 Automated filter changer

As described in section 3.2.3, the largest contribution to the visible extinction signal in ambient air is generally due to scattering by aerosol, which makes filtering of the inlet air necessary. However, manually changing a filter in an airborne instrument inside a pressurized aircraft is far more challenging than in a laboratory environment. The inlet line from the exterior of the aircraft needs to be sealed off and the sampling flow has to be stopped before the filter can be exchanged. After the installation of the new filter, the inlet continuity must be again restored, and the flow through the instrument can be resumed. A manual filter change therefore typically requires a minimum downtime of 10 min with a frequency of typically one filter change per hour, depending on the cleanliness of the atmospheric environment. The frequent and extended downtimes of an instrument in an aircraft do not only affect the spatial coverage of a monitoring mission, and thus the analysis of the data, but it also adds a significant cost to a project. The fuel cost alone of flying the P-3 Hurricane Hunter is ~$10,000 per hour. Although that cost is split over several instruments, it is easy to assign a direct expense of the downtime caused by the filter changes.

The automated filter changer described in section 3.2.3 was one of the first large improvements that made airborne deployment practical. The automated filter changer reduced the filter change time from 10 min to 10-20 s. In addition to the lower downtime, it also allows for autonomous operation of the instrument. An exploded view of the automated filter changer is shown in Figure 3-4. Figure 8-3 shows the filter changer mounted to the ARNOLD instrument.

The greatest challenge in the development of the automated filter changer was the handling and transport of the filters. The filter material is a very thin and delicate porous Teflon membrane. It was not available on a continuous roll, but only as pre-made circular filters with a thin plastic support rim. The filters were not designed to be handled automatically, and they were not uniform or even flat. The spread in curvature varied greatly.[2]

---

[2] The uniformity of the filters has indeed much improved in recent years, but it was a significant challenge when the automated filter changer was initially developed.

The final solution was to place each filter in a support ring before they were loaded in the fresh filter reservoir (to the left in Figure 8-3). The support rings were made of aluminum or Delrin, but mostly aluminum rings were used.

A total of three automated filter changers were built. They have all been in use for ~13 years. One is currently installed on the ARNOLD instrument and another one is installed on the NOAA N_2O_5 and NO_3 CaRDS field instrument "RONALD" (not covered in this thesis). The third one is currently kept as a spare, but has been used by other research groups from time to time. Instruments equipped with the automated filter changers have generated data for a series of publications, [1, 2, 4, 6, 7].
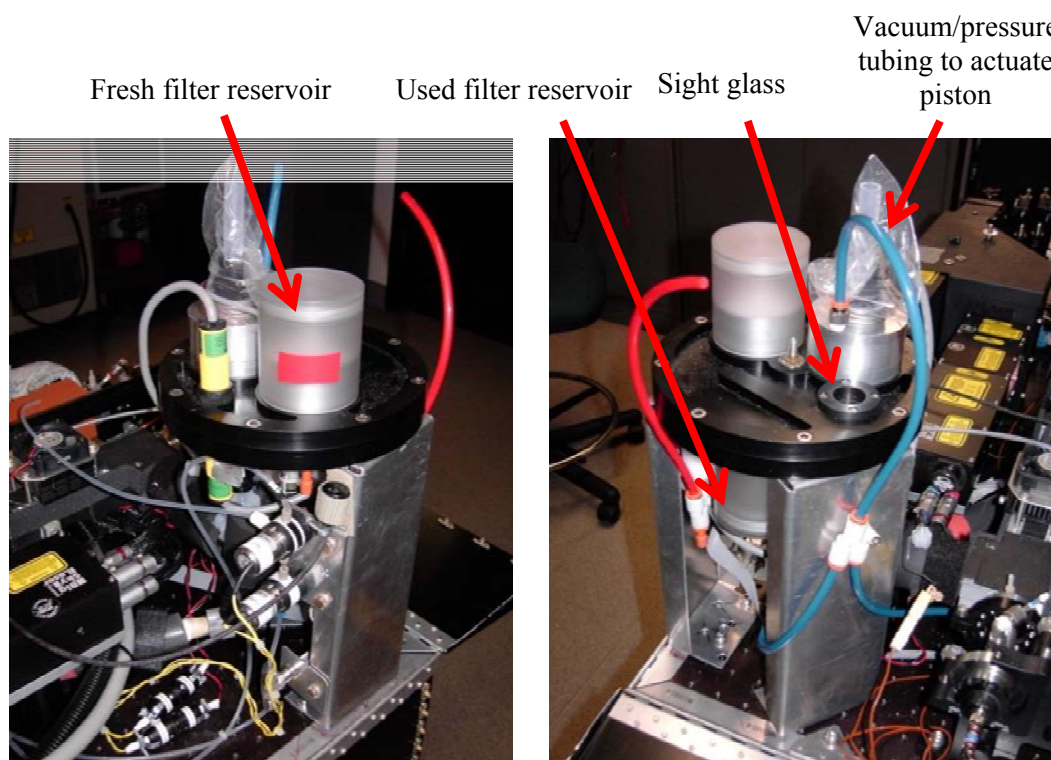

Figure 8-3: The filter changer mounted to the ARNOLD instrument. More details of the design are shown in the exploded view in Figure 3-4.

8.3 Low loss inlet design and flow control

High loss inlets and pressure fluctuations in the gas lines are detrimental to the accuracy of CaRDS instruments. Therefore, proper inlet design and improved flow control are essential for airborne deployment of CaRDS instruments. This section will discuss four major aspects in this context: (i) A low loss Teflon machining technique, (ii) a coaxial flow type zero air addition scheme, (iii) the integration of flow controls, and (iv) isothermal pressure reduction. The improved inlet designs were first used in [2], and have been used in all airborne deployments afterwards [3-5].

8.3.1 Low loss materials and Teflon machining technique

Publication B [2] (Chapter 4) presented a study of gas line transmission losses. This section will present some of the details in the low loss machining, and further work performed to identify the optimum low-loss materials for inlets.

Based on the present knowledge of nitrogen oxide detection at NOAA, unmodified injection-molded FEP (*Fluorinated ethylene propylene,* also known as Teflon) and PFA (*Perfluoroalkoxy alkanes*, a material similar to Teflon) appears to have the lowest surface loss for NO_3 and N_2O_5 of any material that was used at NOAA thus far. While developing prototype instruments, custom shapes are very often needed for parts of the inlet systems that are in contact with N_2O_5 and NO_3. When the surface of virgin cast or injection-molded PFA or FEP is machined, the losses to N_2O_5 and NO_3 increase dramatically. Machined surfaces generally present losses that are many times that of injection-molded PFA or FEP, but the loss depends highly on the way the surface is machined.

To determine the effect of the machining and cleaning processes, the interior of a large number of 4 in. (102 mm) long, ¾ in. (19 mm) (outside diameter), PFA tubes was machined in different ways. The machined pieces were compared against a 4 in. (102 mm) length of ¾ in. (19 mm) injection-molded PFA tubing, which served as the most inert reference. In our experience, FEP and PFA parts are indistinguishable in terms of NO_3 loss, and this was also confirmed at that the beginning of these test experiments. Because of this, only PFA parts were used in the testing. For practical reasons, only losses of NO_3 were measured. N_2O_5 is a less sensitive compound than NO_3, so it was expected that a material with low loss of NO_3 would also result in a low loss of N_2O_5.

Tests for NO_3 losses were performed using the same measurement system described in Figure 4-5 of chapter 4. However, there were several key differences in the configuration used for these loss tests, in contrast to the inlet efficiency test configuration shown in the figure. The nylon tubing section, labeled "h" in Figure 4-5, used NO_3 scrubbing in the inlet efficiency test configuration, became the swappable PFA tubing test section for these loss tests. Also, the second 662 nm NO_3 channel was used instead of the 532 nm NO_2 channel ("i"). Additionally, the 130°C conversion heater ("b") was always used so that the output of the N_2O_5/ NO_3 source was predominately NO_3. Both measurement channels

were operated at room temperature so they would be sensitive to NO_3 and conversion of N_2O_5 would not occur.

Loss was evaluated in each machined test section of PFA by comparison with a reference section of extruded PFA tubing. The reference extruded PFA was placed in the test section, ("h" in figure 4-5.) The system was allowed to stabilize for several minutes. NO_3 was measured on both the upstream channel and the downstream channel, and recorded. Then the machined PFA tubing was substituted, the measurement allowed to stabilize, and the upstream and downstream NO_3 concentrations were again measured and recorded. The reference extruded PFA tubing was then placed in the test section once again. The measurement was then repeated and recorded to check for any possible drift.

The goal of the experiment was to evaluate the relative loss of NO_3 on the machined PFA surface as compared to extruded PFA reference. With the reference section installed, the amount of NO_3 detected in the upstream channel was subtracted from the NO_3 detected in the downstream channel. Subsequently, with the machined section installed, the same difference measurement between the two channels were repeated. The result was the ratio of the machined section loss divided by the reference section loss. Measurements found to have discernable drift between the bracketing reference section measurements were discarded and the measurement sequence was repeated. The surface area of the test sections was very large compared to the rest of the system, and extended residence time within the 4 in. length of the test sections made other, minor, losses in the system negligible.

The parameters that were varied comprised the feed rate, the machining speed, and machining tool features on the lathe. Oven treatment was also tested. All machining tests were performed on a single lathe by a specific machinist using inside boring tools that had different tip curvatures and sizes. The *speed of the tool* relative to the material appeared to have no obvious influence on the surface loss, i.e. all tool surface speeds resulted in the same surface loss. The *feed rate* or *thread pitch* (rate of the tool travel per revolution of the lathe relative to the material) made a large difference to the loss, however. Slower feed rates (finer thread pitches) lead to larger losses, which was surprising. The tool tip radius also strongly influenced the NO_3 losses, which decrease with increasing tool tip radius. The results of this study are illustrated in Figure 8-4. A very finely honed tool cutting edge, (as opposed to a tool of standard sharpness) also affects the losses slightly, i.e. a sharper tool cutting edge will lower the expected losses. A high feed rate using a large radius tool that was carefully sharpened turned out to produce the lowest surface loss. Essentially, a surface having widely spaced shallow scallops was found to have the lowest loss.

Surprisingly, annealing machined parts in an oven did not further minimize the losses in comparison to optimally machined PFA. For the very best machined parts, (lowest loss) the reduction in loss was within the experimental error of the tests, even when the annealing oven temperature was

raised to near the melting point of PFA. Only for the worst (high loss) machined parts heating in an oven lead to a ~50% reduction of loss, bringing the poorly machined part nearer in losses to an optimally machined part. Thus, simply employing a more optimal machining technique during fabrication would result in a far better outcome than oven treatment of a poorly machined part. Also, the oven treatment would often result in geometrical distortion of the part, which would require re-machining to return the part to tolerances. Oven treatment, thus, did not seem a fruitful path.
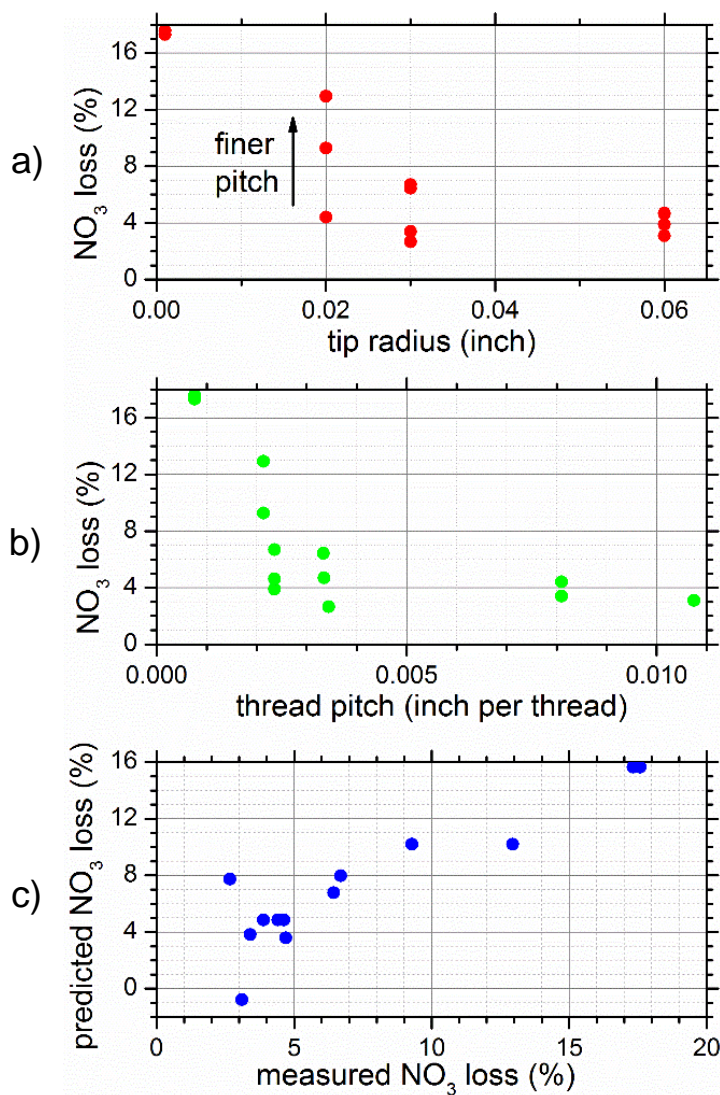
Figure 8-4: (a) NO₃ loss versus the tip radius of the boring bar used for machining the Teflon tube. (b) NO₃ loss versus the thread pitch. (c) Predicted losses from machined PFA versus measured loss using a multivariate linear fit of tip radius and thread pitch versus loss.

The best machined PFA result with the lowest surface loss was a ~50% increase in losses over injection molded PFA. This was achieved by single point machining (one machining pass over the surface) using a very sharp, large radius, facing tool. The tool path was a single pass, large pitch spiral, shown in Figure 8-5d. This result lead to the conclusion that a coarse thread made with a scoop-like tool forming a wide, non-overlapping tool path was the best machining technique for low NO₃ losses.

A more traditional machined surface, comprised of many closely-spaced, sharp, overlapping cuts, was found to be the highest loss surface. This traditional machining process, shown in Figure 8-5a, results in a more visually appealing surface finish, but causes significant surface losses. The losses for the other surfaces shown in Figure 8-5b) and c) were in the range between surfaces shown in Figure 8-5a) and d).

One can interpret the results of the machining process on basis of the interaction between the tool and the polymer chains in the PFA (or FEP) material. During the machining, polymer chains are cut and expose the non-inert ends at the surface. "Pointy" small-radius tools tend to "plow" the surface, cutting many polymer chains on the surface resulting in an increase in the wall losses. Small radius tools also tend to dig into the surface cutting more chains, bringing them to the surface. Conversely, a larger radius, "scoop-like" sharp tool, makes fewer adjacent passes on the surface, and hence cuts fewer chains and thus exposes fewer reactive chain ends. This results in a lower interaction with reactive species in a gas flowing over that surface. Virgin injection-molded PFA has far fewer broken polymer chains and even fewer active sites on its surface. Thus, injection-molded PFA (and FEP) exhibits much lower surface losses.

Figure 8-5: Micrographs showing the inside surface of selected machined PFA tubes in this study. The reticle in each photo shows units in mm. The micrographs were taken with an optical microscope through the end opening of the tube.

8.3.2   Coaxial flow type zero air addition scheme

It was apparent after the first airborne deployment of the ARNOLD instrument (Publication A [1], chapter 3), that pressure control is critical to optimize detection sensitivity and accuracy. Pressure changes can change the alignment of the cavity mirrors, change the density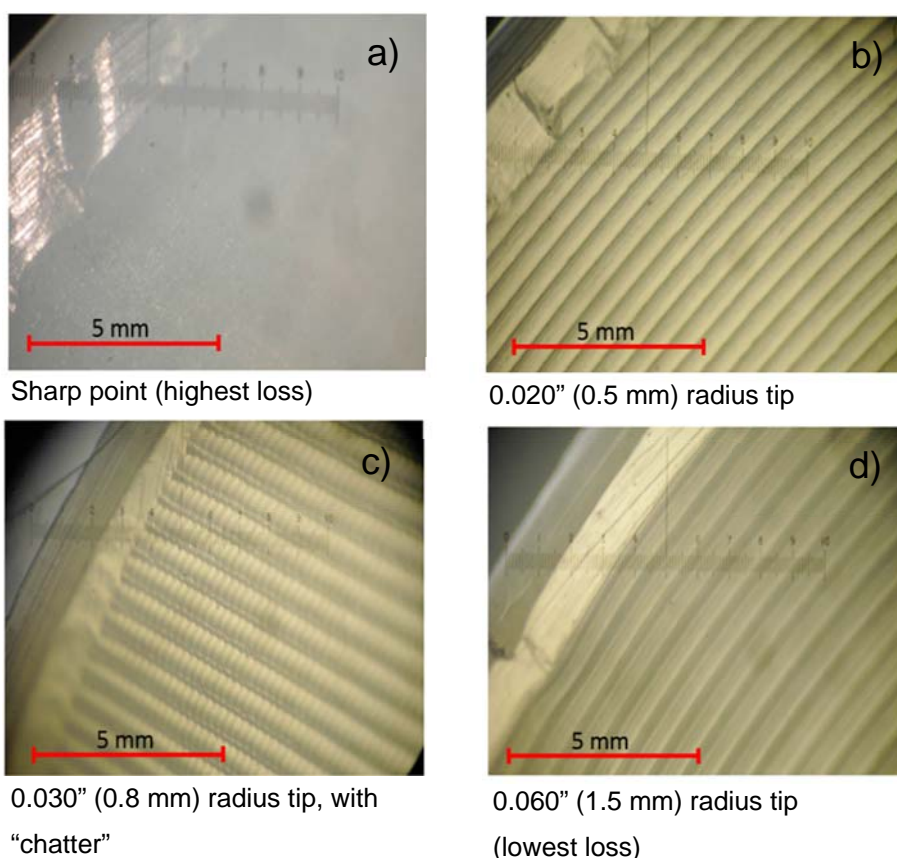 of the gas, and alter the Reynold's number of the flow in the measurement cell, all of which can negatively affect the ring-down time. However, pressure fluctuations were addressed differently in the different instruments. This section will address the coaxial flow zeroing of the NO_2 channels in the NOxCaRD instrument. (The NO_2 channels in the ARNOLD instrument use a very similar experimental approach, but in the NO_3 channels pressure fluctuations are addressed in a completely different manner, which will not be covered here).

The zeroing process of NOxCaRD has been described in Publication E [5] (Chapter 7). The zeroing is necessary to measure τ_0 in equation 7-1, and is accomplished by overflowing the channel with purified air that is either generated onboard by scrubbed ambient air, or supplied from a cylinder of commercial zero air. Traditionally, the zero air is injected through a T-connection in the inlet. The problem with this scheme is the resulting pressure increase in the cavity. This is due to the flow being reversed in the short length of tubing upstream of the T-connection where zero air is introduced. A negative pressure drop at the T-connection becomes a slightly positive pressure increase during the zeroing process. To avoid this pressure increase, a coaxial flow type zero air addition scheme was developed and tested, which was used in [5]. The T-connection and the coaxial zero air addition designs are compared in illustration Figure 8-6.

With the new design, the zero air is added in front of the inlet through an outer, coaxial tube, which minimizes pressure changes. The outer tube forms a small cavity in front of the regular inlet, and during the zeroing process the flow envelopes the entire cavity with zero air. The flow of zero air slightly increases the pressure at the entry length of the inlet. However, this increase is nearly canceled out by the Venturi effect of the zero air flow traveling in the opposite direction, which causes a slight pressure drop. The overhang length of the outer tube is determined experimentally, but is typically 25-50 mm, depending on the severity of the wind traveling perpendicular to the inlet. On the ground, a short overhang suffices because the wind is typically mild. On an airplane, or in more severe winds, a longer overhang is needed to overcome the mixing of ambient air with the overflowing zero air.

Some minor pressure changes may still be present despite the coaxial flow of zero air. Any small change in optical extinction due to pressure difference during the zero air addition is explicitly corrected using the known Rayleigh scattering of zero air, and was never greater than the equivalent of 6 pptv of NO_2 in the field mission reported in ref [103]. Measurements in ambient or humidified air require an additional correction for water vapor, because the Rayleigh scattering cross-section of water vapor is smaller than that of dry air (note: commercial zero air has negligible water content). It is worth

noting, however, that this correction affects both the O_x and NO_2 channels similarly, and hence did not affect the O_3 measurement during the deployment in ref [103].
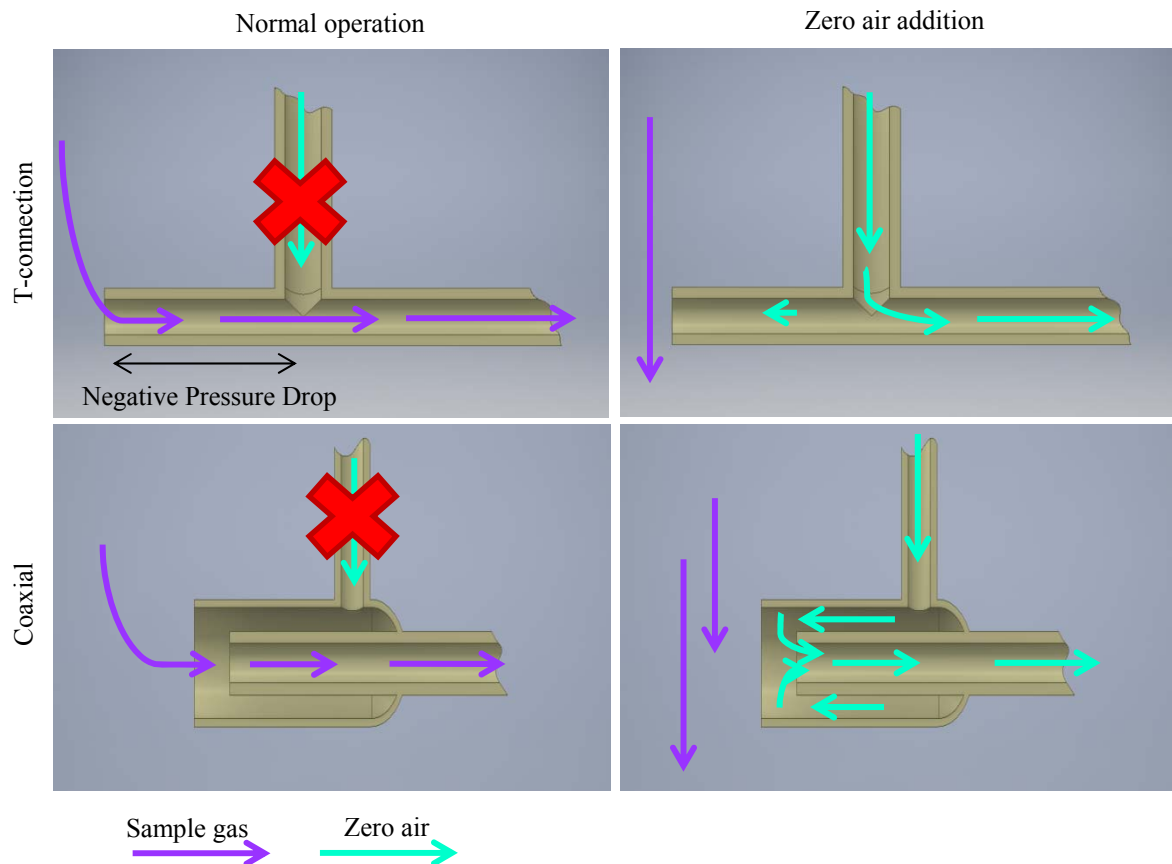
Figure 8-6: Traditional T-connection zero air addition (upper panels) causing pressure fluctuations in the measurement cell versus coaxial zero air addition (lower panels).

8.3.3 Integration of flow controllers

Control of pressure and flow conditions are crucial for the performance of the instrument, especially when it is deployed in highly variable environments. Simple manual flow adjustment using needle valves and monitoring the flow using electronic mass flow meters (as applied in ground based sites) are not appropriate in an aircraft environment. The frequent and rapid ambient pressure changes make manual adjustment of the measurement cell flow in conjunction with a simplistic flow metering impractical. Thus electronic mass flow controllers with integrated control valves were implemented on the first airborne CaRDS instrument. The controllers hold the mass flow in the cells constant as the air pressure varies outside the airplane and also within the cabin of the airplane. In combination with the pressure transducers and the temperature measurements within the measurement cells, an in-house developed LabView program periodically adjusts the settings on the mass flow controllers to maintain a step-wise constant volumetric measurement cell flow as the air density changes with altitude. Since the N_2O_5 to NO_3 conversion process depends on the residence time in the pre-heater the flow time is more important for the conversion than pressure constancy. Thus, to keep the conversion process within

range, the residence time of the incoming air in the heater must remain approximately constant. A constant residence time in the measurement cell also helps maintain data quality. The time resolution of the instrument is not a function of pressure or incoming air temperature because the volumetric flow through the cell is held approximately constant by the controllers (Alicat Scientific).

The residence time in the inlet system varies with changes in the flow. Changes in the residence time adversely affects the reaction time in the O_3, NO, and NO_y mixing volumes, and the N_2O_5 conversion heaters. Holding the flow steady under the varying barometric pressure by using flow controllers makes the measurement possible. Flow controllers were vital to deploy CaRDS instruments on a mobile platform, especially an airplane.

8.3.4   Isothermal pressure reduction

It was known that the inlet efficiency played an important role in the uncertainty of the measurement and it was believed that a faster flow would reduce the inlet losses and increase the inlet transmission efficiency. However, the flow through the cavity must remain laminar, which limits the allowed Reynolds number, Re. As seen in equation 8-1,

$$\mathrm{Re} = \frac{\rho \, v \, l}{\mu},\tag{8-1}$$

can be held constant and the flow velocity increased, if the density of the air is reduced. In equation 8-1 ρ is the density, v is the velocity of the air, l is the characteristic length, and μ is the dynamic viscosity.

It was discovered in early flights with the ARNOLD instrument that high altitude did not decrease the sensitivity of the measurements. This led us to realize that the instrument could be operated continuously at reduced pressure. This would give the necessary density decrease allowing for increased flow velocity while maintaining the same Reynolds number, and thus maintain laminar flow through the system. It was also suspected that the reduced pressure may have other benefits.

Hence the pressure of the sample air is reduced from ambient pressure to ~300 mbar in the NO_3 and N_2O_5 channels in the ARNOLD instrument. At this pressure, the lower number density of the sensed gas species is compensated by the lower scattering losses for a given mirror reflectivity, so that the sensitivity of the instrument is not compromised by using a lower operating pressure. The reduced pressure however, leads to a lower contamination of the inlets and cells over time and therefore significantly reduces the inlet losses. The decrease in inlet loss can be attributed to the evaporation of "wet" and perhaps sticky aerosols in the *isothermal* pressure reducer before the gas reaches the measurement cells, fittings, and filter changer.

The most common solution to create a reduced pressure in a scientific instrument is by the use of a critical orifice, which results in an adiabatic pressure reduction. This is a simple solution, but has the drawback that the temperature changes in an adiabatic pressure reduction. In contrast, if the

temperature of the air is kept constant, the relative humidity will decrease in the pressure reduction, which will dry out aerosols and evaporate VOCs. This in turn was expected to decrease the deposition of humidity, sticky aerosols, and other reactive compounds. It turned that isothermal pressure reduction resulted in longer maintenance intervals, increased accuracy, and less drift. The higher velocity also decreased the residence time in the cell, resulting in increased time resolution. Higher time resolution also translated into higher spatial resolution, which is very important on a fast moving airplane such as the NOAA P-3 Hurricane Hunter that cruises at 208 m/s (466 mph).

The isothermal pressure reduction can be accomplished by a section of smaller diameter tubing in the inlet system just inside the airplane. An 1/8 in. (3.2 mm) internal diameter tubing is inserted in the flow system that otherwise consists of 1/4 in. (6.4 mm) tubing. The narrow tube creates the pressure drop along the length of the narrow section of tubing through the wall friction instead of an abrupt pressure drop that occurs using an orifice. The length of the tube is experimentally determined, and varies slightly with each batch of tubing; a typical length is ~150 mm. The tube section does not use standard fittings. These tend to compress the inner diameter of the tubing where they grip the outer diameter, forming the abrupt orifice which would promote adiabaticity. Instead, the 1/8 in. (3.2 mm) diameter tubing is slightly stretched and then inserted into a thin-walled 1/4 in. (6.4 mm) tubing. Then 1/8 in. diameter tube will relax and form a seal to the 1/4 in. diameter tube. Clamps are added on the outside of the 1/4 in. tube to secure the restrictor without causing any major internal changes of the 1/8 in. diameter tube.

8.4 Cavity stability considerations

The alignment of the cavity mirrors is most critical for the performance of a CaRDS instrument, especially if deployed in a field environment where conditions cannot be controlled as rigorously as in a laboratory. The mirror mounts are subjected to a multitude of forces, all of which act to move the two cavity mirrors out of alignment. The measurement cell is typically sealed to the mirrors, and the cell pressure acts on the mirror face, which is reacted by the mirror mounts. When the internal pressure changes, the mirror mounts can flex and allow the mirror to move out of alignment. Standard optical mirror mounts which use fine screw adjustments acting in opposition to simple coil springs (or perhaps flexure leaf springs) are not designed to tolerate these forces, and the alignment can be permanently altered from its optimum.

The mirror alignment can also be affected by differential thermal expansion and contraction of the cell (or the optical breadboard) itself, which exerts forces on the mirror mounts. Moreover, inertial acceleration forces, due to the movement of the frame of reference on an airplane and of course vibrations in that kind of environment exert forces on the mounts that all can affect the cavity alignment. Finally, mechanical creep often coupled with "stiction" in the cell materials and seals result in changes in the force on the mirror mounts over time, causing long-term misalignment.

A new design of an optical cage for ring-down cavities in conjunction with the development of a clamped/nudged mirror mount system has eliminated many of these alignment and stability issues.
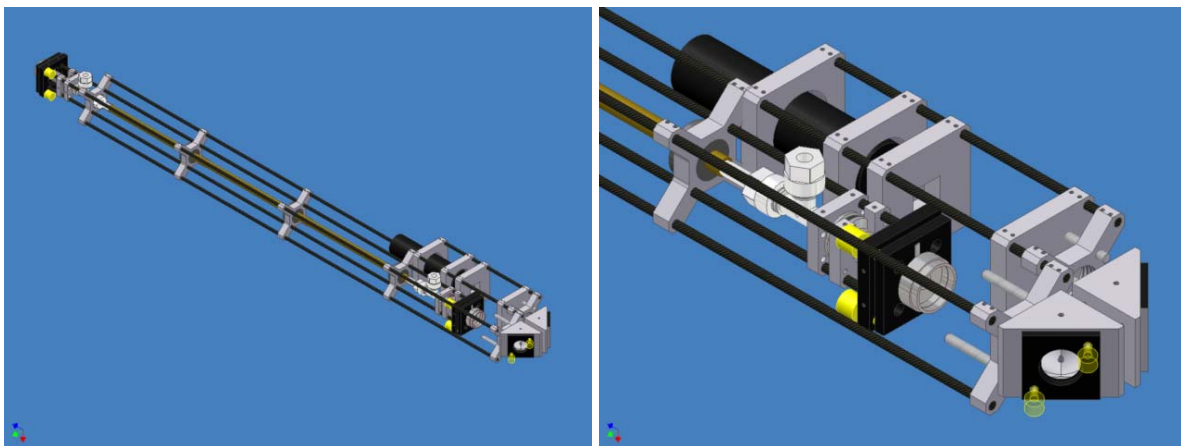
8.4.1 Cage design

In the new design the optical bread board was replaced by a carbon-fiber cage. The cage distributed the forces symmetrically about the mirror axis, as opposed to the asymmetric, cantilevered arrangement of the mount attached to an optical bread board. The carbon-fiber additionally had the very desirable attribute of extremely high modulus (stiffness) and low thermal expansion. The 0.500 in. (12.7 mm) unidirectional pultruded carbon-fiber composite rods have a tensile strength of 200,000 psi (1.375 GPa) and a modulus ("stiffness") of 17,800,000 psi (1227 GPa). More important for optical stability, they have a coefficient of linear thermal expansion of only $1\text{-}2 \times 10^{-6}$ in./in./°F ($1.8\text{-}3.6 \times 10^{-6}$ mm/mm/K) depending on the exact mix of the resin and the carbon-fiber. Aluminum has 20 or 30 times larger thermal expansion coefficient, and steel exhibits a 10 to 20 times larger thermal expansion. The modulus of the carbon fiber rods is approximately twice that of aluminum and two-thirds that of steel. The high modulus in conjunction with the low thermal expansion resist deflection caused by inertial and mechanical loads that the cage is routinely subjected to during flight, shipping, inadvertent rough handling, and pressure changes in the measurement cells. The extremely low thermal expansion makes the cavity length and alignment largely immune to temperature changes.

As with all new design concepts, the cage design went through several iterations. Figure 8-7 illustrates the very first proof-of-concept for the cage design. The selected rods were too thin and too closely spaced, resulting in an unacceptable deflection. This problem was mitigated by increasing the rod diameter to 1/2 in. (12.7 mm) and increasing the spacing. The improved design resulted in the very first version of NOxCaRD (Figure 8-8) described in chapter 5.

The cage type optical system for NOxCaRD was one of three that were designed and built simultaneously. These early cage systems had traditional spring and screw type optical mounts holding the high reflectivity cavity mirrors. They were an improvement over the optical breadboard type systems, but, more importantly, they served as an important stepping stone toward the present cage system design having "nudged and clamped" mirror plates (covered in the next section). The final cage design for NOxCaRD proved extremely robust and is now used for all types of CaRDS instruments in our laboratory and other laboratories.

The carbon-fiber cage has been used in the multichannel instruments NOxCaRD (first use in [3]) and "ACES" *(Airborne Cavity Enhanced Spectrometer)* [5, 7, 131], and will also be implemented in the next generation of the ARNOLD instrument as well as in the CARDINO instrument (see section 1.1). Renderings of the new ARNOLD instrument are found in Figure 2-4 and Figure 2-5. An intermediate version of the ARNOLD instrument with the new optical cage system mounted in the old instrument rack is shown in Figure 8-9 and Figure 8-10.

Figure 8-7: A first proof-of-concept cage design that was built but never integrated into an instrument. The rods were too thin and too closely spaced. It exhibited unacceptable deflection.

Figure 8-8: The earliest version of the new cage design that was employed in the NOxCaRD instrument in 2009.
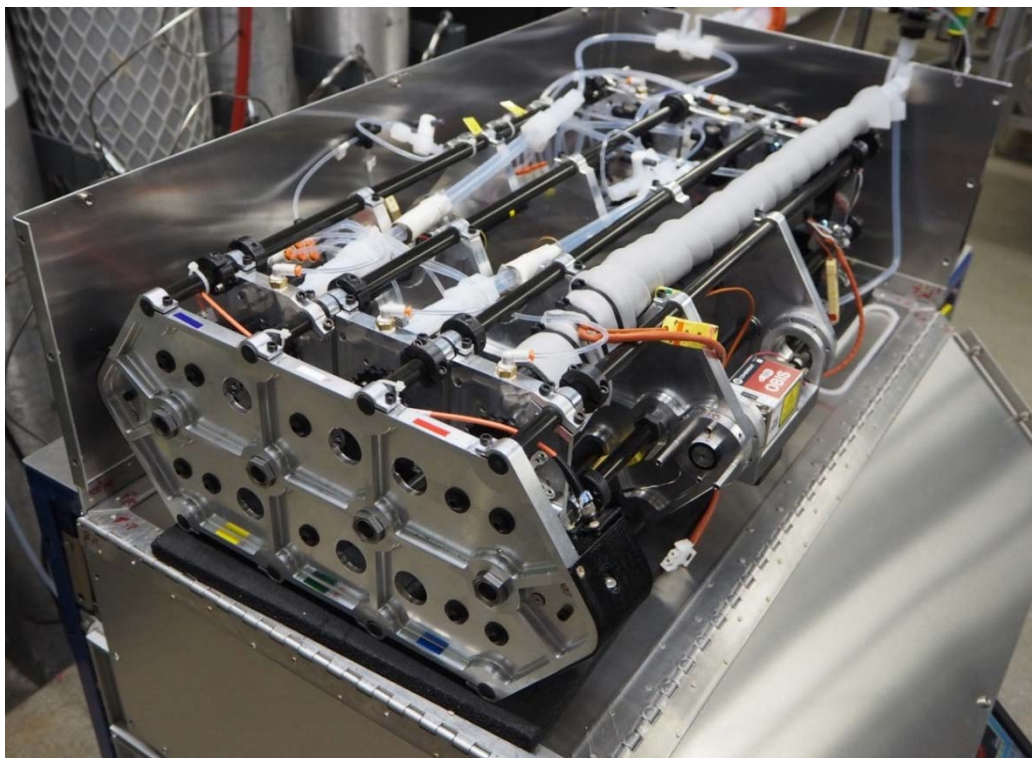
Figure 8-9: An intermediate version of the new 6-channel ARNOLD instrument, with the new optical cage system described in section 2.1 but the old instrument rack and data acquisition system. The instrument measures NO_3, N_2O_5, NO_2, NO, O_3, and NO_y concentrations.

Figure 8-10: The intermediate version of the new ARNOLD instrument. The automated filter changer described in section 8.2 can be seen to the right in the picture.

8.4.2 Clamped/nudged mirror mounts

While the carbon-fiber cage design was crucial to cavity stability, it did not fully solve the cavity mirrors drifting out of alignment due to pressure changes. In order to mitigate this drift problem, an additional design feature in the form of clamped/nudged mirror mounts was added. This consisted of solid aluminum plates designed for the cage system. The high reflectivity cavity mirrors are mounted directly into the aluminum plates, which are then directly clamped to the carbon-fiber rods. The sturdy clamps, shown in Figure 8-11, are located on all four corners of a mirror plate. They are machined as part of the plate itself. The clamps attach at right angles to the carbon-fiber cage rods. Once aligned and clamped, the mirror plates, and thus the cavity mirrors themselves, stay perfectly aligned.

The alignment of the plates does not require a large range of motion, to generate an optically stable cavity. The plates are close to parallel and only small unavoidable machining errors and discrepancies based on the cage assembling need to be compensated for. For a proper alignment the plates merely need to be tilted by a fraction of a degree. This was achieved by means of small "nudger" pieces that were designed to be clamped to the cage rods, one on either side of the mirror plate (see Figure 8-11). Using a fine threaded grub screw in the nudger pieces, the mirror plates can be nudged into alignment while the clamps on the mirror plates were slightly loosened. After successful alignment of the ringdown cavities, the clamps are carefully tightened, and the grub screws in the nudger pieces are loosened. The pieces may then be removed from the carbon-fiber rod, or left in place if desired for future optimizations.

A clamped/nudged mirror mount design further reduced the need for re-alignment of the mirrors. In contrast with traditional CaRDS instruments requiring daily alignments, the current version of NOxCaRD (Figure 2-6), using nudged and clamped cage mirror mounts, has been operated for several years, including multiple deployments to the field, and commercial shipping to and from these field missions, without alignment for three years. The CARDINO instrument, currently being built at UCC, is using this design, and the new ARNOLD instrument has been as well. All details of the holder components in the new ARNOLD optical cage system, including the clamped mirror mounts and nudger pieces are shown in Figure 8-11.

Custom-machined nudger piece.

Nudger made from commercial shaft collar. Much less expensive compared to custom machined nudger pieces.

Adjustment set screw.

Aluminum mirror plate.

Mirror plate adjustment screw.

Mirror plate clamp.

Pultruded carbon-fiber rod.

Recess machined in nudger to allow access for adjustment of mirror plate screw
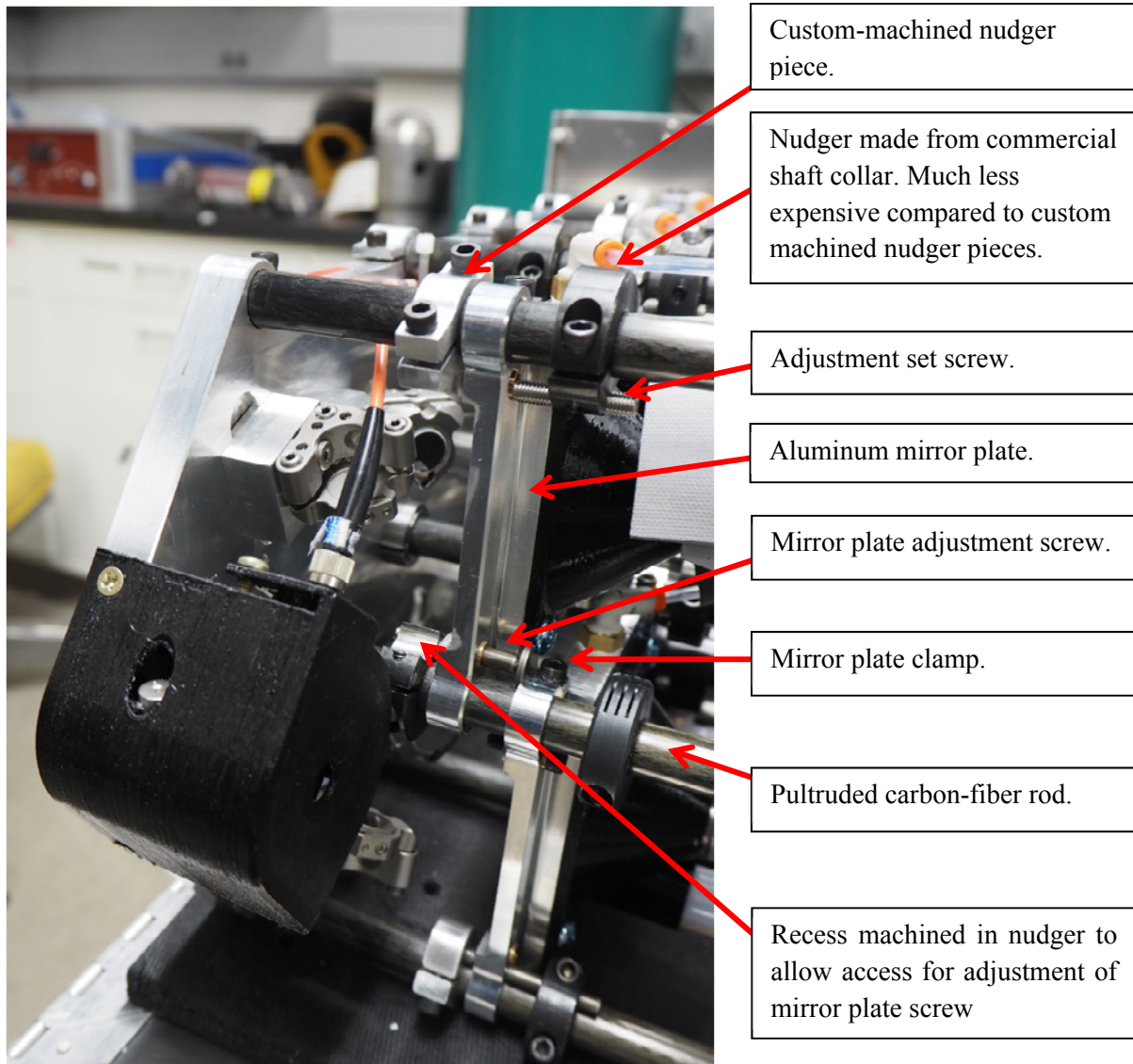
Figure 8-11:   Photo showing the details of the components in the new optical cage system in the ARNOLD instrument, including the clamped mirror mounts and "nudger" pieces.

8.5   Purge system improvements

Purge systems, which keep contaminated air from reaching the cavity mirror surfaces, increase the effective optical path length by keeping the mirrors clean, and thus increase both accuracy and sensitivity of the measurements. However, a poorly integrated purge system can do more harm than good. Throughout the development of CaRDS instruments, several different solutions to properly purge ringdown cavities were tested, including a purgeless system, which was used in the NOxCaRD instrument [5]. This chapter will discuss purge systems and the improvements made, including a coaxial purge used in Ref. [7].

8.5.1   Traditional purge systems

During its first deployment [1] the ARNOLD instrument had a "traditional" purge system. The mirror was mounted in a purge volume separated from the measurement portion of the sample cell by an orifice and purged with dry zero air to maintain mirror cleanliness. This setup was described in section 3.2.1. While the purge volumes kept the mirrors clean, they caused considerable noise in the heated N_2O_5 channel (see section 3.2.2). Improvements of the purge system were therefore necessary.

8.5.2   Purgeless systems

Because of the problems with noise described above, an approach using a purgeless design was tried with limited success. This was used for the first time in the NOxCaRD instrument [5]. The purgeless design simplifies the calibrations and eliminates a possible source of error. However, the elimination of the purge volumes can lead to degradation in mirror reflectivity under some circumstances. Since the sampled air is in direct contact with the mirrors, some compounds can condense onto the mirrors, causing a decrease of the ringdown time. This has been observed in an environment with high relative humidity and required drying of the sampled air. Mirror degradation in the NO_y channel was also encountered under conditions of extremely large hydrocarbon concentration in ambient air.

We are planning to revisit purgeless operation in combination with running the CaRDS systems at reduced pressure. The reduction in humidity and the drying of VOC aerosols concomitant with reduced pressure may be the key to eliminating the purge flows.

8.5.3   Coaxial purge flow

While the purgeless system eliminated noise and calibration errors, the degradation of mirror reflectivity and the degradation of NO_y in the NOxCaRD instrument were unacceptable. The latest design has a coaxial purge flow (not to be confused with coaxial zeroing.) In the new design, the sample flow is introduced coaxially around the mirror purge flow. This approach reduces turbulence in the confluence of the purge flow with the sample flow, and thus allows a significantly shorter purge volume, which is desirable.

The design to experimentally generate a coaxial purge flow, using the mirror mounts discussed in Section 8.4.2, is illustrated in Figure 8-12. A small PTFE piece is inserted directly in front of the mirror, and protrudes out into the measurement cell. Zero air is introduced through radial passages in the PTFE piece, next to the mirror. The sample air is introduced perpendicular to the side of the insert, and flows along the length of the outside of the insert in the annular space between the outer diameter of the insert and the internal diameter of the acetyl flange (see Figure 8-12). The sample flow then merges with the purge flow, in a coaxial manner, as both flows proceed along the measurement cell. A duplicate arrangement is on the opposite end of the measurement cell. This innovation reduced the purge volume

length from ~50 mm to ~15 mm. The design is used in the instruments NOxCaRD, CARDINO, the newest version of ARNOLD.
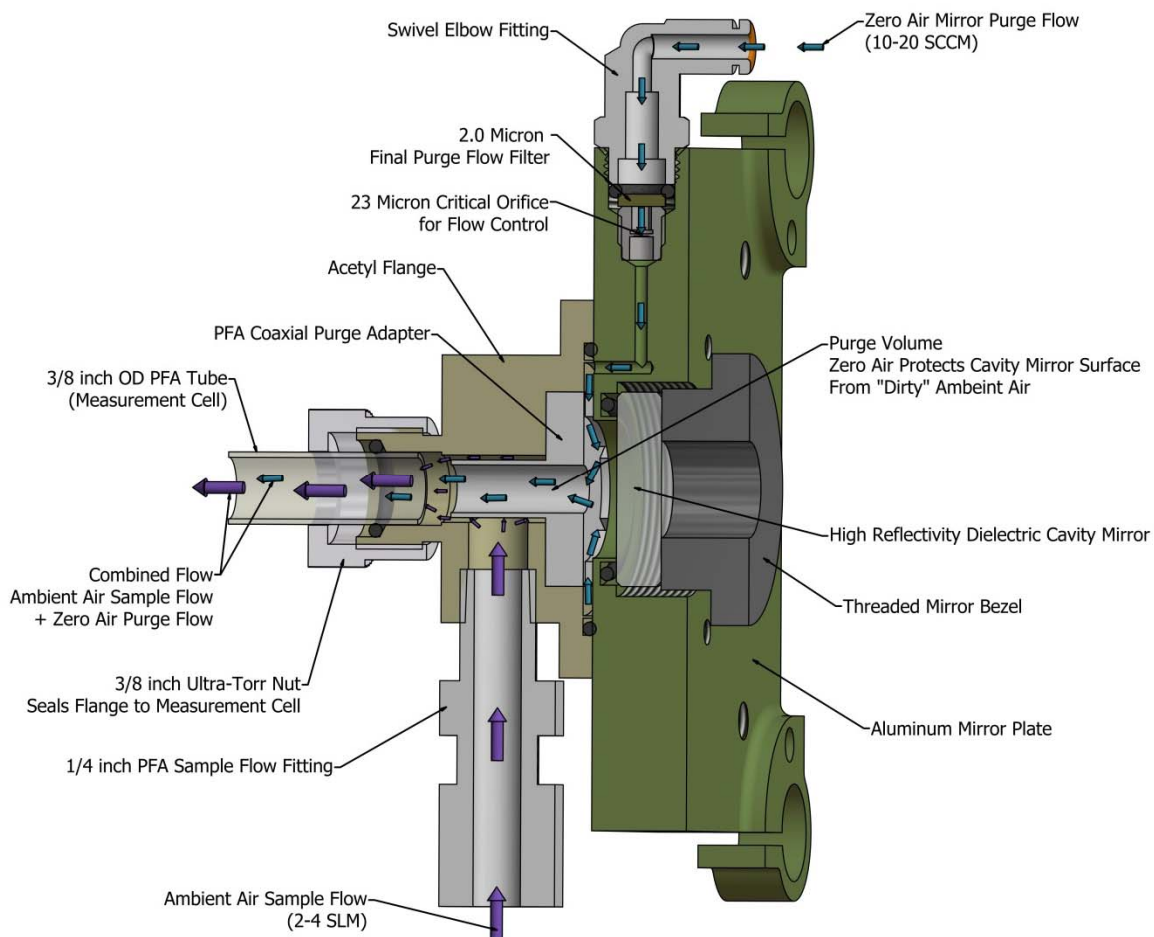

Figure 8-12: Cutaway illustration of the coaxial purge flow design.

9. Conclusions

The work presented in this thesis has shown that pulsed laser-based cavity ring-down spectroscopy (CaRDS) can be used for in-situ detection of nitrogen oxides on airborne platforms. The successful leap from large laboratory instruments with high maintenance requirements to compact and rugged field instruments was possible thanks to extensive engineering work and new innovations. The contributions were mainly in the following areas:

1. **Instrument rack design and vibration isolation:** Welded 4130 chrome-moly steel racks replacing the traditional riveted aluminum rack design resulted in higher strength, lower weight, lower cost, and better vibration isolation. The cost reduction was 80 %, and the mass reduction was 30 %. Pumps and other vibration causing equipment were mounted directly to the aircraft floor, and the entire steel frame, with a lightweight optical table, was vibration isolated.

2. **Automated filter changer:** A unique automated filter changer made the task of hourly changing aerosol filters rapid and even possible on a pressurized airplane. It decreased the downtime from about 10 minutes per hour to 10 seconds per hour, greatly reducing the missed data. It also allowed autonomous operation and decreased the need for a dedicated operator onboard the aircraft.

3. **Low loss inlet design and flow control:** The implementation of flow controllers instead of flow meters, made the instrument capable of automatically compensating for the altitude and density changes on an airborne platform. In combination with a low loss inlet design, the accuracy improved for NO_3 measurements from ± 25 % to $-9/+12$ %, and for N_2O_5 measurements from ± 20-40 % to $-8/+11$ % in the ARNOLD instrument. Coaxial zeroing reduced the disruptive inlet pressure variations and improved both the uptime and accuracy of the NO_2–based channels.

4. **Cage design:** A cage design utilizing carbon fiber composite rods connected to machined aluminum end plates addressed the problem of mirrors drifting out of alignment in non-laboratory environments, and further reduced the vibration sensitivity.

5. **Clamped/nudged mirror mount:** A clamped/nudged mirror mount design further reduced the need for re-alignment of the mirrors. In contrast with traditional CaRDS instruments requiring daily alignments, the instrument NOxCaRD, using nudged and clamped cage mirror mounts, has been operated for more than 2 years without alignment. The next generation of instruments (CARDINO and ARNOLD) will utilize the same design.

6. **Purge system innovation:** Improvements in the purge system, which kept the contaminated air from reaching the mirrors, increased the effective cavity length with about 35 mm and increased both accuracy and sensitivity of the measurements.

The publications [1-5] illustrate the development, application, performance and quality of two specific CaRDS instruments, NOxCaRD and ARNOLD, whose evolution and experimental design features are outlined in this thesis. The next generation of ARNOLD instrument as well as a new instrument CARDINO, which are currently under construction at NOAA and at University College Cork, will utilize all design improvements outlined here. Both instruments are expected to be compact, sensitive, accurate and rugged multi-channel CaRDS devices, highly suitable for airborne measurements.

Acknowledgements

Bibliography

References [1] through [5] are the selected publications presented in chapters 3 through 7.

1. **Dubé, W.P.**, S.S. Brown, H.D. Osthoff, M.R. Nunley, S.J. Ciciora, M.W. Paris, R.J. McLaughlin, and A.R. Ravishankara, *Aircraft instrument for simultaneous, in situ measurement of NO3 and N2O5 via pulsed cavity ring-down spectroscopy.* Rev. Sci. Instrum., 2006. **77**(3): p. 034101-11.

2. Fuchs, H., **W.P. Dubé**, S.J. Ciciora, and S.S. Brown, *Determination of Inlet Transmission and Conversion Efficiencies for in Situ Measurements of the Nocturnal Nitrogen Oxides, NO3, N2O5 and NO2, via Pulsed Cavity Ring-Down Spectroscopy.* Anal. Chem., 2008. **80**(15): p. 6010-6017.

3. Fuchs, H., **W.P. Dubé**, B.M. Lerner, N.L. Wagner, E.J. Williams, and S.S. Brown, *A Sensitive and Versatile Detector for Atmospheric NO2 and NOX Based on Blue Diode Laser Cavity Ring-Down Spectroscopy.* Environ. Sci. Technol., 2009. **43**(20): p. 7831-7836.

4. Wagner, N.L., **W.P. Dubé**, R.A. Washenfelder, C.J. Young, I.B. Pollack, T.B. Ryerson, and S.S. Brown, *Diode laser-based cavity ring-down instrument for NO3, N2O5, NO, NO2 and O3 from aircraft.* Atmos. Meas. Tech., 2011. **4**(6): p. 1227-1240.

5. Wild, R.J., P.M. Edwards, **W.P. Dubé**, K. Baumann, E.S. Edgerton, P.K. Quinn, J.M. Roberts, A.W. Rollins, P.R. Veres, C. Warneke, E.J. Williams, B. Yuan, and S.S. Brown, *A Measurement of Total Reactive Nitrogen, NOy, together with NO2, NO, and O3 via Cavity Ring-down Spectroscopy.* Environ. Sci. Technol., 2014. **48**(16): p. 9609-9615.

6. Thornton, J.A., J.P. Kercher, T.P. Riedel, N.L. Wagner, J. Cozic, J.S. Holloway, **W.P. Dubé**, G.M. Wolfe, P.K. Quinn, A.M. Middlebrook, B. Alexander, and S.S. Brown, *A large atomic chlorine source inferred from mid-continental reactive nitrogen chemistry.* Nature, 2010. **464**(7286): p. 271-274.

7. Edwards, P.M., S.S. Brown, J.M. Roberts, R. Ahmadov, R.M. Banta, J.A. deGouw, **W.P. Dubé**, R.A. Field, J.H. Flynn, J.B. Gilman, M. Graus, D. Helmig, A. Koss, A.O. Langford, B.L. Lefer, B.M. Lerner, R. Li, S.-M. Li, S.A. McKeen, S.M. Murphy, D.D. Parrish, C.J. Senff, J. Soltis, J. Stutz, C. Sweeney, C.R. Thompson, M.K. Trainer, C. Tsai, P.R. Veres, R.A. Washenfelder, C. Warneke, R.J. Wild, C.J. Young, B. Yuan, and R. Zamora, *High winter ozone pollution from carbonyl photolysis in an oil and gas basin.* Nature, 2014. **514**(7522): p. 351-354.

8. Brown, S.S., H. Stark, S.J. Ciciora, R.J. McLaughlin, and A.R. Ravishankara, *Simultaneous in situ detection of atmospheric NO3 and N2O5 via cavity ring-down spectroscopy.* Rev. Sci. Instrum., 2002. **73**(9): p. 3291-3301.

9. Platt, U. and F. Heintz, *Nitrate Radicals in Tropospheric Chemistry.* Israel J. of Chem., 1994. **34**(3-4): p. 289-300.

10. Wayne, R.P., I. Barnes, P. Biggs, J.P. Burrows, C.E. Canosa-Mas, J. Hjorth, G.L. Bras, G.K. Moortgat, D. Perner, G. Poulet, G. Restelli, and H. Sidebottom, *The nitrate radical: Physics, chemistry, and the atmosphere.* Atmos. Environ., Part A, 1991. **25A**(1): p. 1-203.

11. Platt, U.F., A.M. Winer, H.W. Bierman, R. Atkinson, and J.N. Pitts, *Measurement of nitrate radical concentrations in continental air.* Environ. Sci. Technol., 1984. **18**: p. 365-369.

12. Brown, S.S., J.E. Dibb, H. Stark, M. Aldener, M. Vozella, S. Whitlow, E.J. Williams, B.M. Lerner, R. Jakoubek, A.M. Middlebrook, J.A. DeGouw, C. Warneke, P.D. Goldan, W.C. Kuster, W.M. Angevine, D.T. Sueper, P.K. Quinn, T.S. Bates, J.F. Meagher, F.C. Fehsenfeld, and A.R. Ravishankara, *Nighttime removal of NOx in the summer marine boundary layer.* Geophys. Res. Lett., 2004. **31**(7): p. L071081-5.

13. Winer, A.M., R. Atkinson, and J.N. Pitts, *Gaseous Nitrate Radical: Possible Nighttime Atmospheric Sink for Biogenic Organic Compounds.* Science, 1984. **224**: p. 156-159.

14. Platt, U., G. LeBras, G. Poulet, J.P. Burrows, and G. Moortgat, *Peroxy radicals from night-time reaction of NO3 with organic compounds.* Nature, 1990. **348**: p. 147-149.

15. Penkett, S.A., J.N. Blake, P. Lightman, A.R.W. Marsh, P. Anwyl, and G. Butcher, *The seasonal variation of nonmethane hydrocarbons in the free troposphere over the North Atlantic Ocean: Possible evidence for extensive reaction of hydrocarbons with the nitrate radical.* J. Geophys. Res., 1993. **98**: p. 2865-2885.

16. Noxon, J.F., R.B. Norton, and W.R. Henderson, *Observation of atmospheric NO3.* Geophys. Res. Lett., 1978. **5**: p. 675-678.

17. Noxon, J.F., R.B. Norton, and E. Marovich, *Observation of atmospheric NO3.* Geophys. Res. Lett., 1980. **7**: p. 125-128.

18. Platt, U., D. Perner, A.M. Winer, G.W. Harris, and J.N. Pitts, *Detection of nitrate radical in the polluted troposphere by differential optical absorption* Geophys. Res. Lett., 1980. **7**: p. 89-92.

19. Solomon, S., H.L. Miller, J.P. Smith, R.W. Sanders, G.H. Mount, A.L. Schmeltekopf, and J.F. Noxon, *Atmospheric NO3, Measurement technique and the annual cycle at 40 degrees N.* J. Geophys. Res., 1989. **94**: p. 11041-11048.

20. Aliwell, S.R. and R.L. Jones, *Measurement of atmospheric NO3 2. Diurnal variation of stratospheric NO3 at midlatitude.* Geophys. Res. Lett., 1996. **23**: p. 2589-2592.

21. Platt, U., *Air monitoring by spectroscopic techniques*, ed. M.W. Sigrist. Vol. 127. 1994: John Wiley & Sons.

22. Plane, J.M.C. and N. Smith, *Spectroscopy in environmental science*, ed. R.J.H. Clark and R.E. Hester. Vol. 24. 1995: John Wiley & Son Ltd.

23. Allan, B.J., G. McFiggans, J.M.C. Plane, H. Coe, and G.G. McFadyen, *he nitrate radical in the remote marine boundary layer.* J. Geophys. Res., 2000. **105**(D19): p. 24191–24204.

24. Geyer, A., R. Ackermann, R. Dubois, B. Lohrmann, R. Müller, and U. Platt, *Long-term observation of nitrate radicals in the continental boundary layer near Berlin* Atmos. Environ., 2001. **35**(21): p. 3619-3631.

25. Heintz, F., U. Platt, H. Flentje, and R. Dubois, *Long-term observation of nitrate radicals at the Tor Station, Kap Arkona (Rügen).* J. Geophys. Res., 1996. **101**(D17): p. 22891–22910.

26. Atkinson, R., A.M. Winer, and J.N. Pitts, *Estimation of night-time N2O5 concentrations from ambient NO2 and NO3 radical concentrations and the role of N2O5 in night-time chemistry.* Atmos. Environ., 1986. **20**(2): p. 331-339.

27. Mihelcic, D., D. Klemp, P. Müsgen, H.W. Pätz, and A. Volz-Thomas, *Simultaneous measurements of peroxy and nitrate radicals at Schauinsland.* J. Atmos. Chem., 1993. **16**(4): p. 313–335.

28. Geyer, A., B. Alicke, D. Mihelcic, J. Stutz, and U. Platt, *Comparison of tropospheric NO3 radical measurements by differential optical absorption spectroscopy and matrix isolation electron spin resonance.* J. Geophys. Res., 1999. **104**(D21): p. 26097–26105.

29. Brown, S.S., H. Stark, S.J. Ciciora, and A.R. Ravishankara, *In-situ measurement of atmospheric NO3 and N2O5 via cavity ring-down spectroscopy.* Geophys. Res. Lett., 2001. **28**(17): p. 3227–3230.

30. King, M.D., E.M. Dick, and W.R. Simpson, *A new method for the atmospheric detection of the nitrate radical (NO3).* Atmos. Environ., 2000. **34**(5): p. 685-688.

31. Simpson, W.R., *Continuous wave cavity ring-down spectroscopy applied to in situ detection of dinitrogen pentoxide (N2O5)* Rev. Sci. Instrum., 2003. **74**(7): p. 3442-3452.

32. Ayers, J.D., L. Apodaca, W.R. Simpson, and D.S. Baer, *Off-axis cavity ringdown spectroscopy: application to atmospheric nitrate radical detection* Appl. Opt., 2005. **44**(33): p. 239-7242.

33. Ball, S.M., I.M. Povey, E.G. Norton, and R.L. Jones, *Broadband cavity ringdown spectroscopy of the NO3 radical.* Chem. Phys. Lett., 2001. **342**(1-2): p. 113-120.

34. Ball, S.M., J.M. Langridge, and R.L. Jones, *Broadband cavity enhanced absorption spectroscopy using light emitting diode.* Chem. Phys. Lett., 2004. **398**(1-3): p. 68-74.

35. Bitter, M., S.M. Ball, I.M. Povey, and R.L. Jones, *A broadband cavity ringdown spectrometer for in-situ measurements of atmospheric trace gases* Atmos. Chem. Phys., 2005. **5**(9): p. 2547-2560.

36. Wood, E.C., P.J. Wooldridge, J.H. Freese, T. Albrecht, and R.C. Cohen, *Prototype for In Situ Detection of Atmospheric NO3 and N2O5 via Laser-Induced Fluorescence.* Environ. Sci. Technol., 2003. **37**(24): p. 5732-5738.

37. Wood, E.C., T.H. Bertram, P.J. Wooldridge, and R.C. Cohen, *Measurements of N2O5, NO2, and O3 east of the San Francisco Bay* Atmos. Chem. Phys., 2005. **5**: p. 483-491.

38. Matsumoto, J., N. Kosugi, H. Imai, and Y. Kajii, *Development of a Measurement System for Nitrate Radical and Dinitrogen Pentoxide Using a Thermal Conversion/Laser-Induced Fluorescence Technique.* Rev. Sci. Instrum., 2005. **76**: p. 064101–11.

39. Slusher, D.L., L.G. Huey, D.J. Tanner, F.M. Flocke, and J.M. Roberts, *A thermal dissociation–chemical ionization mass spectrometry (TD-CIMS) technique for the simultaneous measurement of peroxyacyl nitrates and dinitrogen pentoxide.* J. Geophys. Res.: Atmos. , 2004. **109**(D19): p. 193151-13.

40. O'Keefe, A. and D.A.G. Deacon, *Cavity ring-down optical spectrometer for absorption measurements using pulsed laser sources.* Rev. Sci. Instrum., 1988. **59**: p. 2544-2555.

41. Busch, K.W. and M.A. Busch, *Introduction to Cavity-Ringdown Spectroscopy*, in *Cavity-Ringdown Spectroscopy*, K.W. Busch and M.A. Busch, Editors. 1999, American Chemical Society. p. 7-19.

42. Ball, S.M. and R.L. Jones, *Broad-Band Cavity Ring-Down Spectroscopy.* Chem. Rev. , 2003. **103**(12): p. 5239-5262.

43. Berden, G., R. Peeters, and G. Meijer, *Cavity ring-down spectroscopy: Experimental schemes and applications.* Int. Rev. Phys. Chem., 2000. **19**: p. 565-607.

44. Brown, S.S., *Absorption Spectroscopy in High-Finesse Cavities for Atmospheric Studies.* Chem. Rev., 2003. **103**(12): p. 5219-5238.

45. Zalicki, P. and R.N. Zare, *Cavity ring-down spectroscopy for quantitative absorption measurements* J. Chem. Phys., 1995. **102**(7): p. 2708-2717.

46. Newman, S.M., I.C. Lane, A.J. Orr-Ewing, D.A. Newnham, and J. Ballard, *Integrated absorption intensity and Einstein coefficients for the O2 a1Δg–X3Σ−g (0,0) transition: A comparison of cavity ringdown and high resolution Fourier transform spectroscopy with a long-path absorption cell.* J. Chem. Phys., 1999. **110**(22): p. 10749-10757.

47. Pettersson, A., E.R. Lovejoy, C.A. Brock, S.S. Brown, and A.R. Ravishankara, *Measurement of aerosol optical extinction at 532 nm with pulsed cavity ring down spectroscopy.* J. Aerosol Sci., 2004. **35**(8): p. 995-1011.

48. Osthoff, H.D., S.S. Brown, T.B. Ryerson, T.J. Fortin, B.M. Lerner, E.J. Williams, A. Pettersson, T. Baynard, **W.P. Dubé**, S.J. Ciciora, and A.R. Ravishankara, *Measurement of atmospheric NO2 by pulsed cavity ring-down spectroscopy.* J. Geophys. Res.: Atmos. , 2010. **111**(2): p. 1-10.

49. Yokelson, R.J., J.B. Burkholder, R.W. Fox, R.K. Talukdar, and A.R. Ravishankara, *Temperature Dependence of the NO3 Absorption Spectrum.* J. Phys. Chem., 1994. **98**(50): p. 13144–13150.

50. R., P., *Tables of the Refractive Index for Standard Air and the Rayleigh Scattering Coefficient for the Spectral Region between 0.2 and 20.0 μ and Their Application to Atmospheric Optics* J. Opt. Soc. Am., 1957. **47**(2): p. 176-182.

51. Aldener, M., S.S. Brown, H. Stark, E.J. Williams, B.M. Lerner, W.C. Kuster, P.D. Goldan, P.K. Quinn, T.S. Bates, F.C. Fehsenfeld, and A.R. Ravishankara, *Reactivity and loss mechanisms of NO3 and N2O5 in a polluted marine environment: Results from in situ measurements during New England Air Quality Study 2002.* J. Geophys. Res., 2006. **111**(D23): p. 2156-2202.

52. Brown, S.S., H. Stark, T.B. Ryerson, E.J. Williams, D.K. Nicks, M. Trainer, F.C. Fehsenfeld, and A.R. Ravishankara, *Nitrogen oxides in the nocturnal boundary layer: Simultaneous in situ measurements of NO3, N2O5, NO2, NO, and O3.* J. Geophys. Res., 2003. **108**(D9): p. 2156-2202.

53. Sander, S., D. Golden, M. Kurylo, G. Moortgat, P. Wine, A. Ravishankara, C. Kolb, M. Molina, B. Finlayson-Pitts, and R. Huie, *Chemical kinetics and photochemical data for use in atmospheric studies evaluation number 15.* 2006, Pasadena, CA: Jet Propulsion Laboratory, National Aeronautics and Space Administration, 2006.

54. Vandaele, A.C., C. Hermans, P.C. Simon, M. Carleer, R. Colin, S. Fally, M.F. Mérienne, A. Jenouvrier, and B. Coquart, *Measurements of the NO2 absorption cross-section from 42 000 cm−1 to 10 000 cm−1 (238–1000 nm) at 220 K and 294 K.* J. Quant. Spectrosc. Radiat. Transf., 1998. **59**(3): p. 171-184.

55. Brown, S.S., H.D. Osthoff, H. Stark, **W.P. Dubé**, T.B. Ryerson, C. Warneke, J.A. de Gouw, A.G. Wollny, D.D. Parrish, F.C. Fehsenfeld, and A.R. Ravishankara, *Aircraft observations of daytime NO3 and N2O5 and their implications for tropospheric chemistry.* J. Photochem. Photobiol. A, 2005. **176**(1–3): p. 270-278.

56. Davidson, J.A., A.A. Viggiano, C.J. Howard, I. Dotan, F.C. Fehsenfeld, D.L. Albritton, and E.E. Ferguson, *Rate constants for the reactions of O2+, NO2+, NO+, H3O+, CO3−, NO2−, and halide ions with N2O5 at 300 K* J. Chem. Phys., 1978. **68**: p. 2085-2087.

57. M., M.D. and F.D. W., *Mathematical treatment of the wall loss of a trace species in denuder and catalytic converter tubes* Anal. Chem., 1987. **59**(23): p. 2753-2759.

58. Rudich, Y., R.K. Talukdar, T. Imamura, R.W. Fox, and A.R. Ravishankara, *Uptake of NO3 on KI solutions: rate coefficient for the NO3 + I− reaction and gas-phase diffusion coefficients for NO3.* Chem. Phys. Lett., 1996. **261**(4-5): p. 467-473.

59. Burkholder, J.B. and R.K. Talukdar, *Temperature Dependence of the ClONO2 UV Absorption Spectrum.* Geophys. Res. Lett., 1994. **21**(7): p. 581-584.

60. Orphal, J., C.E. Fellows, and P.M. Flaud, *The visible absorption spectrum of NO3 measured by high-resolution Fourier transform spectroscopy.* J. Geophys. Res., 2003. **108**: p. 40771-12.

61. Brown, S.S., H. Stark, and A.R. Ravishankara, *Cavity ring-down spectroscopy for atmospheric trace gas detection: application to the nitrate radical (NO3).* Appl. Phys. B, 2002. **75**(2): p. 173-182.

62. Werle, P., R. Mücke, and F. Slemr, *The limits of signal averaging in atmospheric trace-gas monitoring by tunable diode-laser absorption spectroscopy (TDLAS).* Appl. Phys. B, 1993. **57**(2): p. 131-139.

63. Aldener, M., S.S. Brown, H. Stark, J.S. Daniel, and A.R. Ravishankara, *Near-IR absorption of water vapor: Pressure dependence of line strengths and an upper limit for continuum absorption.* J. Mol. Spectrosc., 2005. **232**(2): p. 223-230.

64. Geyer, A., B. Alicke, S. Konrad, T. Schmitz, J. Stutz, and U. Platt, *Chemistry and oxidation capacity of the nitrate radical in the continental boundary layer near Berlin.* J. Geophys. Res., 2001. **106**(D8): p. 8013–8025

65.   Warneke, C., J.A. de Gouw, P.D. Goldan, W.C. Kuster, E.J. Williams, B.M. Lerner, R. Jakoubek, S.S. Brown, H. Stark, M. Aldener, A.R. Ravishankara, J.M. Roberts, M. Marchewka, S. Bertman, D.T. Sueper, S.A. McKeen, J.F. Meagher, and F.C. Fehsenfeld, *Comparison of daytime and nighttime oxidation of biogenic and anthropogenic VOCs along the New England coast in summer during New England Air Quality Study 2002.* J. Geophys. Res, 2004. **109**: p. D103091-14.

66.   Atkinson, R., *Kinetics and Mechanisms of the Gas‑Phase Reactions of the NO3 Radical with Organic Compounds.* J. Phys. Chem. Ref. Data, 1991. **20**(3): p. 459-507.

67.   Dentener, F.J. and P.J.J. Crutzen, *Reaction of N2O5 on tropospheric aerosols: Impact on the global distributions of NOx, O3, and OH.* J. Geophys. Res., 1993. **98**(D4): p. 7149–7163

68.   Plane, J.M.C. and C. Nien, *Differential optical absorption spectrometer for measuring atmospheric trace gases.* Rev. Sci. Instrum., 1992. **63**: p. 1867-1876.

69.   Brown, S.S., T.B. Ryerson, A.G. Wollny, C.A. Brock, R. Peltier, A.P. Sullivan, R.J. Weber, J.S. Holloway, **W.P. Dubé**, M. Trainer, J.F. Meagher, F.C. Fehsenfeld, and A.R. Ravishankara, *Variability in nocturnal nitrogen oxide processing and its role in regional air quality.* Science, 2006. **311**(5757): p. 67-70.

70.   Stark, H., S.S. Brown, P.D. Goldan, M. Aldener, W.C. Kuster, R. Jakoubek, F.C. Fehsenfeld, J. Meagher, T.S. Bates, and A.R. Ravishankara, *Influence of nitrate radical on the oxidation of dimethyl sulfide in a polluted marine environment.* J. Geophys. Res.: Atmos. , 2007. **112**(D10): p. D10S041-11.

71.   Brown, S.S., **W.P. Dubé**, H.D. Osthoff, D.E. Wolfe, W.M. Angevine, and A.R. Ravishankara, *High resolution vertical distributions of NO3 and N2O5 through the nocturnal boundary layer.* Atmos. Chem. Phys., 2007. **7**: p. 139-149.

72.   Atkinson, R. *IUPAC Subcommittee on Gas Kinetic Data Evaluation for Atmospheric Chemistry*. 2003; Available from: http://iupac.pole-ether.fr/.

73.   Liu, B.Y.H. and K.W. Lee, *An Aerosol Generator of High Stability.* Am. Ind. Hyg. Assoc. J., 1975. **36**(12): p. 861-865.

74.   Osthoff, H.D., M.J. Pilling, A.R. Ravishankara, and S.S. Brown, *Temperature dependence of the NO3 absorption cross-section above 298 K and determination of the equilibrium constant for NO3+NO2↔N2O5 at atmospherically relevant conditions.* Phys. Chem. Chem. Phys., 2007. **9**: p. 5785-5793.

75.   Crutzen, P.J., *Influence of nitrogen oxides on atmospheric ozone content.* Q. J. R. Meteorol. Soc., 1970. **96**(408): p. 320-325.

76.   Kley, D. and M. McFarland, *Chemiluminescence detector for NO and NO2.* Atmos. Tech., 1980. **12**: p. 62-69.

77.   Ryerson, T.B., E.J. Williams, and F.C. Fehsenfeld, *An efficient photolysis system for fast-response NO2 measurements.* J. Phys. Chem., 2000. **105**(D21): p. 26447–26461.

78.   Winer, A.M., J.W. Peters, J.P. Smith, and J.N. Pitts, *Response of commercial chemiluminescent nitric oxide-nitrogen dioxide analyzers to other nitrogen-containing compounds.* Environ. Sci. Technol., 1974. **8**(13): p. 1118–1121.

79.   Dunlea, E.J., *Evaluation of nitrogen dioxide chemiluminescence monitors in a polluted urban environment.* Atmos. Chem. Phys., 2007. **7**: p. 2691-2704.

80.   Li, Y.Q., K.L. Demerjian, M.S. Zahniser, D.D. Nelson, J.B. McManus, and S.C. Herndon, *Measurement of formaldehyde, nitrogen dioxide, and sulfur dioxide at Whiteface Mountain using a dual tunable diode laser system.* J. Geophys. Res., 2004. **109**: p. D16S081-11.

81.   Thornton, J.A., P.J. Woolridge, and R.C. Cohen, *Atmospheric NO2: In situ laser‑induced fluorescence detection at parts per trillion mixing ratios.* Anal. Chem., 2000. **72**(3): p. 528-539.

82.   Czyzewski, A., K. Ernst, G. Karasinki, H. Lange, P. Rairoux, W. Skubiszak, and T. Stacewicz, *Cavity ring-down spectroscopy for trace gas analysis.* Acta Phys. Pol. B, 2002. **33**: p. 2255 – 2267.

83.   Mazurenka, M., R. Wada, A.J.L. Shillings, T.J.A. Butler, J.M. Beames, and A.J. Orr-Ewing, *Fast Fourier transform analysis in cavity ring-down spectroscopy: application to an optical detector for atmospheric NO2.* Appl. Phys. B: Laser Opt., 2005. **81**: p. 135-141.

84.   Wada, R. and A.J. Orr-Ewing, *Continuous wave cavity ring-down spectroscopy measurement of NO2 mixing ratios in ambient air.* The Analyst, 2005. **130**: p. 1595-1600.

85.   Miyazaki, K., J. Matsumoto, S. Kato, and Y. Kajii, *Development of atmospheric NO analyzer by using a laser-induced fluorescence NO2 detector.* Atmos. Environ., 2008. **42**(33): p. 7812-7820.

86.   Hargrove, J. and J. Zhang, *Measurements of NOx, acyl peroxynitrates, and NOy with automatic interference corrections using a NO2 analyzer and gas phase titration.* Rev. Sci. Instrum., 2008. **79**: p. 0461091-3.

87.   Kebabian, P.L., E.C. Wood, S.C. Herndon, and A. Freedman, *A Practical Alternative to chemiluminescence-based detection of nitrogen dioxide: cavity attenuated phase shift spectroscopy.* Environ. Sci. Technol., 2008. **42**(16): p. 6040–6045.

88.   Baer, D.S., J.B. Paul, M. Gupta, and A.O. O'Keefe, *Sensitive asorption measurements in the near-infrared region using off-axis integrated-cavity-output spectroscopy.* Appl. Phys. B: Lasers Opt., 2002. **75**(2-3): p. 261–265.

89.   Voigt, S., J. Orphal, and J.P. Burrows, *The temperature and pressure dependence of the absorption cross-sections of NO2 in the 250-800 nm region measured by Fourier transform spectroscopy.* J. Photochem. Photobiol. A, 2002. **149**(1-3): p. 1-7.

90.   Rothman, L.S., *HITRAN database.* J. Quant. Spectrosc. Radiat. Transfer, 2005. **96**: p. 139.

91.   Bodhaine, B.A., N.B. Wood, E.G. Dutton, and J.R. Slusser, *On Rayleigh optical depth calculations.* J. Atmos. Ocean. Technol., 1999. **16**(11): p. 1854-1861.

92.   Sutton, J.A. and J.F. Driscoll, *Rayleigh scattering cross sections of combustion species at 266, 355, and 532 nm for thermometry applications.* Opt. Lett., 2004. **29**(22): p. 2620-2622.

93.   *MPI Mainz UV VIS spectral atlas of gaseous molecules.* Available from: http://www.atmosphere.mpg.de/enid/2295.

94.   Volkamer, R., P. Spietz, J. Burrows, and U. Platt, *High-resolution absorption cross-section of glyoxal in the UV VIS and IR spectral ranges.* J. Photochem. Photobiol., 2005. **172**(1): p. 35-46.

95.   Washenfelder, R.A., A.O. Langford, H. Fuchs, and S.S. Brown, *Measurement of glyoxal using an incoherent broadband cavity enhanced absorption spectrometer.* Atmos. Chem. Phys., 2008. **8**: p. 7779-7793.

96.   Volkamer, R., L.T. Molina, M.J. Molina, T. Shirley, and W.H. Brune, *DOAS measurement of glyoxal as an indicator for fast VOC chemistry in urban air.* Geophys. Res. Lett., 2005. **32**: p. L088061-4.

97.   Huisman, A.J., J.R. Hottle, K.L. Coens, J.P. DiGangi, M.M. Galloway, A. Kammrath, and F.N. Keutsch, *Laser-Induced phosphorescence for the in situ detection of glyoxal at part per trillion mixing ratios.* Anal. Chem., 2008. **80**(15): p. 5884–5891.

98.   Harwood, M.H., R.L. Jones, R.A. Cox, E. Lutman, and O.V. Rattigan, *Temperature-dependent absorption cross sections of N2O5.* J. Photochem. Photobiol. A, 1993. **73**(3): p. 167-175.

99.   Jones, C.L. and J.H. Seinfeld, *The oxidation of NO2 to nitrateday and night.* Atmos. Environ., 1983. **17**(11): p. 2370-2373.

100. Finlayson-Pitts, B.J., M.J. Ezell, and J.N. Pitts, *Formation of chemically active chlorine compounds by reactions of atmospheric NaCl particles with gaseous N2O5 and ClONO2.* Nature, 1989. **337**(6204): p. 241-244.

101. Brown, S.S., **W.P. Dubé**, H.D. Osthoff, J. Stutz, T.B. Ryerson, A.G. Wollny, C.A. Brock, C. Warneke, J.A. de Gouw, E. Atlas, J.A. Neuman, J.S. Holloway, B.M. Lerner, E.J. Williams, W.C. Kuster, P.D. Goldan, W.M. Angevine, M. Trainer, F.C. Fehsenfeld, and A.R. Ravishankara, *Vertical profiles in NO3 and N2O5 measured from an aircraft: Results from the NOAA P-3 and surface platforms during the New England Air Quality Study 2004.* J. Geophys. Res, 2007. **112**(D22): p. D223041-17.

102. Fuchs, H., S.M. Ball, B. Bohn, T. Brauers, R.C. Cohen, H.P. Dorn, **W.P. Dubé**, J.L. Fry, R. Häseler, U. Heitmann, R.L. Jones, J. Kleffmann, T.F. Mentel, P. Müsgen, F. Rohrer, A.W. Rollins, A.A. Ruth, A. Kiendler-Scharr, E. Schlosser, A.J.L. Shillings, R. Tillmann, R.M. Varma, D.S. Venables, G. Villena Tapia, A. Wahner, R. Wegener, P.J. Wooldridge, and S.S. Brown, *Intercomparison of measurements of NO_2 concentrations in the atmosphere simulation chamber SAPHIR during the NO3Comp campaign.* Atmos. Meas. Tech., 2010. **3**(1): p. 21-37.

103. Washenfelder, R.A., N.L. Wagner, **W.P. Dubé**, and S.S. Brown, *Measurement of Atmospheric Ozone by Cavity Ring-down Spectroscopy.* Environ. Sci. Technol., 2011. **45**(7): p. 2938-2944.

104. Brown, S.S., H. Stark, and A.R. Ravishankara, *Applicability of the steady state approximation to the interpretation of atmospheric observations of NO3 and N2O5.* J. Geophys. Res.: Atmos. , 2003. **108**(D17): p. 45391-10.

105. Atkinson, D.B., *Solving chemical problems of environmental importance using cavity ring-down spectroscopy.* The Analyst, 2003. **128**(2): p. 117-125.

106. Schuster, G., I. Labazan, and J.N. Crowley, *A cavity ring down/cavity enhanced absorption device for measurement of ambient NO3 and N2O5.* Atmos. Meas. Tech., 2009. **2**: p. 1-13.

107. Everest, M.A. and D.B. Atkinson, *Discrete sums for the rapid determination of exponential decay constants.* Rev. Sci. Instrum., 2008. **79**(2 Pt 1): p. 0231081-10.

108. Langridge, J.M., S.M. Ball, A.J. Shillings, and R.L. Jones, *A broadband absorption spectrometer using light emitting diodes for ultrasensitive, in situ trace gas detection.* Rev. Sci. Instrum., 2008. **79**(12): p. 1231101-10.

109. Ryerson, T.B., L.G. Huey, K. Knapp, J.A. Neuman, D.D. Parrish, D.T. Sueper, and F.C. Fehsenfeld, *Design and initial characterization of an inlet for gas-phase NOy measurements from aircraft.* J. Geophys. Res.: Atmos. , 1999. **104**(D5): p. 5483-5492.

110. Ryerson, T.B., M. Trainer, W.M. Angevine, C.A. Brock, R.W. Dissly, F.C. Fehsenfeld, G.J. Frost, P.D. Goldan, J.S. Holloway, G. Hubler, R.O. Jakoubek, W.C. Kuster, J.A. Neuman, D.K. Nicks Jr., D.D. Parrish, J.M. Roberts, D.T. Sueper, E.L. Atlas, S.G. Donnelly, F. Flocke, A. Fried, W.T. Potter, S. Schauffler, V. Stroud, A.J. Weinheimer, B.P. Wert, C. Wiedinmyer, R.J. Alvarez, R.M. Banta, L.S. Darby, and C.J. Senff, *Effect of petrochemical industrial emissions of reactive alkenes and NOx on tropospheric ozone formation in Houston, Texas,.* J. Geophys. Res., 2003. **108**(ACH8-1-24).

111. Pollack, I.B., B.M. Lerner, and T.B. Ryerson, *Evaluation of ultraviolet light-emitting diodes for detection of atmospheric NO2 by photolysis - chemiluminescence.* J. Atmos. Chem., 2010. **65**(2): p. 111-125.

112. Fahey, D., C. Eubank, G. Hübler, and F. Fehsenfeld, *Evaluation of a catalytic reduction technique for the measurement of total reactive odd-nitrogen NOy in the atmosphere.* J. Atmos. Chem., 1985. **3**: p. 435–468.

113. Williams, E.J., K. Baumann, J.M. Roberts, S.B. Bertman, R.B. Norton, F.C. Fehsenfeld, S.R. Springston, L.J. Nunnermacker, L. Newman, K. Olszyna, J. Meagher, B. Hartsell, E. Edgerton,

J.R. Pearson, and M.O. Rodgers, *Intercomparison of ground-based NOy measurement techniques.* J. Geophys. Res.: Atmos., 1998. **103**(D17): p. 22261-22280.

114. Crosley, D.R., *NOy Blue Ribbon panel.* J. Geophys. Res.: Atmos., 1996. **101**(D1): p. 2049-2052.

115. Kliner, D.A.V., B.C. Daube, J.D. Burley, and S.C. Wofsy, *Laboratory investigation of the catalytic reduction technique for measurement of atmospheric NOy.* J. Geophys. Res.: Atmos., 1997. **102**(D9): p. 10759-10776.

116. Neuman, J.A., L.G. Huey, T.B. Ryerson, and D.W. Fahey, *Study of Inlet Materials for Sampling Atmospheric Nitric Acid.* Environ. Sci. Technol., 1999. **33**: p. 1133-1136.

117. Wooldridge, P.J., A.E. Perring, T.H. Bertram, F.M. Flocke, J.M. Roberts, H.B. Singh, L.G. Huey, J.A. Thornton, G.M. Wolfe, J.G. Murphy, J.L. Fry, A.W. Rollins, B.W. LaFranchi, and R.C. Cohen, *Total Peroxy Nitrates (Σ PNs) in the atmosphere: the Thermal Dissociation-Laser Induced Fluorescence (TD-LIF) technique and comparisons to speciated PAN measurements.* Atmos. Meas. Tech., 2010. **3**: p. 593-607.

118. Di Carlo, P., E. Aruffo, M. Busilacchio, F. Giammaria, C. Dari-Salisburgo, F. Biancofiore, G. Visconti, J. Lee, S. Moller, C.E. Reeves, S. Bauguitte, G. Forster, R.L. Jones, and B. Ouyang, *Aircraft based four-channel thermal dissociation laser induced fluorescence instrument for simultaneous measurements of NO2, total peroxy nitrate, total alkyl nitrate, and HNO3.* Atmos. Meas. Tech., 2013. **6**: p. 971-980.

119. Pérez, I.M., P.J. Wooldridge, and R.C. Cohen, *Laboratory evaluation of a novel thermal dissociation chemiluminescence method for in situ detection of nitrous acid.* Atmos. Environ., 2007. **41**: p. 3993-4001.

120. Thaler, R.D., L.H. Mielke, and H.D. Osthoff, *Quantification of Nitryl Chloride at Part Per Trillion Mixing Ratios by Thermal Dissociation Cavity Ring-Down Spectroscopy.* Anal. Chem., 2011. **83**: p. 2761-2766.

121. Day, D.A., P.J. Wooldridge, M.B. Dillon, J.A. Thornton, and R.C. Cohen, *A thermal dissociation laser-induced fluorescence instrument for in situ detection of NO2, peroxy nitrates, alkyl nitrates, and HNO3.* J. Geophys. Res.: Atmos., 2002. **107**: p. ACH 4-1.

122. Mazurenka, M.I., B.L. Fawcett, J.M. Elks, D.E. Shallcross, and A.J. Orr-Ewing, *410-nm diode laser cavity ring-down spectroscopy for trace detection of NO2.* Chem. Phys. Lett., 2003. **367**: p. 1-9.

123. Hargrove, J., L. Wang, K. Muyskens, M. Muyskens, D. Medina, S. Zaide, and J. Zhang, *Cavity Ring-Down Spectroscopy of Ambient NO2 with Quantification and Elimination of Interferences.* Environ. Sci. Technol., 2006. **40**: p. 7868-7873.

124. Castellanos, P., W.T. Luke, P. Kelley, J.W. Stehr, S.H. Ehrman, and R.R. Dickerson, *Modification of a commercial cavity ring-down spectroscopy NO2 detector for enhanced sensitivity.* Rev. Sci. Instrum., 2009. **80**: p. 1131071-6.

125. Rollins, A.W., J.D. Smith, K.R. Wilson, and R.C. Cohen, *Real Time In Situ Detection of Organic Nitrates in Atmospheric Aerosols.* Environ. Sci. Technol., 2010. **44**: p. 5540-5545.

126. Johnston, H.S., C.A. Cantrell, and J.G. Calvert, *Unimolecular decomposition of NO3 to form NO and O2 and a review of N2O5/NO3 kinetics.* J. Geophys. Res.: Atmos., 1986. **91**: p. 5159-5172.

127. Reisen, F. and J. Arey, *Atmospheric Reactions Influence Seasonal PAH and Nitro-PAH Concentrations in the Los Angeles Basin.* Environ. Sci. Technol., 2005. **39**: p. 64-73.

128. Axson, J.L., R.A. Washenfelder, T.F. Kahan, C.J. Young, V. Vaida, and S.S. Brown, *Absolute ozone absorption cross section in the Huggins Chappuis minimum (350 - 470 nm) at 296 K.* Atmos. Chem. Phy., 2011. **11**: p. 11581-11590.

129. Roberts, J.M., P. Veres, C. Warneke, J.A. Neuman, R.A. Washenfelder, S.S. Brown, M. Baasandorj, J.B. Burkholder, I.R. Burling, T.J. Johnson, R.J. Yokelson, and J. de Gouw, *Measurement of HONO, HNCO, and other inorganic acids by negative-ion proton-transfer chemical-ionization mass spectrometry (NI-PT-CIMS): application to biomass burning emissions.* Atmos. Meas. Tech., 2010. **3**: p. 981-990.

130. Helmig, D., C.R. Thompson, J. Evans, P. Boylan, J. Hueber, and J.H. Park, *Highly Elevated Atmospheric Levels of Volatile Organic Compounds in the Uintah Basin, Utah.* Environ. Sci. Technol., 2014. **48**: p. 4707-4715.

131. Brown, S.S., J.A. Thornton, W.C. Keene, A.A.P. Pszenny, B.C. Sive, **W.P. Dubé**, N.L. Wagner, C.J. Young, T.P. Riedel, J.M. Roberts, T.C. VandenBoer, R. Bahreini, F. Öztürk, A.M. Middlebrook, S. Kim, G. Hübler, and D.E. Wolfe, *Nitrogen, Aerosol Composition, and Halogens on a Tall Tower (NACHTT): Overview of a wintertime air chemistry field study in the front range urban corridor of Colorado.* J. Geophys. Res.: Atmos. , 2013. **118**(14): p. 8067-8085.